FACULDADE DE ENGENHARIA DA UNIVERSIDADE DO PORTO

Development of a Universal Thermosetting Putty for High-Performance Bicycle Frames: An Integrated Materials Engineering and Process Optimization Approach

António Afonso Pacheco Lousa Ciravegna da Fonseca

Mestrado em Engenharia Mecânica

Supervisor: Prof. Doutor Rúben Filipe da Silva Santos

Second Supervisor: Prof. Doutor José Carlos Magalhães Duque da Fonseca

July 22, 2026

Development of a Universal Thermosetting Putty for High-Performance Bicycle Frames: An Integrated Materials Engineering and Process Optimization Approach

António Afonso Pacheco Lousa Ciravegna da Fonseca

Mestrado em Engenharia Mecânica

Approved in oral examination by the committee:

President: Prof. Teresa Margarida Guerra Pereira Duarte

Examiner: Prof. João Augusto Sousa Bastos

Member: Prof. Rúben Filipe da Silva Santos

July 22, 2026

Resumo

A expansão do mercado europeu de bicicletas elétricas (e-bikes) impulsionou a procura por quadros de alumínio 6061 com uma estética contínua, exigindo a aplicação de betumes de nivelamento cosmético sobre as soldaduras estruturais. No entanto, a integração deste processo num ambiente de fabrico de alto rendimento cria um conflito termomecânico. A instalação atual opera um sistema de matriz dupla: os betumes de poliéster insaturado oferecem uma cura rápida, mas sofrem desgaseificação térmica durante o ciclo de pintura eletrostática a pó a 180°C, enquanto os betumes de epóxi sobrevivem ao forno, mas introduzem atrasos operacionais devido ao longo tempo de cura. Esta investigação visa desenvolver uma matriz de nivelamento universal para otimizar a cadeia de valor de acabamento de superfícies.

Uma metodologia sequencial de duas fases foi executada dentro dos limites operacionais da linha de fábrica. A Fase 1 utilizou uma metodologia Analytical Hierarchy Process (AHP) para avaliar 32 combinações de formulação-primário face a restrições termodinâmicas e de tempo de ciclo, demonstrando empiricamente que primários líquidos intermediários (1K e 2K) retêm compostos voláteis em expansão e exacerbam a falha térmica na estufa. Consequentemente, a Fase 2 empregou um Design of Experiments (DoE) para desenvolver um nanocompósito através de mistura centrífuga planetária. A dopagem de uma matriz epóxi de base (NT) com 0.6% em volume de nanoplaquetas de grafeno estabeleceu uma rede de percolação semicondutora. Esta modificação estabilizou a deposição eletrostática do pó, resolvendo o efeito de gaiola de Faraday e alcançando uma classificação de adesão Classe 0 sem degradar a resistência térmica inata da matriz. A investigação entregou um protótipo validado no Nível de Prontidão Tecnológica (Technology Readiness Level (TRL)) 4, fornecendo um plano técnico para abordar o estrangulamento do sistema de dupla matriz e apoiar a transição para um padrão de produção em massa.

Palavras-chave: Betumes termofixos • Matrizes de poliéster • Matrizes epóxi • Nanoplaquetas de grafeno • AHP • DoE • Revestimento a pó • Otimização de processos de fabrico

Abstract

The expansion of the European e-bike market has driven the demand for aluminum 6061 frames featuring a seamless aesthetic, necessitating the application of cosmetic leveling putties over structural welds. However, integrating this process into high-throughput manufacturing creates a thermomechanical conflict. The current facility operates a dual-matrix system: unsaturated polyester putties offer rapid curing but experience thermal outgassing during the 180°C electrostatic powder coating cycle, while high-temperature epoxy putties survive the oven but introduce a curing bottleneck. This research aims to develop a universal leveling matrix to streamline the surface finishing value stream.

A sequential, two-phase methodology was executed within the operational boundaries of the active factory line. Phase 1 utilized an Analytical Hierarchy Process (AHP) methodology to evaluate 32 commercial formulation-primer combinations against thermodynamic and cycle-time constraints, demonstrating that intermediate 1K and 2K liquid primers trap expanding volatiles and exacerbate thermal failure. Consequently, Phase 2 employed a Design of Experiments (DoE) to develop a nanocomposite via planetary centrifugal compounding. The doping of a baseline epoxy matrix (NT) with 0.6% by volume of graphene nanoplatelets established a semi-conductive percolation network. This modification stabilized electrostatic powder deposition, resolving the Faraday cage effect and achieving a Class 0 adhesion score without degrading the matrix's innate 180°C thermal resistance. The research delivered a validated Technology Readiness Level (TRL) 4 prototype, providing a technical framework to address the dual-matrix bottleneck and transition toward a mass-production standard.

Keywords: Thermosetting putty • Polyester matrices • Epoxy matrices • Graphene nanoplatelets • AHP • DoE • Powder coating • Manufacturing process optimization

The United Nations Sustainable Development Goals

This research contributes to sustainable manufacturing by improving the efficiency and robustness of the surface finishing process used in aluminium bicycle frame production. The development of a universal thermosetting putty reduces production waste, minimizes rework, decreases material consumption, and improves First Time Yield (FTY), thereby supporting more resource-efficient manufacturing. Furthermore, the proposed solution contributes to cleaner production through better process stability and the potential reduction of energy consumption associated with repeated curing operations. The adoption of advanced nanocomposite materials also promotes industrial innovation and strengthens the competitiveness of European manufacturing.

This work aligns most strongly with the following Sustainable Development Goals (SDG):

SDG 8 Decent Work and Economic Growth

SDG 9 Industry, Innovation and Infrastructure

SDG 12 Responsible Consumption and Production

SDG	Target	Contribution	Possible Performance Indicators
8	8.2	Increased manufacturing productivity through process optimization	Productivity, cycle time, labour efficiency
9	9.4	Development of an innovative thermosetting nanocomposite for advanced manufacturing	TRL level, successful industrial validation, process capability, innovation adoption
	9.5	Applied industrial Research and Development (R&D) integrating materials engineering and process optimization	Number of new formulations developed, experimental validation
12	12.2	More efficient use of raw materials through reduced defects and rework	Material consumption per frame, putty waste reduction
	12.4	Improved chemical management and optimized coating processes	Reduced defective coatings, reduced chemical losses
	12.5	Reduction of industrial waste through higher FTY	Scrap rate, rework rate, Cost of Poor Quality (COPQ) reduction

Acknowledgements

This dissertation marks the culmination of an academic and professional journey that I hold in high regard. This path would not have been possible without the support and guidance of many individuals.

First and foremost, I would like to express my sincere gratitude to my supervisors at FEUP, Professor Doutor Rúben Filipe da Silva Santos and Professor Doutor José Carlos Magalhães Duque da Fonseca. Thank you for your guidance, availability, and the valuable technical insights and support you provided throughout this process. I also extend my thanks to Professora Doutora Teresa Duarte for her assistance during logistical challenges, and to Professora Doutora Susana Olhero for granting me access to the research facilities at the University of Aveiro.

I would also like to thank Triangle's – Cycling Equipments S.A. for the opportunity to be part of the team, which allowed me to conduct this research in a demanding and authentic industrial environment. My thanks go to Daniela for my integration into the company, and to my mentor, Eng. Rui Miguel Silva, for the autonomy and trust he placed in me. A special thank you to Andreilson for the many hours of hard work and the time we shared on the factory floor.

I extend my appreciation to FEUP for the academic environment provided and for the knowledge I have gained throughout this Master's program.

I am deeply grateful to those who are closest to my heart and have stood by me through this journey; your love, support, and motivation made this work possible.

Finally, a special thank you to my sister and my parents. To my parents, in particular, I am eternally grateful for the support, teachings, and love you have given me throughout my life. You have shaped me not only as a professional but, more importantly, as a person. I will always be grateful to you.

Afonso

Declaração de Honra

Declaro que a presente dissertação é de minha autoria e não foi previamente apresentada e avaliada nesta ou em outra instituição. As referências a outros autores (afirmações, ideias, pensamentos), assim como a utilização de trabalhos publicados respeitam escrupulosamente as regras da atribuição, e encontram-se devidamente indicadas no texto e nas referências bibliográficas, de acordo corn as normas de referenciação. Tenho consciência de que a prática de plágio ou de autoplágio constituem ilícitos académicos, conforme estabelecido no Código de Ética da U.Porto.

Mais declaro que incluí texto(s) publicado(s) em coautoria, tendo especificado, com transparência e rigor, a colaboração de cada coautor e informado sobre a eventual existência de alguma outra dissertação em que também tenha sido incluído. São também incluídos a autorização da revista em que se encontra publicado, assim como a acordo expresso assinado por todos as coautores para a inclusão do artigo.

Declaro, ainda, que utilizei ferramentas de Inteligência Artificial de forma limitada para apoiar a estruturação de texto e o aperfeiçoamento linguístico. Todo o conteúdo final foi revisto e validado pelo autor.

António Afonso Pacheco Lousa Ciravegna da Fonseca

"The last clear definite function of man—muscles aching to work, minds aching to create beyond the single need—this is man."

John Steinbeck, The Grapes of Wrath

Contents

1 Introduction **1**
- 1.1 Context and Motivation . . . 1
- 1.2 Problem Statement . . . 2
- 1.3 Objectives and Scope . . . 3
- 1.4 Scientific Contribution and Research Hypotheses . . . 4
- 1.5 Methodology Overview . . . 5
- 1.6 Structure of the Dissertation . . . 5
- 1.7 Sustainability Impact and SDG Alignment . . . 5

2 Current State Analysis **7**
- 2.1 Macro Production Flow . . . 7
- 2.2 The Surface Finishing Value Stream . . . 10
  - 2.2.1 Pre-Application Phase: Chemical Passivation Line . . . 10
  - 2.2.2 Core Application Phase: Putty Deposition and Thermal Curing . . . 12
  - 2.2.3 The Coating Phase . . . 15
- 2.3 Current KPI Analysis and Process Diagnostics . . . 21
  - 2.3.1 Framework and Data Extraction Strategy . . . 21
  - 2.3.2 Phase 1 Investigation: Pre-Coating Preparation . . . 21
  - 2.3.3 Phase 2 Investigation: The "Ghost Rework" Discovery . . . 23
  - 2.3.4 Phase 3 Validation: The Final Coating Facility . . . 23
  - 2.3.5 Diagnostic Synthesis and Justification for the DoE Methodology . . . 29

3 Literature Review **30**
- 3.1 The Role of aluminum alloy 6061 in the Bicycle and E-Bike Industry . . . 30
- 3.2 Aluminum Treatments and Coating Processes . . . 31
  - 3.2.1 Adhesion and Surface Treatments . . . 32
  - 3.2.2 Coating Processes . . . 34
  - 3.2.3 Critical Discussion and Experimental Implications . . . 36
- 3.3 Metal Surface Repair and Covering of Welding Seams . . . 37
  - 3.3.1 Market Trends of Putties . . . 37
  - 3.3.2 The Role of Industrial Putties . . . 38
  - 3.3.3 Current Problems and Bottlenecks . . . 39
  - 3.3.4 Critical Discussion and Experimental Implications . . . 41
- 3.4 Thermosetting Polymer Matrices . . . 42
  - 3.4.1 Polyester resins . . . 42
  - 3.4.2 Epoxy resins . . . 44
  - 3.4.3 Critical Discussion and Experimental Implications . . . 45
- 3.5 Polymer Modification and Functional Fillers . . . 45

3.5.1 Different Filler Approaches . . . 46
3.5.2 Critical Discussion and Experimental Implications . . . 48
3.6 Methodological Foundations for Process Optimization . . . 48
3.6.1 Methodological Foundations for Process Optimization . . . 48

4 Methodology and Experimental Work **50**
4.1 Experimental Architecture and Protocol . . . 51
4.1.1 Evaluation Methodology . . . 51
4.1.2 Heuristic Stage-Gate Screening Protocol . . . 56
4.1.3 Phase 2: Parallel DoE Architecture . . . 63
4.2 Route Mapping and Iterative Process . . . 66
4.2.1 Independent Variables and the Initial Experimental Matrix . . . 67
4.2.2 Logistics Expansion and Supplier Engagement . . . 67
4.2.3 Updated Experimental Matrix and Contingency Execution . . . 68
4.2.4 Thermal Incompatibility and Elimination of the 1K Primer . . . 69
4.2.5 Methodological Pivot and Supplier Feedback Loop . . . 71
4.2.6 Engineering Contingencies and Circular Economy Limitations . . . 73

5 Results and Discussion **75**
5.1 Initial Screening Phase . . . 75
5.1.1 Performance of Baseline Putties . . . 75
5.1.2 Addition of the 2k Primer . . . 79
5.1.3 Phase 1 Conclusion: The Operational Paradox and the Limit of Commercial Baselines . . . 85
5.1.4 Performance of Modified Formulas . . . 86
5.1.5 Stage-Gate Synthesis: Declaration of the Top 3 . . . 91
5.1.6 Sensitivity Analysis . . . 92
5.2 Phase 2: Design of Experiments (DoE) on Selected Matrices . . . 94
5.2.1 The Legacy Polyester . . . 94
5.2.2 The Legacy Epoxy (ES) . . . 97
5.2.3 Evaluation of the NT Matrix . . . 99
5.3 Cross-Matrix Synthesis and Final Operational Capability . . . 102
5.3.1 Visualizing the Performance Envelopes . . . 102
5.3.2 Consolidated Operational Metrics and Global Efficiency . . . 103

6 Conclusions and Future Works **105**
6.1 Industrial Pragmatism vs. Academic Evaluation . . . 105
6.2 Methodological Constraints and Statistical Limitations . . . 106
6.3 The Operational Trade-off and Process-Driven Problem Solving . . . 107
6.4 Efficacy of Nanomaterial Doping and Interfacial Primers . . . 107
6.5 Validation of the Weighted Evaluation Framework . . . 108
6.6 Future Works . . . 108

References **111**

A Methodology and Experimental Work **117**
A.1 Methodology Tools . . . 117
A.1.1 Variable Definitions for the Weighted Decision Matrix . . . 117
A.1.2 AHP Tools . . . 119

A.1.3 Mapping of the samples 121

B Results and Software Data **122**
B.1 PD Data 122
B.2 ES Data 123
B.3 NT Data 124

List of Figures

2.1 Primary anatomical nomenclature of a standard bicycle frame. 8
2.2 Macro Production Flow of the Factory. 8
2.3 Schematic representation of the continuous chemical passivation line and integrated water demineralization group. 11
2.4 Chemical architecture of the three primary polymeric putty matrices utilized on the factory floor. 13
2.5 The two legacy putties. 13
2.6 Sequential phases and thermal parameters of the liquid painting value stream. . . 16
2.7 Examples of the difficulty in the powder coating deposition. 18
2.8 Sequential phases and thermal parameters of the powder painting value stream. . 19
2.9 Process Flow of E-Bike Frames - Passivation Line and Putty Application. 20
2.10 Process Flow of E-Bike Frames - Coating Lines and Final Phase. 20
2.11 Designation of manufacturing sample models, tracking their respective putty matrices and production line routings. 21
2.12 Defect Pareto Analysis for Model C (Nave 4, 2025). Source: Minitab. 25
2.13 Statistical Process Control (SPC) P-Chart for the expanded 2025 baseline (Model A). The dots correspond to the Not OK (NOK) values. Source: Minitab. 26
2.14 SPC P-Chart for Model C during the 2026 Post-Transition monitoring period. The dots correspond to the NOK values. Source: Minitab. 27
2.15 Binomial Process Capability Analysis for Model C, Post-Transition Period. Source: Minitab. 28

3.1 Outgassing phenomena with the polyester putty underneath the coating. 42

4.1 Linear progression of the methodology. 50
4.2 Functional mapping, weight assignment, and primary evaluation rationale for process variables. 53
4.3 Chronological stage-gate screening sequence. Formulations progress horizontally through distinct processing gates, where critical empirical variables (V_1–V_7) are measured. 58
4.4 Decision-tree logic dictating the strategic allocation of functional modifiers. . . . 61
4.5 Technology Readiness Level (TRL) denominations. Source: Autohas-waechtershaeuser [7]. 62
4.6 The three-stage centrifugal compounding protocol. Dashed boxes indicate carefully simulated procedures designed to maintain an identical shear history and uniform thermal stress. 63
4.7 Adaptive experimental architecture and active statistical treatments based on Phase 2 primer compatibility. 64

4.8 Process incompability with the 1k primer. 69
4.9 Root-Cause Analysis (RCA) of the 1k primer failure. 70
4.10 Comparative curing kinetics for the Factor X_2 evaluation. 72

5.1 Baseline Performance Envelope: Isolating the highest and lowest scoring formulations of the standard polyester family against the baseline epoxy matrix. 76
5.2 The Interfacial Paradox: Comparing the unprimed (dashed) versus primed (solid) states of the polyesters that suffered the biggest impact. 83
5.3 Strategic allocation of functional nanomaterials for the variants. 87
5.4 Modified Performance Envelope: Isolating the highest and lowest scoring unprimed modified polyesters against the modified epoxy matrix. 88
5.5 RCA of the epoxies' V4 results with the 2k primer. 91
5.6 Sensitivity Analysis to stress-test the formulation selection algorithm. 93
5.7 Tukey Pairwise Comparisons for V_1. 94
5.8 Comparative analysis of Chemical Resistance. 95
5.9 Boxplot of V_7 for the PD family. 96
5.10 Comparative analysis of Electrostatic Adhesion. 96
5.11 Interval Plot for the Chemical Resistance Scores. 98
5.12 Boxplot graph for Electrostatic Adhesion (ES matrix). 99
5.13 Interval Plot regarding Condition after First Sanding. 100
5.14 Interval Plot of Chemical Resistance Scores (NT Matrix). 101
5.15 Radar chart evaluating PD family mean performance across the variables. 102
5.16 Comparative performance envelope showcasing the operational footprint of the ES and NT matrices and the incremental shifts of the nanocomposite formulations. 103

A.2 Weight Intervals of the AHP Process. 120
A.1 Principal eigen value = 7.240; Eigenvector solution: 5 iterations, delta = 8.6E-8. . 121

B.1 Data for V_1, PD family. 122
B.2 Data for PD family, V_3 and V_6. 123
B.3 Residual Analysis V_7, PD family. 123
B.4 Data for PD family, Efficiency. 123
B.5 Data for ES family, V_3 and V_6. 124
B.6 Data for ES family, Efficiency. 124
B.7 Data for NT family, V_3 and V_7. 124
B.8 Data for NT family, Efficiency. 125

List of Tables

2.1 Visual Acceptance Matrix for Final Coating Inspection. 17
2.2 Nave 3 Pre-Coating Inspection Metrics: 2025 Baseline. 22
2.3 Nave 3 Pre-Coating Inspection Metrics: 2026 Post-Transition Period. 22
2.4 Nave 4 Final Coating Inspection Metrics: 2025 Baseline. 24
2.5 Nave 4 Final Coating Inspection Metrics: 2026 Post-Transition Period. 26

4.1 Evaluation metrics, assigned weights, and impact levels for the Weighted Decision Matrix. 53
4.2 Translation matrix of ISO 2409 adhesion classes into the custom quantitative scoring system. 55
4.3 Experimental Protocol: Factors and levels of the Screening Phase. 57
4.4 Nomenclature and technical specifications of the base putty matrices utilized in the study. 58
4.5 Target volumetric concentrations and primary functional rationale for matrix integration. 59
4.6 Phase 2 Experimental Design: Rigorous DoE parameters for the top 3 screening candidates. 63
4.7 Initial Experimental Design (DoE) factors and categorical levels. 67
4.8 Comparative Thermal Outgassing Analysis: Baseline vs. 1K Primer Variation. . . 69

5.1 Baseline Screening Results for Unmodified Putty Formulations (-0). 76
5.2 Thickness Results for Unmodified Putty Formulations (-0). 78
5.3 Comparative Screening Results: 2K Primer M vs. 2K Primer R. 79
5.4 Decisive Tie-Breaking Metrics: V_6 Score and Final Efficacy. 79
5.5 hermal Performance of Epoxy Control Group. 81
5.6 Comparative Analysis: Unprimed Baselines (-0) vs. 2K Primer R (-2R) on Polyester Matrices. 82
5.7 Comparative Analysis: Unprimed Baselines (-0) vs. 2K Primer R (-2R) on Epoxy Matrices 84
5.8 Baseline Screening Results for Modified Putty Formulations (-0). 88
5.9 Baseline Screening Results for Modified Putty Formulations (-2R). 90
5.10 Final Stage-Gate Screening Scores for the Selected DoE Candidates. 92
5.11 Descriptive statistics for Electrostatic Adhesion (V_6) of the NT formulas. 102
5.12 Final operational capability, statistical significance, and global efficiency profiles. 104

A.1 Qualitative evaluation scale for variable V_1. 117
A.2 Qualitative evaluation scale for variable V_2. 118

A.3 Qualitative evaluation scale for variable V_3. Porosity counts were evaluated strictly within a standardized localized zone of approximately 5–7 cm × 2–3 cm directly over the primary weld. . . . 118
A.4 Qualitative evaluation scale for variable V_4. Porosity counts were evaluated strictly within a standardized localized zone of approximately 5–7 cm × 2–3 cm directly over the primary weld. . . . 118
A.5 Qualitative evaluation scale for variable V_5. . . . 119
A.6 Qualitative evaluation scale for variable V_7. Porosity counts were evaluated strictly within a standardized localized zone of approximately 5–7 cm × 2–3 cm directly over the primary weld. . . . 119
A.7 AHP Pairwise Comparison Relations. . . . 120
A.8 Priorities and Weight Intervals. . . . 120
A.9 Mapping matrix of sample group identifiers to their corresponding chemical formulations and replicate distributions. . . . 121

B.1 Thickness Measurements: Primer Head-2-Head. . . . 122

List of Acronyms

AHP Analytical Hierarchy Process
ANOVA Analysis of Variance
COPQ Cost of Poor Quality
CR Consistency Ratio
CS Chain Stay
DMA Dynamic Mechanical Analysis
DoE Design of Experiments
DSC Differential Scanning Calorimetry
DT Down Tube
ERP Enterprise Resource Planning
FT Front Triangle
FTY First Time Yield
HT Head Tube
KPIs Key Performance Indicators
NOK Not OK
RCA Root-Cause Analysis
R&D Research and Development
RT Rear Triangle
SDG Sustainable Development Goals
SPC Statistical Process Control
SS Seat Stay
ST Seat Tube
TGA Thermogravimetric Analysis
TRL Technology Readiness Level
TT Top Tube
UV Ultra-Violet
VOC Volatile Organic Compounds

Chapter 1

Introduction

This chapter establishes the foundational framework for the research, delineating the scope and strategic significance of the dissertation. It begins by defining the Industrial Context and Motivation (1.1), highlighting the structural manufacturing shifts and volume demands within the European e-bike sector. This is followed by the Problem Statement (1.2), which diagnoses the specific operational inefficiencies—namely the dual-matrix finishing bottleneck—that necessitate this engineering intervention. Subsequently, the Research Objectives and Hypotheses (1.3 and 1.4) are articulated to define the boundaries of the scientific inquiry, alongside a brief overview of the sequential, two-phase Methodology (1.5) employed to empirically validate the proposed solutions. The chapter then formally establishes the Structure of the Dissertation (1.6), providing a cohesive narrative roadmap of the document's overall organization. Finally, it concludes with the project's Alignment with Sustainable Development Goals (1.7).

1.1 Context and Motivation

The manufacturing operations analyzed in this dissertation take place at Triangle's - Cycling Equipments S.A., a leading manufacturer specialized in high-performance bicycle and e-bike frames. The rapid expansion of the European electrical bicycle (e-bike) sector has placed unprecedented volume and quality demands on localized manufacturing facilities. As production scales to meet market needs, industrial finishing lines are forced to balance high-throughput targets with increasingly strict aesthetic standards. In the premium mobility segment, consumers demand a seamless, "carbon-look" aesthetic, which strictly dictates the complete concealment of all structural aluminum weld joints prior to surface finishing.

To achieve this continuous surface topography, manufacturers must apply polymeric leveling putties over the weld beads. However, introducing these manual leveling processes into a high-volume industrial environment creates a manufacturing conflict. Modern frame finishing relies on electrostatic powder coating, a process that inherently mandates a thermal curing cycle of temperatures surrounding 180°C. Adding to that, central to this finishing sequence is the chemical passivation line—a continuous, automated process utilizing acidic baths to decontaminate the

aluminum substrate and establish a conversion layer, before the painting process. This layer is essential for corrosion resistance and serves as the primary molecular anchor for polymer coatings. However, as this thesis will demonstrate, this chemical preparation step introduces significant structural challenges when interacting with the leveling putties currently utilized on the shop floor.

The primary motivation for this dissertation stems from the systemic operational failures occurring at this exact intersection of aesthetics and thermodynamics. Standard polymeric formulations are fundamentally incompatible with the thermal and chemical requirements of the powder coating line. When subjected to the curing ovens, inadequate putties suffer from outgassing, porosity, and structural degradation, directly resulting in spikes in the Cost of Poor Quality (COPQ) and continuous cycle-time disruptions. Therefore, there is an urgent industrial mandate to engineer a thermomechanically stabilized matrix capable of surviving the finishing line without throttling global factory throughput.

1.2 Problem Statement

Currently, the manufacturing facility operates parallel finishing lines: a high-demand liquid coating process with extended cycle times, and an electrostatic powder coating process with rapid cycle times. To accommodate the distinct thermodynamic requirements of these two lines, the factory is forced to utilize a fragmented, two-putty system. A polyester-based matrix is applied for liquid coating, while an epoxy-based matrix is utilized for powder coating.

This dual-system architecture creates considerate operational inefficiencies. The polyester matrix cannot be universally applied because it lacks the structural integrity to withstand the high-temperature (180°C) curing ovens of the powder line, where it suffers from outgassing and porosity. Conversely, deploying the epoxy matrix universally creates a significant production bottleneck in the liquid line; it requires an one-hour thermal curing cycle in an industrial oven (leading to energy expenditure) and presents significant ergonomic challenges during manual application.

When a putty formulation fails to maintain its structural integrity or electrostatic adhesion after exiting the curing oven, it triggers a continuous cycle of unaccounted extensive rework. This hidden rework impacts line efficiency, particularly during high-demand scenarios or periods of limited workforce availability. The required rework drastically decreases the First Time Yield (FTY) and consumes labor hours that could otherwise be allocated to processing multiple new frames. Furthermore, maintaining two disparate chemical systems introduces high process variability, increasing the likelihood of operator application errors on the shop floor, expanding material expenditures, and compounding supply-chain dependencies.

The operational failures of these leveling matrices are governed by a strict chemical relationship between thermal stability and process agility. Polyester formulations cure rapidly but fundamentally lack the cross-linked thermal stability necessary to prevent volatile expansion and surface degradation in a 180°C environment. In contrast, epoxy formulations provide the requisite thermodynamic resistance but lack the rapid polymerization kinetics required to maintain continuous

manufacturing flow. Consequently, an industrial trade-off emerges: the existing formulations cannot simultaneously satisfy the thermal requirements of electrostatic deposition and the temporal constraints of a high-throughput factory.

The existing commercial market and current scientific literature fail to offer a multifunctional, "universal" putty capable of resolving these competing variables. There remains a critical industrial gap regarding the development of a single leveling matrix that survives demanding outgassing parameters without disrupting manufacturing throughput. Consequently, a systematic engineering intervention is required to rigorously screen existing commercial baselines and, if necessary, develop a structurally adequate nanocomposite to bridge this gap.

1.3 Objectives and Scope

The primary macro-level objective of this dissertation is to develop and empirically validate a Technology Readiness Level (TRL) 4 prototype for a single, universal leveling putty, designed to replace the inefficient dual-matrix system. This optimized formulation targets the facilitation of ergonomic application and mechanical sanding, the elimination of temperature-induced downstream rework, and the increase of global process productivity across the manufacturing line.

To systematically investigate and validate a universal solution prototype through three distinct engineering pathways:

- **Process Diagnostic:** To comprehensively map the current factory layout and establish a rigorous diagnostic of the surface finishing operations, isolating the exact mechanisms of thermomechanical failure and identifying key areas for process improvement.

- **Methodological Framework:** To define and implement an objective, mathematically weighted evaluation matrix capable of empirically ranking competing leveling systems against the factory's rigid thermal, chemical, and temporal constraints.

- **Tripartite Solution Exploration:** To systematically investigate and implement a universal solution through three distinct engineering pathways:

    1. *Market Benchmarking:* Conducting a rigorous screening of existing commercial formulations to determine if an off-the-shelf matrix can satisfy the factory's process requirements.
    2. *Process Optimization:* Investigating the integration of intermediate inter-layers (e.g., 2K liquid primers) to artificially mitigate adhesion and porosity failures within the current production line.
    3. *Research and Development (R&D):* Synthesize a novel, custom formulation via the targeted doping of a baseline matrix with additives, effectively altering its fundamental thermodynamic and electrostatic properties to survive the manufacturing environment.

1.4 Scientific Contribution and Research Hypotheses

This research bridges the gap between materials engineering and industrial process engineering by systematically diagnosing the dual-matrix bottleneck and establishing the validated technical blueprint for its resolution. The investigation is guided by two primary hypotheses:

Hypothesis 1: As detailed in subsequent chapters, the current standard putties suffer from chemical degradation in the acidic passivation baths and act as electrical insulators, causing Faraday cage effects during electrostatic powder coating. It is hypothesized that process-level adjustments—specifically the application of an intermediate two-component (2k) liquid primer—will successfully mitigate chemical degradation during acidic passivation and artificially resolve electrostatic adhesion failures at the putty interface. However, the ultimate viability of this solution is hypothesized to be fundamentally limited by intrinsic thermodynamic incompatibilities. Beyond merely withstanding the vapor pressure generated by the underlying putty matrix, the 2K primer itself is subjected to the 180°C powder-coating curing cycle.The primer's own cross-linking kinetics and volatile retention may prove thermodynamically unstable at these peak temperatures, inducing autonomous outgassing that negate any mechanical FTY improvements. Operationally, the mandatory application and intermediate curing of this wet inter-layer inherently introduces an additional manufacturing step. Therefore, even if the primer successfully contains the thermal outgassing, it is hypothesized that the resulting cycle-time penalty will fail to satisfy the macro-objective of streamlining global factory throughput.

Hypothesis 2: It is hypothesized that if a baseline thermosetting matrix is structurally modified via the targeted doping of aluminum oxide (Al_2O_3) and graphene nanoplatelets, the resulting composite will systematically alter the material's thermal transport and electrical characteristics. Under this framework, the integration of alumina is evaluated for its role in enhancing bulk thermal resistance, providing a baseline of dimensional stability. Concurrently, graphene is integrated to establish an electrically conductive percolation network for electrostatic powder deposition while independently contributing to the matrix's thermal dissipation. While graphene and alumina both influence thermal properties, they are utilized here for complementary effects: alumina provides high-volume bulk thermal stability, whereas graphene enables localized electrical percolation and rapid interfacial heat dissipation. If this dual-nanomaterial network successfully facilitates rapid internal heat dissipation and prevents localized thermal accumulation, it is hypothesized that thermal outgassing will be suppressed during the downstream curing cycle without extending the baseline polymerization cycle times. In the epoxy matrices, it is hypothesized that the targeted integration of graphene will establish a semi-conductive percolation network, directly resolving the matrix's inherent electrical insulation and stabilizing electrostatic powder adhesion. Consequently, the verification of these material interactions is evaluated based on its capacity to improve the global FTY and reduce the COPQ on the assembly line.

1.5 Methodology Overview

To scientifically validate the proposed hypotheses, this research employs a sequential, two-phase engineering methodology designed to efficiently allocate experimental resources. The initial phase consists of a broad industrial screening of existing commercial leveling matrices, the application of intermediate 2K liquid primers, and preliminary additive integrations. These systems are evaluated utilizing a strict stage-gate method that incorporates the Analytical Hierarchy Process (AHP) decision matrix. This mathematical framework filters and ranks the formulations based on their ability to satisfy the factory's non-negotiable thermal, chemical, and temporal variables.

Following this broad screening, the second phase deliberately narrows the focus exclusively to the top three highest-scoring formulations. To ensure proper scientific rigor and obtain a definitive empirical result, these three winning matrices undergo targeted experimental synthesis. The objective of this phase is not exhaustive parametric optimization, but rather the highly rigorous, definitive validation of whether these top-tier composites can physically resolve the thermomechanical and FTY failures on the production line.

1.6 Structure of the Dissertation

This dissertation is logically organized into six chapters to reflect the progression from industrial problem identification to experimental resolution. Chapter 1 establishes the industrial context, defines the operational reality, and outlines the research objectives, hypotheses, and sustainability alignment. Building upon this foundation, Chapter 2 provides a detailed current state analysis by mapping the factory's macro production flow and diagnosing the specific mechanisms behind the coating failures and undocumented rework loops. Chapter 3 then explores the fundamental materials science of polymeric matrices, thermal degradation mechanisms, and the role of nanomaterial fillers through a comprehensive literature review. Subsequently, Chapter 4 details the methodology and experimental work, explicitly defining the physical testing parameters, the logistical implementation of the stage-gate screening approach, and the consolidation of the final protocol for in-house additive doping. Chapter 5 presents the results and discussion, rigorously analyzing the empirical data from the initial screening and the sequent second stage, alongside a sensitivity analysis. Finally, Chapter 6 synthesizes the conclusions, evaluating project outcomes and reflecting on the broader impact of the work, finally identifying opportunities for continuous improvement in Future Works.

1.7 Sustainability Impact and SDG Alignment

This research supports sustainable manufacturing by improving the efficiency and robustness of bicycle frame surface finishing. By developing a universal thermosetting putty that minimizes rework and reduces energy consumption from repeated curing cycles, the project promotes resource-efficient production and strengthens European manufacturing competitiveness.

The work aligns with three key Sustainable Development Goals (SDG). Regarding SDG 8 (Decent Work and Economic Growth), process optimization increases manufacturing productivity, thereby improving cycle times and labour efficiency. In alignment with SDG 9 (Industry, Innovation and Infrastructure), this research delivers an innovative thermosetting nanocomposite validated through successful industrial trials and applied R&D, contributing directly to process capability and innovation adoption. Finally, the project supports SDG 12 (Responsible Consumption and Production) by enabling more efficient raw material use and improved chemical management. These advancements reduce industrial waste, scrap rates, and rework loops, ultimately lowering the COPQ and ensuring higher FTY when it reaches eventually a TRL of 8 or 9.

Chapter 2

Current State Analysis

Before proposing any chemical or procedural optimization, it is imperative to thoroughly map and understand the existing production environment. The purpose of this chapter is to establish the baseline reality of the factory's surface preparation and painting operations (the "As-Is" state).

This analysis will dissect the complete process flow of the aluminum bicycle frames, focusing afterwards from the stage of the initial putty application stations through the final curing ovens. By examining the distinct technological parameters of both the liquid and powder coating lines, and tracking the specific routing of varying frame models (Models A, B, and C), a clear picture of the thermodynamic and logistical constraints will emerge.

Furthermore, this chapter will identify current systemic bottlenecks, gaps in quality control infrastructure, and the specific failure modes that currently plague the production line.

2.1 Macro Production Flow

The manufacturing process at Triangle's relies on the transformation of the 6061 aluminum alloy (AA 6061), acquired in various geometries (lengths, thicknesses, and diameters), alongside auxiliary raw materials necessary to guide the bicycle frame from initial stock to a fully welded, painted product tailored to client specifications.

Before analyzing the production line, it is essential to establish the structural anatomy of the bicycle frames, as these distinct geometric zones later dictate the rigor of the quality inspection criteria.

A standard bicycle frame is fundamentally composed of two main structures: the Front Triangle (FT) and the Rear Triangle (RT), compromised by the different tubes as seen in Figure 2.1.

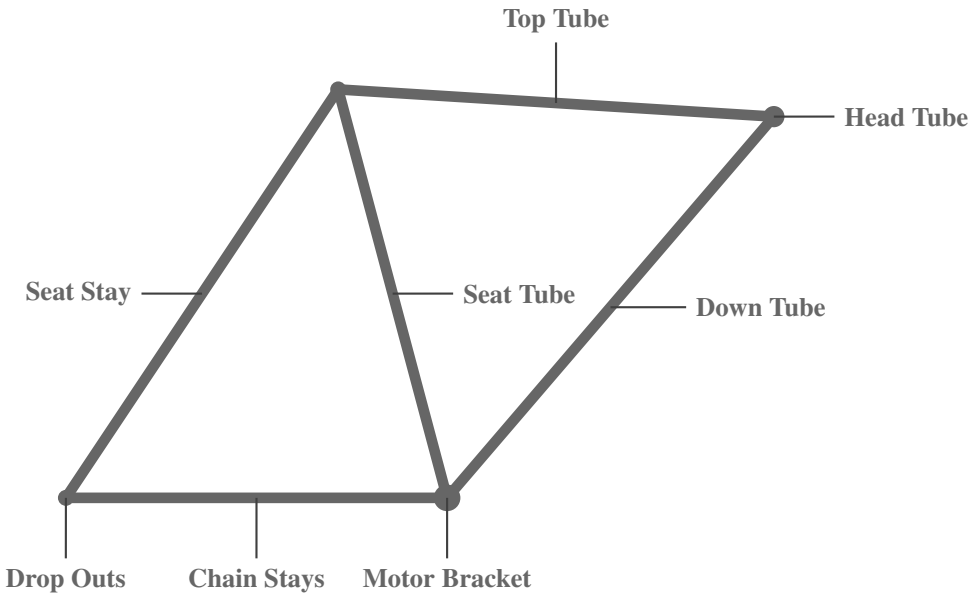

Figure 2.1: Primary anatomical nomenclature of a standard bicycle frame.

While this represents the standard skeletal framework, frame geometries vary significantly based on the model. For instance, step-through models often lack a Top Tube (TT), while frames designed for particular environments (such as e-mountain bikes) feature more robust configurations to support heavier dynamic loads. Furthermore, not all models are manufactured entirely in-house. Depending on complex geometric requirements (such as specific hydroformed tubes whose production scale is currently outsourced) or specific mechanical joints (e.g., coupling mechanisms rather than welded connections between the FT and RT), certain components are imported and integrated into the line.

To manage this complex assembly, the factory is organized into specialized pavilions that execute a macro production flow comprising four primary stages.

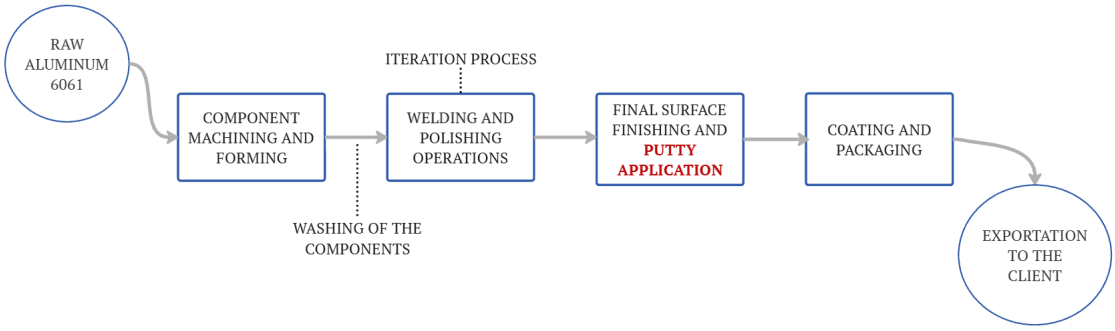

Figure 2.2: Macro Production Flow of the Factory.

1. Component Machining and Forming

The process begins with the mechanical transformation of the raw AAl 6061 stock. Tubes are cut, deformed, and shaped to their precise dimensional tolerances utilizing Computer Numerical

Control machining, laser cutting, and mechanical presses. Prior to advancing to the next stage, these individual components undergo a mandatory washing cycle in a dedicated tank to remove machining residues, oils, and particulate matter that could critically compromise subsequent welding operations.

2. Welding and Polishing operations

This stage involves the structural assembly of the machined tubes through a highly interweaved sequence of robotic and manual operations. Different robotic welding cells are programmed with specific, highly optimized trajectories to handle distinct frame junctions (e.g., a cell programmed to weld the Head Tube (HT)/TT junction cannot inherently weld the Seat Tube (ST)/Seat Stay (SS) junction). Manual welding is strictly deployed to correct defects that the robotic arms cannot resolve or to access complex geometries constrained by the robot's kinematics. Following welding, the frames undergo robotic and manual polishing. Notably, this phase operates iteratively rather than linearly; a frame may undergo welding, proceed to polishing, and return to welding to complete specific structural passes. It is at the conclusion of this stage that the physical "body" of the bicycle is fully formed.

3. Final Surface Finishing and Putty Application

Once the structural assembly is complete, the frames enter the crucial surface finishing phase which is called Nave 3. This stage includes heat treatments (T4 and T6 ovens) to relieve internal stresses and restore the mechanical properties of the alloy, followed by additional polishing and shot-blasting operations. This stage also houses the continuous passivation line. It is important to note that the passivation line serves a dual purpose throughout the factory: it acts as a general cleaning station for incomplete frames during earlier stages, and later as the critical chemical surface preparation step before painting. Frames are suspended on a continuous overhead conveyor for automated passage through these chemical baths. Specifically regarding the scope of this work, the application of polymeric putty occurs within a dedicated cabin during this stage. Before entering the cabin, frames are polished, passed through the passivation line, and thoroughly dried. The putty is manually applied under two primary operational conditions:

- **Systematic Application**: To conceal weld seams, creating a continuous, "seamless" aesthetic mimicking carbon fiber frames.
- **Sporadic Rework**: To correct localized leveling defects or dents that could not be resolved during the mechanical polishing phases.

Crucially, the specific chemical formulation of the putty (e.g., polyester versus epoxy) is dictated entirely by the subsequent coating technology assigned to that specific frame model.

4. Coating and Packaging

Following putty application, curing, and manual sanding, the frame undergoes a rigorous final surface inspection. Once approved, it is routed through the passivation line one final time

to ensure absolute surface cleanliness. After drying, the frames diverge into two distinct coating lines in Nave 4: liquid painting or electrostatic powder coating. While both lines share similar macro-objectives, they operate under vastly different thermodynamic and chemical parameters. Following a final post-painting inspection, the frames enter the packaging sector, where they undergo one last review and localized touch-ups before being dispatched to the client.

The following sections will dissect the micro-operations of the third and fourth stages—specifically, the pre-putty surface preparation, the application constraints, the final passivation cycle, and the thermodynamic realities of the respective coating lines.

2.2 The Surface Finishing Value Stream

2.2.1 Pre-Application Phase: Chemical Passivation Line

As outlined in section 2.1, prior to entering the putty application booth, the aluminum frames undergo mechanical polishing followed by a mandatory chemical surface treatment. This treatment is executed within a continuous, automated passivation line where the frames are suspended on an overhead conveyor system and routed through a series of enclosed spray tunnels.

As seen in Figure 2.3, the surface preparation protocol consists of six distinct processing stages, supported by an integrated water demineralization plant:

- **Stages 1 & 2: Chemical Degreasing.** The frames are sprayed with a heated aqueous acidic solution (38°C) strictly maintained at a pH < 1. This chemical agent is formulated to strip the substrate of residual machining oils, lubricants, and particulate matter. Crucially, it serves to activate the aluminum surface, establishing the optimal boundary conditions for the subsequent conversion layer.

- **Stage 3: Normal Water Rinse.** An ambient-temperature water rinse removes the chemical residues from the degreasing stage, preventing cross-contamination and unwanted pH shifts in the downstream baths.

- **Stage 4: Demineralized Pre-Rinse.** A continuously recirculated bath of demineralized (DI) water prepares the substrate for chemical conversion. The final spray ramp of this stage draws directly from the demineralization unit.

- **Stage 5: Chemical Passivation (Conversion).** This is the core of the pre-treatment process. The frames are sprayed with an acidic passivating solution diluted in Deionized (DI) water, operating within a highly controlled window of pH 2.8 to 3.5. This conversion agent reacts chemically with the aluminum substrate to synthesize a microscopic, invisible conversion layer. This layer provides temporary corrosion resistance and acts as the primary molecular anchor for the subsequent polymer coatings.

- **Stage 6: Final Demineralized Rinse.** A critical final wash utilizing continuously recirculated Deionized water, terminating with a direct high-purity water spray to remove any unreacted passivation product.

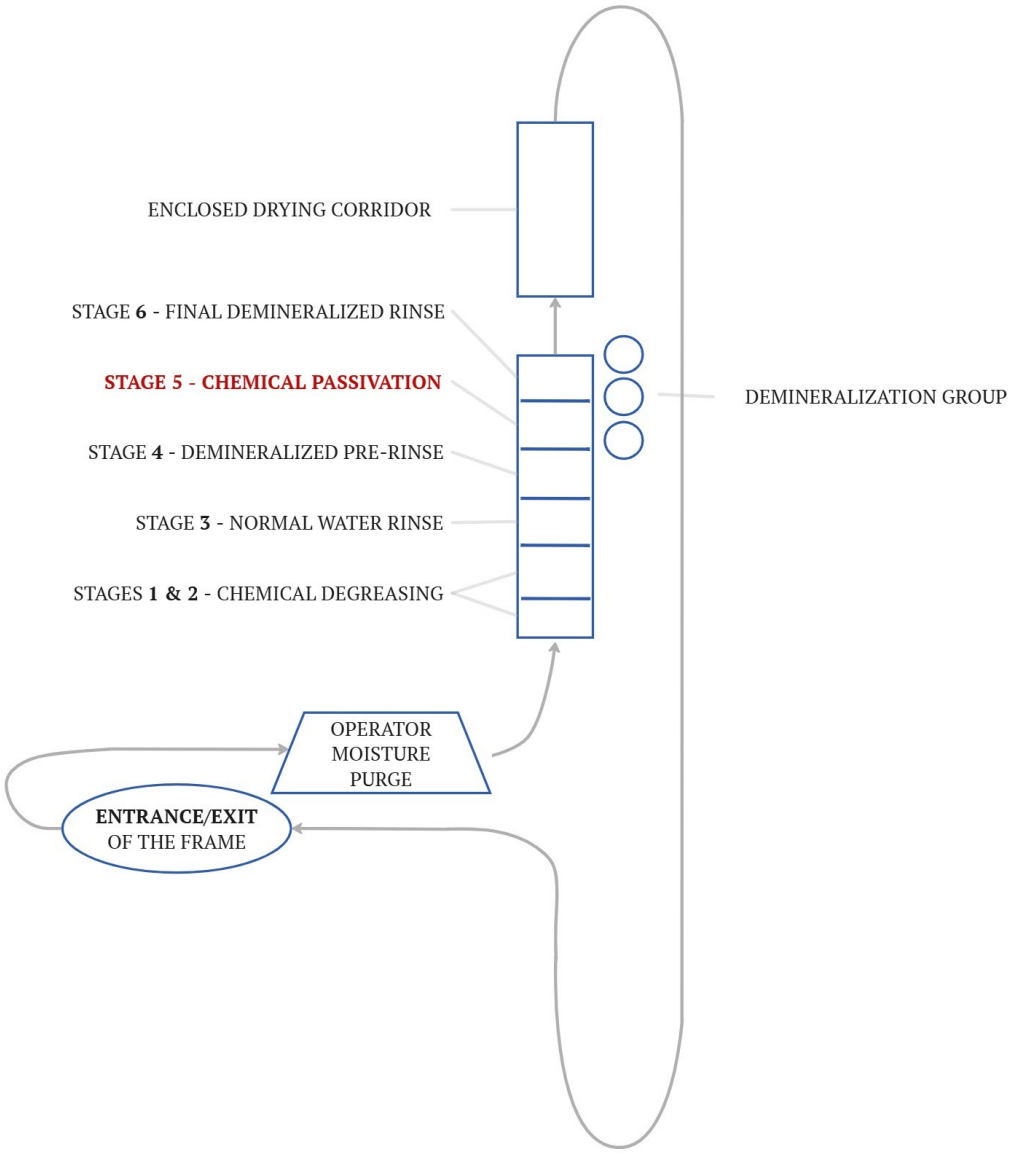

Figure 2.3: Schematic representation of the continuous chemical passivation line and integrated water demineralization group.

Legend: Oval: *Process boundaries (Start/End);* ***Rectangles:*** *Automated processing stages;* ***Trapezoid:*** *Manual operator task;* ***Circles:*** *Water filtration and storage units;* ***Solid Arrows:*** *Direction of conveyor flow.*

To protect the integrity of the highly sensitive passivation layer, the electrical conductivity of the water in Stage 6 must be strictly maintained below 30 µS. Elevated electrical conductivity indicates the presence of dissolved ions (e.g., chlorides, sulfates, calcium, and magnesium). If

these trace minerals are deposited onto the frame and allowed to dry, they react with the conversion layer, creating initiation sites for premature corrosion, osmotic blistering, and catastrophic adhesion failure of the paint system.

Following the final rinse, the conveyor routes the frames through an enclosed drying corridor. Upon exiting the tunnel and returning to the loading station, any residual moisture trapped in the frame's geometry is manually purged by an operator using compressed air. Once fully dry and chemically passivated, the frames are cleared to enter the dedicated application booth, officially initiating the putty application phase.

A key remark is necessary: applying the putty after passivation is nonviable because the manual mechanical sanding required to level the putty would destroy the chemical conversion (passivation) layer on the surrounding substrate, compromising both corrosion resistance and powder paint adhesion. Therefore, the passivation is strictly needed after the putty application.

2.2.2 Core Application Phase: Putty Deposition and Thermal Curing

The application of polymeric putty is a highly specialized manual operation within the surface finishing value stream. While theoretically the majority of aluminum frames should not require geometric correction (the best scenario would be if only the frames that need to have the weld covered had putty applied), practical manufacturing variances—such as irregular weld seams, localized depressions, or excessive material removal by automated polishing robots—necessitate the use of putty. The primary objective of this phase is to establish a mathematically continuous, seamless surface topography prior to the application of the final coating system.

Material Matrices: polyester vs. epoxy The choice of putty formulation is strictly dictated by the thermal demands of the downstream coating process. The factory currently utilizes two distinct chemical streams, alongside a third experimental variant (Figure 2.4).

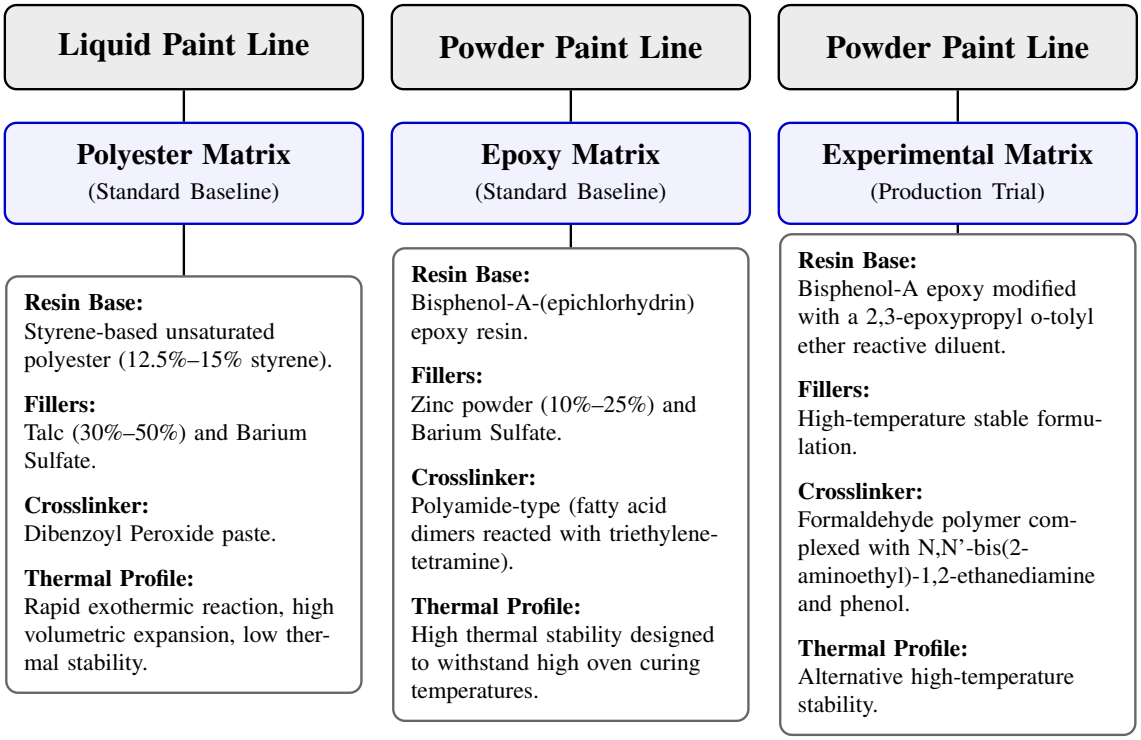

Figure 2.4: Chemical architecture of the three primary polymeric putty matrices utilized on the factory floor.

The Application Protocol and Operator Constraints The compounding of the putty is executed manually by the operators. Using clean spatulas, the base matrix and catalyst are mixed until a uniform color gradient is achieved, confirming a homogeneous distribution of the hardener. The stoichiometric mixing ratios vary significantly by matrix: the polyester system requires a 50:1 ratio (2% Dibenzoyl Peroxide), the epoxy putty requires a 2:1 ratio, and the experimental epoxy system utilizes a 4:1 ratio.

(a) Polyester putty applied to junction of HT, TT and Down Tube (DT).

(b) Epoxy putty applied to junction of HT, TT and DT.

Figure 2.5: The two legacy putties.

The deposition process is highly dependent on operator skill. While operators prefer to over-apply the putty to guarantee sufficient material for subsequent sanding, care is taken since there exists the known risk that thicker localized applications increase the probability of entrapped air (cause of porosity) and uneven curing gradients. Furthermore, improper stoichiometric mixing—specifically, a deficit of catalyst in the epoxy matrix—can lead to significant solvent popping or "bubbling" during the high-temperature oven cycle.

Thermal Curing and The Sanding Cycle The curing kinetics represent one of the most significant cycle-time bottlenecks in the factory. For the polyester matrix, the exothermic crosslinking is rapid; the working window is approximately 3 to 5 minutes, with full hardening allowing for mechanical sanding after just 20 minutes at ambient temperature.

Conversely, the high-temperature epoxy matrices require a longer thermal curing cycle. Batches than can be compromised from 30 to 50 frames approximately are loaded into an industrial oven programmed for a 60-minute cycle (20 minutes of ramp-up heating, 20 minutes at a peak oven temperature of 200°C, and 20 minutes of controlled cooling). It is critical to note that due to thermodynamic heat transfer limitations, the surface of the aluminum frame may not reach the peak 200°C ambient oven temperature.

Once cured, the putty undergoes an iterative, manual sanding protocol. Operators utilize progressively finer abrasives, beginning with a 120-grit and concluding with a 320-grit finish. In geometrically complex zones with tight internal angles, orbital sanding is prohibited due to the risk of cutting into the bare aluminum; these areas must be finished entirely by hand.

Defect Detection and Rework Because the final paint layer amplifies rather than hides substrate imperfections, defect detection is paramount. Operators rely heavily on human sensory feedback—visual inspection for micro-porosities and tactile (touch) feedback to ensure absolute surface continuity between the putty and the native aluminum substrate.

If major geometric deviations or large porosities are detected, the entire application and curing cycle must be repeated. For minor micro-porosities identified on powder-coated frames, a rapid-cure, solvent-borne metallic filler is utilized as an immediate spot-correction countermeasure. Chemically defined as a highly metallized paste containing aluminum powder and elemental zinc dust, this formulation is suspended in a highly volatile solvent blend primarily composed of xylene, Methyl Ethyl Ketone, and toluene. The rapid volatilization of these solvents allows the localized patch to solidify in seconds, effectively sealing the micro-porosity while completely bypassing the need for a secondary 60-minute thermal oven cycle.

Final Quality Inspection and Iterative Rework Following the primary putty application and curing cycles, the frame advances to the final finishing inspection station. At this stage, the substrate is rigorously evaluated against the factory's stringent quality standards to ensure perfect

geometric continuity and the complete absence of surface defects. Because this phase relies heavily on manual craftsmanship, it is inherently highly iterative; localized corrections are frequently necessary before the frame can be cleared for painting.

If superficial porosities or minor topological deviations are detected, operators employ two primary countermeasures: mechanical polishing to physically level the defect, or the application of a highly specialized spot-correction matrix. For the latter, the factory utilizes a solvent-free, Ultra-Violet (UV)-curable mono-compound filler. Rather than relying on thermal crosslinking or solvent volatilization, this advanced matrix is composed of urethane and bisphenol-A epoxy acrylates blended with reactive monomeric diluents, such as isobornyl acrylate and hexanediol diacrylate. The curing mechanism is driven by a specialized photoinitiator—ethyl phenyl(2,4,6-trimethylbenzoyl)phosphinate—which triggers near-instantaneous photopolymerization upon exposure to ultraviolet light. This targeted UV-cure technology allows operators to seal microporosities rapidly without subjecting the frame to an additional thermal oven cycle.

Once the surface topography is certified as structurally and visually flawless, the frame is routed back through the chemical passivation line for a final decontamination and conversion cycle. Only after being thoroughly passivated and dried is the frame officially released to the painting facility, thereby concluding the surface finishing value stream.

2.2.3 The Coating Phase

Following the complete mechanical leveling of the frame and its chemical passivation, the substrate enters the final stage of the surface finishing value stream: the coating phase. This phase serves a dual purpose, providing both the ultimate aesthetic finish required by the client and the critical environmental barrier against corrosion and UV degradation. To accommodate varying mechanical and aesthetic specifications, the factory operates two distinct, parallel coating facilities: a solvent-borne liquid paint line and an electrostatic powder paint line. The routing of a frame through either stream dictates profoundly different thermal cycles, process times, and chemical interactions with the underlying putty matrix.

2.2.3.1 Liquid Paint Line

The liquid paint application operates as an independent facility, frequently described as a "factory within a factory". Due to the high sensitivity of the coating process to dust and airborne particulates, the painting line is physically isolated from the remaining machining and surface finishing operations to mitigate the risk of cross-contamination. This is a continuous and highly iterative process, characterized by rigorous controls of viscosity, surface roughness, and thermo-hygrometric monitoring, since the volatilization rates of the solvents (thinners) fluctuate significantly with ambient temperature variations (particularly during the summer months).

The Sequential Application Protocol The liquid painting process follows a strictly phased value stream, dictated by evaporation kinetics (flash-off) and thermal curing times.

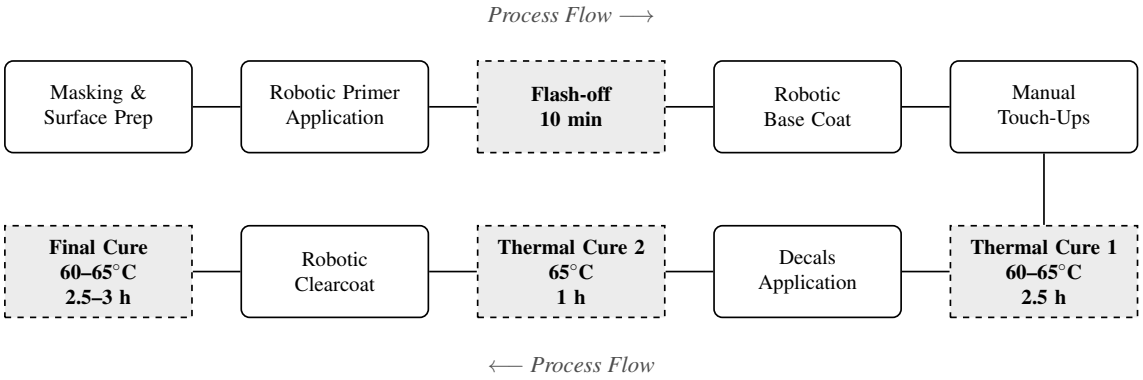

Figure 2.6: Sequential phases and thermal parameters of the liquid painting value stream.

The operational specifics of each stage of Figure 2.6 include:

1. **Masking and Surface Preparation:** Protective masking is applied to the CNC (Computer Numerical Control)-machined holes and threads. The substrate undergoes manual degreasing to eliminate residual moisture and passivation contaminants. Precise geometric positioning on the overhead conveyor (e.g., aligning the seat tube parallel to the hanger) is strictly maintained to ensure the kinematic accuracy of subsequent robotic applications.

2. **Primer and Base Coat Deposition:** The primer acts as a foundational seal for the substrate. The catalyzed pigmented paint is applied via a hydraulic robot, whose kinematic trajectories and color formulations are rigidly governed by a Programmable Logic Controller (PLC) utilizing model-specific identification codes.

3. **Manual Touch-Ups:** Prior to the primary thermal curing, operators manually intervene to cover geometrical "shadows" and complex internal angles that are naturally inaccessible to the standard robotic trajectories, ensuring uniform coverage.

4. **Decals and Clearcoat Application:** Following a preliminary quality inspection, water-based decals are applied to the substrate. An independent robotic system subsequently deposits the final protective clearcoat, programmed for either a specific matte or gloss finish, preparing the frame for the final thermal cycle.

Interaction with the polyester Putty Matrix The painting phase does not conceal topographical defects; conversely, the paint film acts as a visual amplifier of substrate imperfections. The interface between the areas leveled with polyester putty and the liquid paint presents significant chemical and mechanical challenges. Notably, the aqueous passivation line is engineered exclusively for bare aluminum alloys; the high-pressure spray in the initial stages frequently degrades the applied putty patches.

Additionally, excessively thick putty applications tend to entrap solvents within the matrix. During the extended 60°C oven cycles, these entrapped solvents undergo thermal expansion, inducing topographical micro-blistering and porosity. When the primer is applied over these micro-porosities, "sinkage" occurs (the paint collapsing into the void), necessitating the rejection of the frame and its return to the putty application phase.

Quality Control Criteria and Process Bottlenecks Due to the high susceptibility to putty- or polishing-induced defects, the final inspection station employs a rigorous visual acceptance matrix, detailed in Table 2.1.

Table 2.1: Visual Acceptance Matrix for Final Coating Inspection.

Zone	Visibility	Anatomical Frame Regions	Acceptance Criteria
A	Critical	HT, upper and lateral faces of the DT, TT, and motor bracket.	Zero tolerance for visible defects.
B	Medium	Lateral faces of the ST; outer and upper faces of the Chain Stay (CS), SS, and dropouts.	Defects perceptible from a distance of 50 cm mandate immediate rework.
C	Low	Inferior and inner faces of the frame geometry.	Maximum of three micro-defects (diameter < 5 mm) accepted.

The stringency of these criteria, compounded by the extended oven cycle times, dictates the overall factory throughput time. While standard monochromatic models require approximately 1.5 days to process, complex configurations demanding re-masking for a secondary color or dual-suspension geometries extend the value stream cycle up to 3 days.

Furthermore, the coating facility operates under strict time contingencies. Because it is the final major manufacturing phase prior to assembly and shipping, any upstream delays—whether in welding, machining, or the iterative putty application cycle—directly compress the schedule for the painting department. Consequently, the coating line is frequently forced to operate under forced time constraints, eliminating any buffer capacity to absorb the extended rework loops caused by putty-induced porosity or sinkage.

2.2.3.2 Powder Paint Line

In contrast to the solvent-borne liquid line, the powder coating facility utilizes a dry electrostatic deposition method to achieve the final aesthetic finish. This process applies a dry, free-flowing, thermoset polymer powder that offers superior mechanical resistance to physical impacts, albeit presenting a higher chemical sensitivity to surface contaminants such as greases and outgassing phenomena.

Electrostatic Application and Topological Challenges During application, the powder particles are imparted with a negative electrical charge and sprayed toward the grounded aluminum frame. However, this electrostatic mechanism introduces specific topological challenges. The powder naturally gravitates toward the closest grounded surfaces and sharp edges. Consequently, achieving uniform coverage in geometrically complex regions—such as inner angles and tight weld joints—is inherently difficult. The fixed spraying distance of the application guns exacerbates this issue, often resulting in insufficient coating thickness in recessed areas.

(a) (b)

Figure 2.7: Examples of the difficulty in the powder coating deposition.

Furthermore, the putty matrix acts as a thermal and electrical insulator. If the applied putty layer is excessively thick, it locally reduces the electrical conductivity of the substrate. This impedes the electrostatic adhesion of the powder, confirming operators' observations that excessive putty application directly correlates with poor localized paint adherence.

The Sequential Application Protocol While the powder coating line shares the identical visual acceptance matrix (Zones A, B, and C) detailed in Table 2.1, its process flow is distinct. Notably, unlike the liquid line, the powder coating process does not utilize a primer layer. The pigmented powder is deposited directly onto the passivated aluminum and putty substrate, meaning the frame only undergoes two primary thermal cycles. The general value stream follows the stages in Figure 2.8.

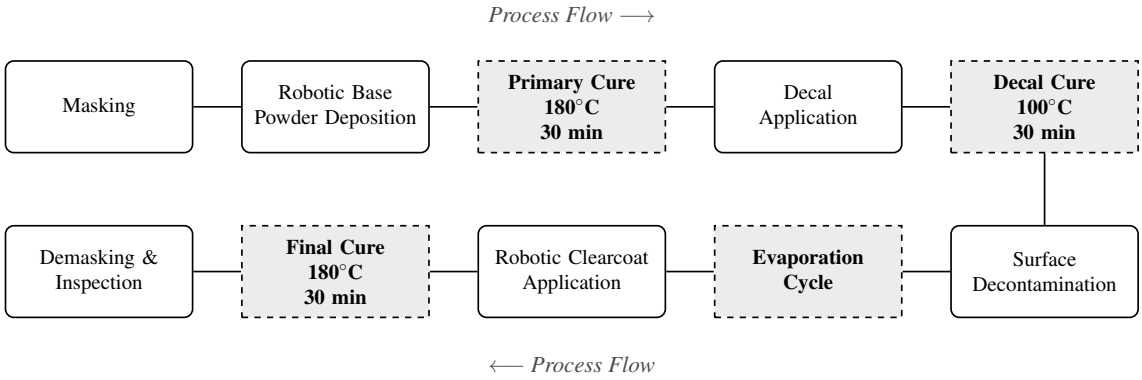

Figure 2.8: Sequential phases and thermal parameters of the powder painting value stream.

The operational constraints of these stages include:

- **Masking Sensitivity:** Because the powder is electrostatically charged, it aggressively permeates and adheres to any improperly sealed crevice. This makes the masking of threads and tolerances significantly more critical and time-consuming than in the liquid process.
- **Thermal Decontamination:** Water-based decals are applied while the frame retains residual heat from the primary cure. This heat can degrade the decal adhesive and leave brown stains, requiring a manual decontamination wash with warm water before the frame enters the evaporation cycle.

Note: There is a specific manufacturing exception regarding the primerless application for one particular frame model, which will be detailed and analyzed in section 2.3.

Thermodynamic Incompatibilities with Putty Matrices The 180°C thermal cycle of the powder line dictates the strict formulation requirements discussed in Section 2.2.2. When standard liquid-line polyester putty is erroneously processed through the powder oven, significant thermodynamic incompatibilities occur. The heat causes rapid volumetric expansion and volatile release (outgassing) of the entrapped air and solvents within the inappropriate matrix, resulting in ruptured blisters, significant sinkage, and complete failure of the coating interface. Even with the correct high-temperature epoxy putty, excessive application thicknesses exponentially increase the risk of these outgassing defects, reinforcing the critical need for geometric precision during the manual sanding phase.

To finalize the process flow, figures 2.9 and 2.10 illustrate the routing logic for puttied frames. The specific classification criteria dictating these routes (Model A, B, and C) are formally defined in Section 2.3.1.

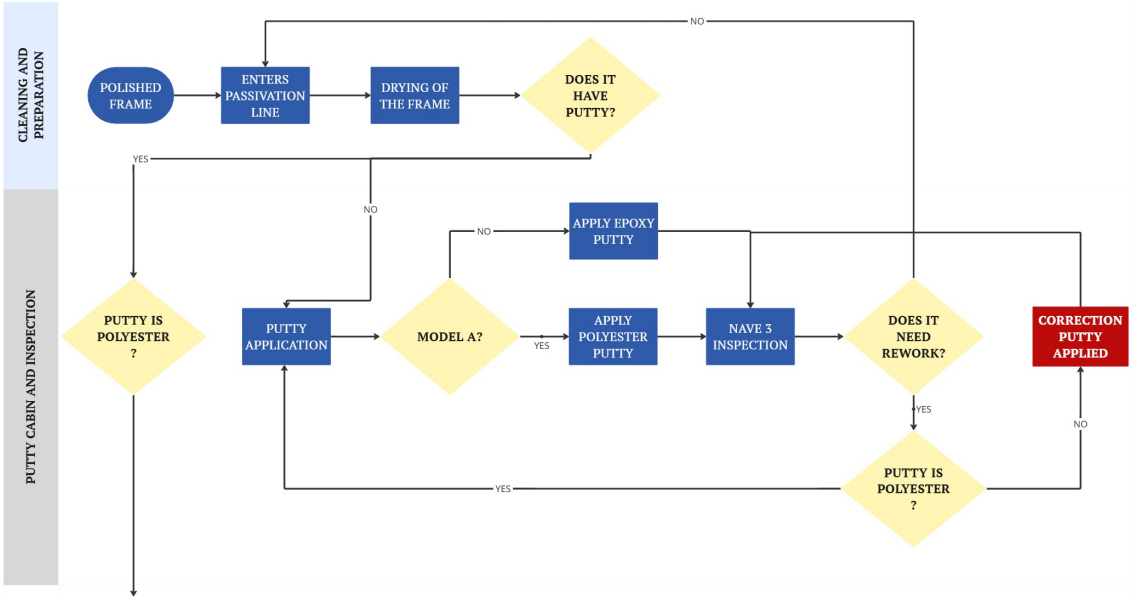

Figure 2.9: Process Flow of E-Bike Frames - Passivation Line and Putty Application. *Legend:* ***Oval:*** *Process boundary (Start);* ***Blue Rectangles:*** *Standard processing and manual application stages;* ***Yellow Diamonds:*** *Decision points and conditional routing;* ***Red Rectangle:*** *Defect correction and rework protocol;* ***Solid Arrows:*** *Direction of process flow.*

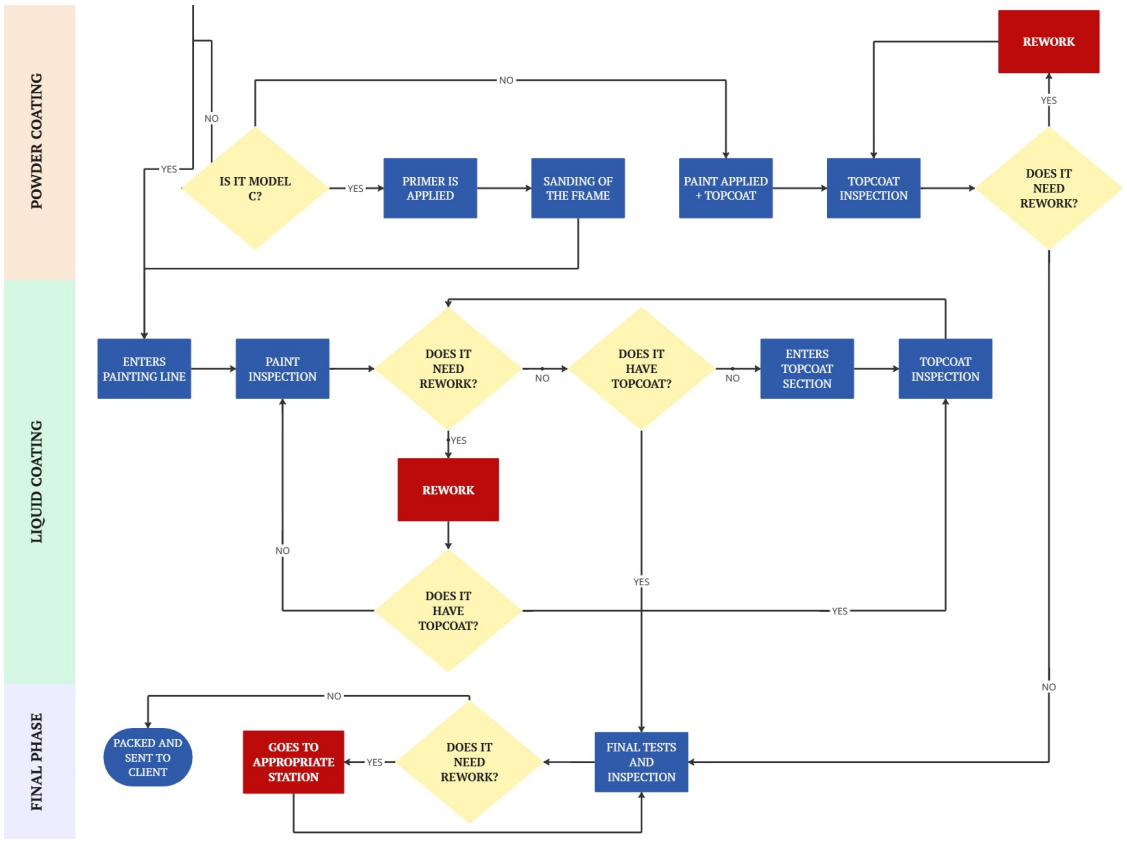

Figure 2.10: Process Flow of E-Bike Frames - Coating Lines and Final Phase.

2.3 Current KPI Analysis and Process Diagnostics

To quantify the inefficiency of the current value stream and formally justify the necessity for a rigorous optimization of the polymeric putty formulations, a detailed extraction of Key Performance Indicators (KPIs) was conducted. The diagnostic strategy was executed sequentially, initially focusing on the preparation phase before pivoting to the final coating phase upon discovering critical data tracking limitations on the factory floor.

2.3.1 Framework and Data Extraction Strategy

The diagnostic study centered on three high-volume aluminum frame models to ensure statistical significance. It is critical to note that for these selected baselines, putty is strictly applied as a localized rework measure to correct surface leveling defects, rather than as a systematic application to conceal structural weld seams. While the facility does produce a specific frame model D that mandates systematic putty application over its welds, a preliminary data review revealed that the historical production volume and subsequent Nave 4 inspection data for this model were insufficient to draw statistically valid conclusions. Therefore, to protect confidential manufacturing data while ensuring a robust sample size, the chosen high-volume models are designated as follows (Figure 2.11).

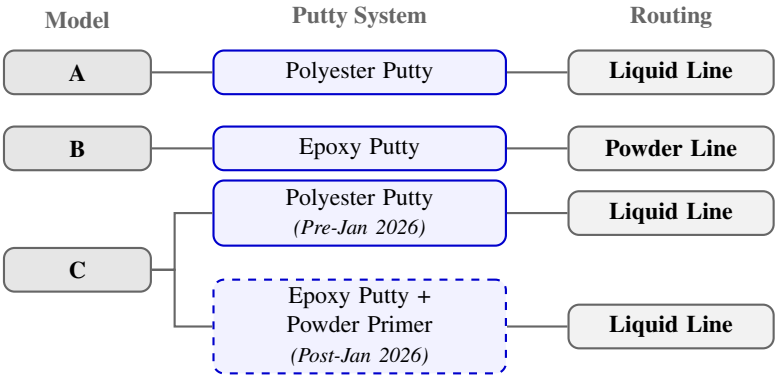

Figure 2.11: Designation of manufacturing sample models, tracking their respective putty matrices and production line routings.

Data collection established two temporal comparison periods: the full calendar year of 2025 (legacy baseline) and the interval from February 1 to March 6, 2026 (post-transition monitoring). January 2026 was excluded to eliminate statistical noise generated by the process-change learning curve.

2.3.2 Phase 1 Investigation: Pre-Coating Preparation

The initial data extraction focused on the inspection station immediately following mechanical sanding. The historical performance of the legacy process during the 2025 baseline is detailed in Table 2.2.

To note that, to preserve the empirical integrity of the manufacturing data captured on Triangle's production line, the evaluation tables utilize the standard shop-floor binary designations OK (Pass) and Not OK (NOK). Within the framework of this quality audit, a designation of NOK directly corresponds to a state of Non Conforming Quality (NCQ). Any formulation or component flagged as NCQ/NOK indicates a structural or dimensional deviation that violates engineering limits, thereby mandating a complete process rejection or downstream rework operation.

Table 2.2: Nave 3 Pre-Coating Inspection Metrics: 2025 Baseline.

Model	Volume Produced	NOK	Porosity Occurrences
Model A	43,826	6,440 (14.69%)	237 (0.54%)
Model B	23,742	5,021 (21.15%)	242 (1.02%)
Model C	6,617	3,264 (49.33%)	451 (6.82%)

Note: All percentages presented in the table above, and the subsequent ones, represent the proportion relative to the total volume produced/inspected for that specific model, rather than a percentage of the total defects.

It is critical to note that the 451 porosity occurrences recorded for Model C represent 13.82% of all defects for that specific model alone, signaling a material or process incompatibility.

The discrepancy in Model C prompted a segregated temporal analysis, which revealed a critical statistical anomaly. Between July 1 and November 1, out of 1,972 units produced, the system recorded zero occurrences of porosity. However, between November 1 and December 31, out of 4,645 units, porosity spiked to 451 occurrences.

A factory-floor investigation revealed that this was a recording hierarchy failure, not a sudden change in chemical performance. When Model C initiated production in July, it suffered from a significant incidence of mechanical polishing marks (constituting 66% of all defects). Because operators prioritized logging this mechanical defect, simultaneous putty porosities were simply ignored in the system. Once the polishing process stabilized in November, operators resumed logging the porosities.

Following that, the KPIs of the 2026 Post-Transition Period were analysed to see if the overall results changed. We can see the results in Table 2.3.

Table 2.3: Nave 3 Pre-Coating Inspection Metrics: 2026 Post-Transition Period.

Model	Volume Produced	NOK (%)	Porosity Occurrences (%)
Model A	3,078	387 (12.57%)	18 (0.58%)
Model B	285	84 (29.47%)	3 (1.05%)
Model C	5,008	1,411 (28.17%)	173 (3.45%)

Diagnostic Conclusion on Nave 3 Data Despite the apparent stabilization observed in the post-transition metrics, this phase of the investigation was ultimately deemed inconclusive for isolating the root cause of polymeric failure. Firstly, factory protocols dictate that defects larger than 1 mm are routed to cold welding, restricting putty application to minor surface corrections. Secondly, inspectors in Nave 3 cannot reliably visually distinguish between air bubbles trapped in the putty mixture and native porosity originating from the aluminum substrate or the weld bead. It was concluded that the values of porosity in the system do not reflect the source of this defect. Therefore, the data in this stage of the process is fundamentally insufficient to quantify the chemical efficacy of the polymers.

2.3.3 Phase 2 Investigation: The "Ghost Rework" Discovery

Beyond the reporting inaccuracies of Nave 3, the factory-floor diagnosis exposed an invisible COPQ regarding the new Model C process. It was observed that applying the powder primer over the epoxy putty frequently triggers outgassing during the 180°C oven cycle. When the frame exits the oven, the primer exhibits numerous crater defects, mandating a rigorous, manual sanding step before it can enter the liquid paint line. This highly iterative step is completely unrecorded by the facility's Enterprise Resource Planning (ERP) system, constituting a "ghost rework" loop that falsely inflates apparent productivity while masking the true cycle time.

Furthermore, a more disruptive manifestation of this hidden factory (work that is being conducted without being recorded) was observed during the qualitative assessment of a separate production line, Model D as mentioned in 2.3.1. Notably, Model D is currently the sole frame design in production that explicitly requires full aesthetic concealment of its structural weld seams. On this line, frames frequently pass the initial inspection in Nave 3 and proceed to the painting department. However, the subsequent application of the liquid primer exposes latent micro-porosities and structural leveling defects that were previously undetectable. As a result, these frames must be physically routed backward from the painting line to the putty cabin for secondary material application and re-sanding before re-entering the paint queue. This reverse routing creates a manufacturing bottleneck and significantly compounds the undocumented COPQ, something that is not accurately captured in the primary defect logs. Consequently, the official FTY metrics are artificially inflated, rendering the primary defect logs unreliable for process optimization.

2.3.4 Phase 3 Validation: The Final Coating Facility

Due to the inconclusive nature of Nave 3 and the discovery of the ghost rework, it was determined that the true thermomechanical impact and interfacial adhesion failures of the putties could only be accurately quantified via the KPIs of the Coating Facility (Nave 4).

The historical performance and defect distribution across the final coating facility prior to any process interventions are summarized in Table 2.4. Zone A refers to the zone previously exposed in Table 2.1.

Table 2.4: Nave 4 Final Coating Inspection Metrics: 2025 Baseline.

Model	Volume Inspected	FTY	NOK	Porosity	Zone A Defects
Model A	11,046	55%	3159 (28,6%)	408 (3.8%)	2,851 (25,8%)
Model B	8,958	72%	2,532 (28.3%)	496 (6.0%)	2,362 (26.4%)
Model C	2,022	39%	1,002 (49.6%)	260 (13.2%)	887 (88.5%)

The following contextual constraints apply to the 2025 baseline:

- **Model A (Polyester):** The presented data isolates complex frame geometries. A highly simplified sub-model was intentionally removed from this dataset as it positively skewed the overall metrics. Furthermore, chemical incompatibilities were observed with metallic paint formulations (e.g., the Metallic Sand finish exhibited an isolated 43.6% rejection rate).

- **Model B (Epoxy):** Represents the standard performance baseline for the electrostatic powder coating line utilizing the high-temperature epoxy matrix.

- **Model C:** The significant reduction of the FTY (39.0%) and the high concentration of defects in Zone A (88.52%) were the direct consequences of routing the thermally unstable polyester putty through the 180°C powder primer oven, which induced significant thermal outgassing.

Methodological Framework for Statistical Analysis Before proceeding with the quantitative Six Sigma evaluation, a critical methodological boundary must be established regarding the structural integrity of the data source. As identified in the diagnostic of Nave 3 (Section 2.3.3), the factory's ERP logging system contains inherent causal attribution limits, most notably the conflation of defect typologies and the pervasive presence of unrecorded 'ghost rework' loops.

Recognizing that these unrecorded loops inherently underreport the true defect rate, executing a pure, absolute Process Capability (Z-score) calculation is statistically constrained. Therefore, the following Statistical Process Control (SPC) and binomial capability analyses are not deployed to definitively diagnose the specific chemical root cause of the putty failure, nor to claim absolute statistical precision of the factory line. Rather, the ERP data is utilized strictly to establish an Optimistic Upper Bound of macroscopic systemic capability.

By mathematically evidencing that the legacy manufacturing process operates fundamentally out of control and is statistically incapable—even when evaluated against this artificially favorable, underreported dataset—the necessity for a foundational chemical redesign is definitively validated. The subsequent isolation and resolution of the putty's specific thermodynamic failure modes are therefore addressed experimentally, entirely independent of the flawed ERP baseline, through the Design of Experiments (DoE) executed in Chapter 4.

Defect Pareto Analysis To quantitatively isolate the primary drivers behind Model C's 39% FTY, a formal Defect Pareto Analysis was executed on the 1,002 recorded NOK instances from the 2025 baseline. While Table 2.4 highlights a concentration of defects in Zone A, the Pareto analysis dissects these occurrences into mutually exclusive root causes.

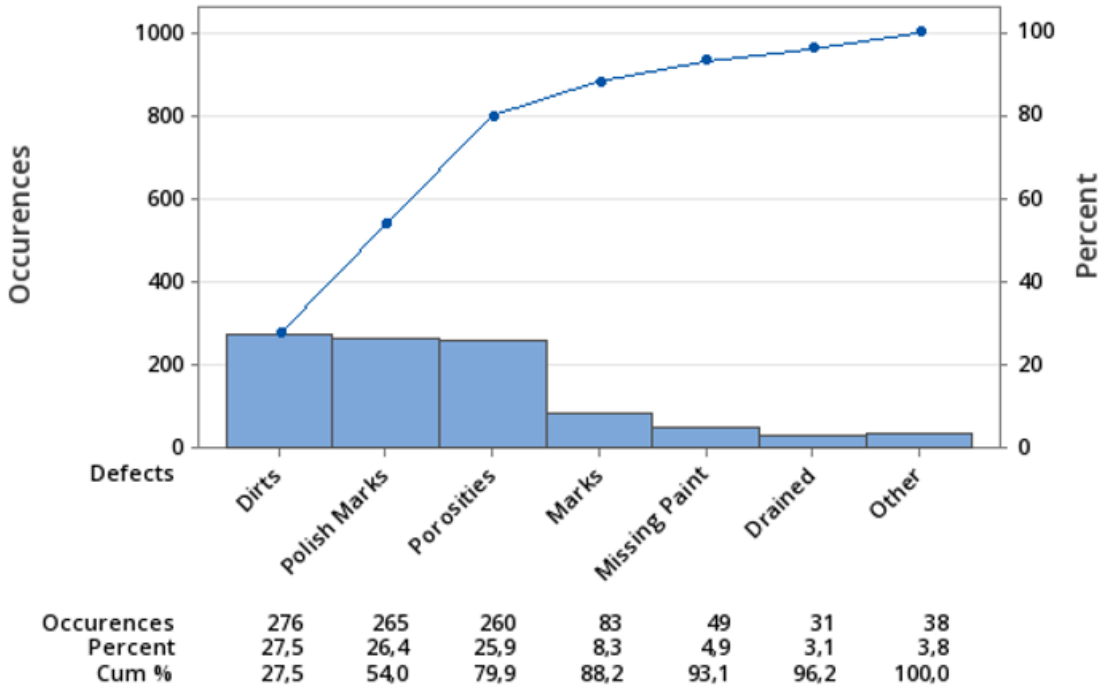

Figure 2.12: Defect Pareto Analysis for Model C (Nave 4, 2025). Source: Minitab.

The data mathematically confirms the Pareto principle, demonstrating that surface contamination (Dirts), mechanical preparation errors (Polish Marks), and thermal outgassing (Porosities) account for 79.9% of all NOK occurrences.

As evidenced by Figure 2.12, the defect distribution strictly adheres to the 80/20 rule (the Pareto principle). The data visually and mathematically proves that the factory's rejection rate is not driven by random, special-cause anomalies (such as handling scratches or missing paint), but rather by systemic, common-cause variations intrinsic to the surface preparation and curing phases. Specifically, the incidence of thermal porosity (accounting for over 25% of all isolated defects) statistically validates the operational necessity for a thermomechanical redesign of the leveling matrix, rather than relying on superficial adjustments to the painting parameters.

Process Stability and Control Limit Analysis Having established thermal outgassing as one of the primary failure modes, it is imperative to evaluate the temporal stability of the surface finishing process. An annual aggregate (such as the 28.6% NOK rate for Model A) is mathematically insufficient to determine if a manufacturing process is stable. To quantify this, the historical inspection data for Model A was chronologically sequenced and subjected to SPC.

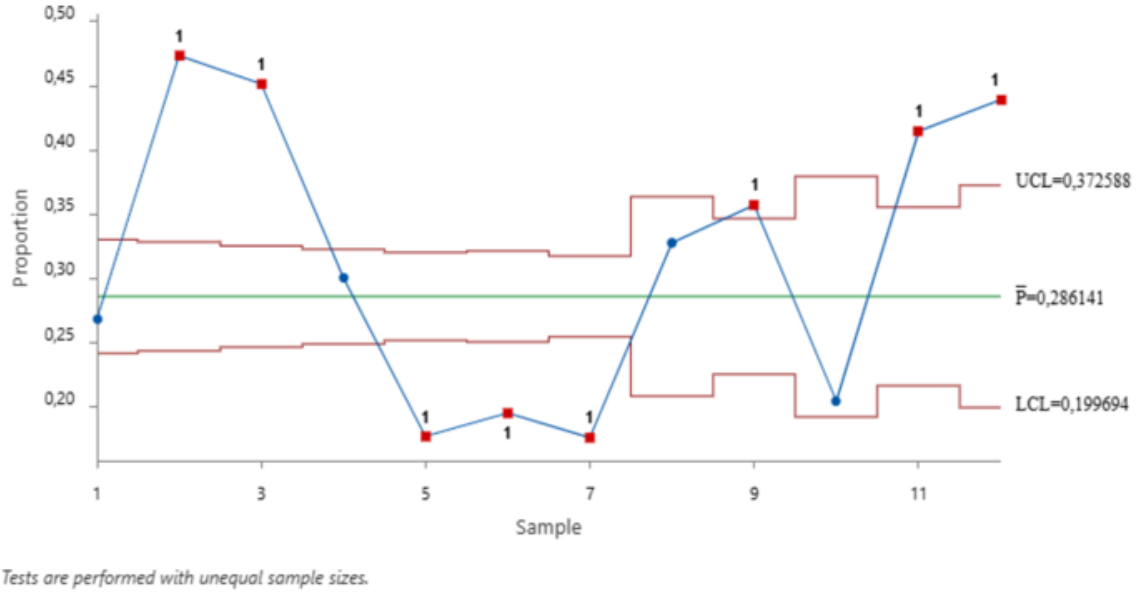

Figure 2.13: SPC P-Chart for the expanded 2025 baseline (Model A). The dots correspond to the NOK values. Source: Minitab.

The central baseline average ($\bar{P}$) rests at 28.6% NOK. Because the monthly inspection volumes vary, the control limits adjust accordingly.

The resulting P-Chart (Figure 2.13) mathematically invalidates the assumption of a stable process during the 2025 calendar year. Rather than a consistent defect rate, the chronological data reveals an erratic system that routinely breached its operational parameters. The NOK spikes observed in Q1 (reaching approximately 45% and 47% in February and March) and Q4 (breaching the Upper Control Limit again in late autumn) prove that the surface finishing process was condition by shifting external variables over the course of the year.

This month-to-month volatility—likely driven by seasonal ambient humidity changes, operator mixing variance, or micro-fluctuations in oven thermodynamics—confirms that the defect generation is a common-cause variation acting upon a fundamentally unstable process. Superficial procedural corrections are mathematically incapable of stabilizing a chemical system with this degree of inherent chronological volatility.

After carefully retrieving the data of the legacy base, the Post-Transition Period was analysed as seen in Table 2.5.

Table 2.5: Nave 4 Final Coating Inspection Metrics: 2026 Post-Transition Period.

Model	Volume Inspected	FTY	Total NOK	Porosity	Zone A Defects
Model A	3,273	62%	891 (27.2%)	134 (5.2%)	663 (20.3%)
Model B	207	65%	73 (35.3%)	6 (2.9%)	72 (34.8%)
Model C	2,278	67%	497 (21.8%)	79 (3.6%)	424 (18.6%)

As in the previous case, the following contextual constraints apply to this time period:

- **Model A:** While the overall FTY showed a marginal improvement to 62%, porosities increased to 5.2%. Furthermore, the instability of the Copper Metallic paint exhibited acute chemical incompatibility, resulting in a 95.8% rejection rate (isolated within a specific batch of 137 frames).
- **Model B:** Demonstrated a drop in FTY to 65% with a NOK rate of 35.3%, although reported porosities decreased to 2.9%.
- **Model C (The Transition Effect):** The shift to the epoxy matrix for the hybrid powder primer routing generated a substantial recovery in Nave 4 metrics. The FTY surged to 67%, and the global NOK rate dropped to 21.8%. Porosity incidence retreated to a manageable 3.6%. Nevertheless, process instability persisted with the Pure White color formulation (78.7% NOK rate across 74 frames).

Process Stability Analysis While the 2025 baseline established the inherent instability of the legacy process, it is critical to evaluate the systemic improvements implemented during the early 2026 Post-Transition period (as detailed in Table 2.5). Most notably, the strategic routing correction for Model C—shifting from the thermally unstable polyester putty to the epoxy matrix prior to the powder primer—yielded a substantial recovery. The overall FTY surged from an initial 39% to 67%, and the recorded incidence of porosity dropped from 13.2% to 3.6%.

However, an average defect reduction does not inherently equate to statistical stability. To determine if the routing correction stabilized the line, the weekly production data for Model C (Feb 1 - Mar 6, 2026) was subjected to SPC analysis.

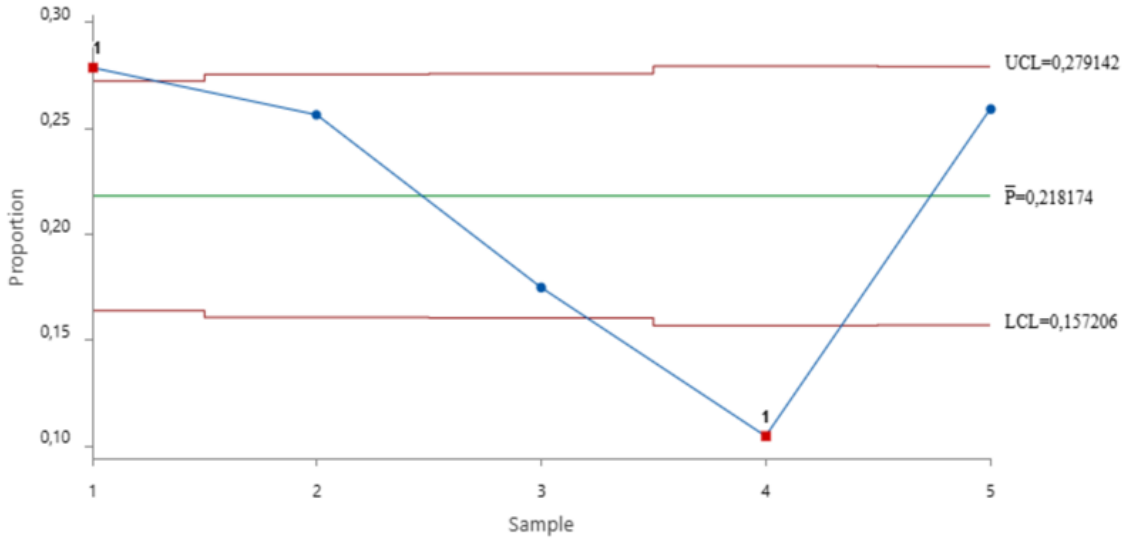

Figure 2.14: SPC P-Chart for Model C during the 2026 Post-Transition monitoring period. The dots correspond to the NOK values. Source: Minitab.

Despite the routing corrections lowering the central baseline average ($\bar{P}$) to 21.8%, the process remains highly volatile. As evidenced by Figure 2.14, the Post-Transition process remains out of statistical control. The presence of common-cause variation is mathematically confirmed by the Upper Control Limit (UPL) breach in Week 1, followed by a significant drop below the Lower Control Limit (LCL) in Week 4. This erratic chronological behavior proves that while the immediate outgassing symptom was partially mitigated, the underlying thermomechanical sensitivity of the baseline matrices remains unresolved.

Process Capability Analysis To conclusively address the operational viability of the surface finishing value stream, a Binomial Process Capability Analysis was executed on the 2026 Post-Transition data. While continuous variables utilize standard C_p/C_{pk} indices, the binary nature of visual paint inspection (Pass/Fail) requires a binomial evaluation against the Upper Specification Limit (USL). For premium E-bike frames (Zone A), the allowable defect target is strictly 0%.

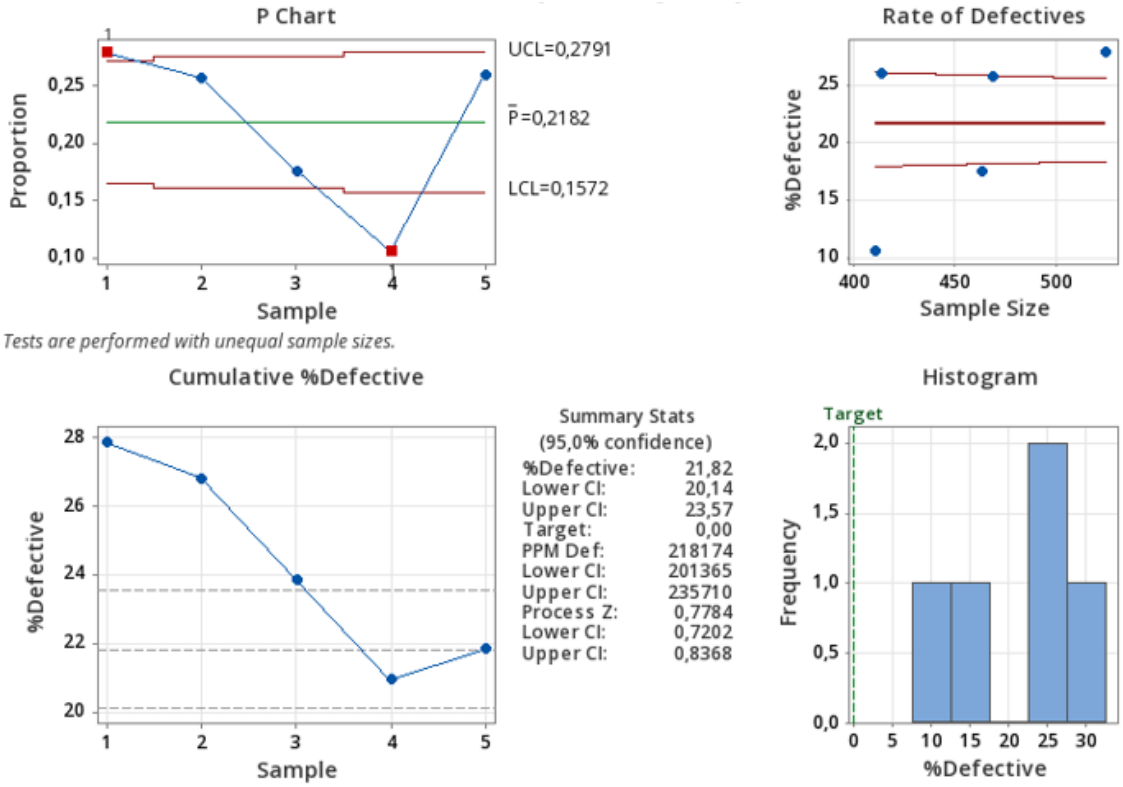

Figure 2.15: Binomial Process Capability Analysis for Model C, Post-Transition Period. Source: Minitab.

The analysis evaluates the 21.8% defect rate against a 0% target, calculating the overall process Sigma level (Process Z).The capability report (Figure 2.15) mathematically quantifies the state of the manufacturing bottleneck. The analysis yields a Process Z (Sigma level) of 0.7784, which is significantly below the standard industrial capability minimum threshold of 4.0 (equivalent to a C_{pk} of 1.33), as established by Montgomery [36]. A capability score this low mathematically

confirms that the current polymeric surface finishing process is structurally incapable of meeting quality specifications, regardless of logistical routing adjustments or operator diligence.

2.3.5 Diagnostic Synthesis and Justification for the DoE Methodology

The investigative progression from Nave 3 to Nave 4 confirms that "Zone A" is a universal manufacturing constraint. While the material routing correction for Model C drastically improved the visible KPIs in Nave 4, the manufacturing process remains at the absolute limit of its capability. The rejection episodes associated with specific colors strongly suggest unpredictable thermodynamic reactions at the putty/paint/oven interface.

It is imperative to note a critical diagnostic constraint inherent to the Nave 4 dataset, mirroring the limitations previously identified in Nave 3. The defect categorizations within the ERP's rely entirely on macroscopic visual inspection after the final coating layers have been applied and thermally cured. Consequently, a defect logged generically as "porosity" cannot be definitively and exclusively attributed to the outgassing or chemical failure of the polymeric putty matrix. This metric inevitably encompasses native porosity originating from the underlying aluminum substrate or the weld beads, which has propagated through the primer and paint films. This systemic ambiguity in the factory's reporting architecture further emphasizes the impossibility of isolating the putty's true thermodynamic performance using exclusively macroscopic, production-line data.

Furthermore, the factory's operational reality introduces a notorious traceability constraint. Because the facility tracks production by bulk manufacturing lots rather than individual frame serial numbers, it is virtually impossible to digitally trace which specific frames received leveling putty, or on which exact geometric zone it was applied in the ERP. Once the frame receives the opaque primer or topcoat, the putty becomes entirely invisible. Building on that, there is no formal inspection or digital registry logging the structural state of the putty immediately after it exits the chemical passivation line.

Historically, this lack of isolated chemical data has forced the facility into symptom-based troubleshooting. A prominent example occurred when porosity issues plagued painted frames prepped with the legacy polyester putty. Operating under the assumption that the chemical passivation baths were the root cause, management deactivated the first two degreasing stages of the continuous line to observe the effect. While this temporarily resolved the porosity—likely because the porous putty was no longer absorbing cleaning agents—it introduced a secondary failure: paint delamination caused by residual grease left on the bare aluminum, ultimately forcing the immediate reactivation of the degreasing stages.

Adding to that, the current ERP is fundamentally incapable of mapping the costs associated with the unrecorderd rework resulting from the outgassing of the epoxy putty. Given the impossibility of extracting isolated root causes in a factory-floor environment plagued by recording inconsistencies, shifting priorities, and overlapping variables, it becomes scientifically imperative to isolate these chemical factors. This diagnostic conclusion directly justifies the necessity of implementing the DoE detailed in Chapter 4.

Chapter 3

Literature Review

The development of a unified bi-component putty for e-bike frame finishing requires a multidisciplinary understanding of metallurgy, surface chemistry, and polymer science. While the overarching industrial goal is to streamline the manufacturing process, the root causes of the current production bottlenecks, such as thermal degradation, surface porosities, and electrostatic repulsion, are fundamentally chemical and physical in nature.

To systematically address the incompatibility between surface correction putties and the subsequent liquid and powder coating lines, it is necessary to examine the underlying mechanisms of each process step. This chapter establishes the theoretical foundation for the experimental work of this thesis.

The review begins by a brief analysis of the base material, AA 6061, in the bike industry, followed by its specific surface characteristics. Subsequently, it explores the chemical mechanisms of surface preparation and passivation, which are critical for ensuring adhesion and corrosion resistance, and lastly different coating realities, distinguishing the characteristics between the powder and liquid painting mechanisms. The chapter then transitions to the usage of putties in the industry to solve process problems, as well as the natural effects they cause, transitioning into the chemistry and rheology of polymeric bi-component systems, detailing their curing kinetics and thermal stability. Finally, the state-of-the-art of additives and fillers, highlighting the alteration of properties that they cause in order to adjust to demands and the consequent side-effects that surge with this modification of the base putty. By integrating these domains, this chapter defines the physical and thermochemical boundaries within which the new putty formulation must successfully operate.

3.1 The Role of aluminum alloy 6061 in the Bicycle and E-Bike Industry

The European bicycle industry has been undergoing a profound structural transformation. According to data from CONEBI [21], despite economic readjustments and global supply chain challenges observed between 2023 and 2024, the sector has demonstrated strong resilience. A 2022 report from CONEBI [19] shows that this stability is driven by a macro-trend of *reshoring*

(the relocation of Asian production back to Europe) where countries like Portugal take the lead in manufacturing volume. In this context of local production optimization and competitiveness, the choice of frame construction materials becomes a critical success factor for European manufacturers.

The most significant catalyst in this industry has been the exponential growth of e-bikes, whose sales have seen drastic increases, exceeding 50% growth in key years as reported by CONEBI [19]. The integration of electric motors and high-capacity batteries requires frames with much more complex geometries, larger tube cross-sections, and consequently, a fatigue and torsional resistance vastly superior to that of conventional bicycles. It is here that traditional materials reach their limits and where aluminum alloys, specifically the 6xxx series, consolidate their dominance in the mid-to-high-end segments.

According to Market Research Intellect [34], market projections up to 2033 indicate that aluminum frames will continue to hold the largest global market share. The 6061-T6 aluminum alloy (Al-Mg-Si) is the gold standard due to its high balance between lightweighting, mechanical strength, and, crucially, high formability and weldability. Unlike carbon fiber, which presents high production costs and end-of-life recycling challenges, AA 6061 is highly compliant with the European Union's ESG (Environmental, Social, and Governance) directives. Being 100% recyclable and allowing for advanced hydroforming processes (to create organic shapes that seamlessly accommodate batteries), AA 6061 offers a sustainable and scalable response.

3.2 Aluminum Treatments and Coating Processes

Being an ever-growing market as well as having high quality demands, as noted by CONEBI [20], the successful manufacture of high-tech bicycle frames requires rigorous material preparation processes. Due to its intrinsic characteristics, aluminum presents specific challenges when subjected to aesthetic and functional finishing phases, particularly during the application of bicomponent putties and the subsequent liquid and powder coating lines that are present in the production line.

To ensure the final quality of the product and an effective transition between the polishing and painting stages , the metallic surface must undergo specific cleaning and protective treatments. As stated by Silva et al. [46], surface preparation is then a crucial step: the presence of moisture or dust can cause the applied putty to detach even after painting or lead to a higher content of porosities only noticeable in final steps of the process, compromising the entire production cycle. Furthermore, treatments such as passivation are implemented to form a very thin layer that protects the aluminum against corrosion and significantly improves paint adhesion. However, the acidic nature of these conversion baths poses a significant challenge when porous polymeric materials, such as polyester putties, are already present on the frame prior to the washing cycle, leading to chemical degradation and porosity issues in subsequent steps.

This section explores the essential treatments applied to aluminum within the industrial context of bicycle production. It will address the physical-chemical mechanisms governing adhesion and surface preparation, the coating and passivation processes, and finally, the main obstacles and

defects, such as porosities and issues related to thermal reactions or the Faraday cage effect, that frequently arise during these critical stages.

3.2.1 Adhesion and Surface Treatments

To achieve a highly durable bond between AA 6061 substrates and polymeric materials, in this case the polyester or epoxy putties and subsequent powder or liquid paints, proper surface preparation is fundamentally critical. The quality of these bonded joints is largely determined by the adhesion forces present at the interface between the aluminum and the applied polymer, a relationship recently quantified by Tajti, Berczeli, and Weltsch [51]. Bond failures typically occur in three ways: adhesive failure (the putty peels off the metal), cohesive failure (the putty detaches from the aluminum substrate), or a mixed adhesion-cohesion failure. The primary goal of surface treatments is to shift the failure mode from a weak adhesive failure to a stronger cohesive failure, ensuring the interface is stronger than the material itself, a principle noted by Silva et al. [47].

The native aluminum oxide layer that forms at room temperature is thin (typically 1-2 μm), highly porous, and mechanically weak, as argued by Ardelean et al. [5]. Furthermore, untreated aluminum surfaces are typically coated with rolling oils, grease, moisture, and dust transferred during manufacturing and storage. If these surfaces are not properly pre-treated, the putty or paint will adhere only to this weak boundary layer of contaminants rather than the base metal, leading to significantly reduced bond strength, a phenomenon emphasized by Tajti, Berczeli, and Weltsch [51]. Cleaning with solvents (such as isopropyl alcohol or methanol) is the mandatory first step to degrease the surface, which alone has been shown to double the shear strength of bonds in some metallic applications by altering the balance of the surface free energy.

Within the company's production line, the bike frames (even prior to complete assembly) regularly enter the passivation line to perform this cleaning process, with the passage through this stage mandatory before the application of the putty.

Mechanical abrasion is also commonly used to create a macro- and micro-roughness profile that allows for the mechanical interlocking of the putty or paint. In their methodology, Tajti, Berczeli, and Weltsch [51] demonstrate that techniques like sanding (using sandpaper or veil polishing) and sandblasting effectively remove the weak native oxide layer and introduce deep scratches. For example, sandblasting with quartz particles can drastically increase the maximum surface roughness (*Rmax*) from 1.8 μm to over 34 μm, . However, the same study cautions that an increase in roughness does not universally guarantee higher adhesion. If the epoxy or polyester putty is too viscous to properly wet the deep microscopic crevices, microscopic air bubbles become trapped in the roughness profile (a phenomenon known as Cassie-Baxter wetting), acting as stress concentrators and ultimately reducing bond strength. Therefore, mechanical treatments must be balanced with the viscosity and wetting properties of the chosen putty.

For optimal adhesion, there must be a precise balance between mechanical roughness and high surface free energy (SFE), specifically a high polar component, which enhances chemical interaction with the adhesive. Advanced treatments, such as laser irradiation followed by immersion in hot deionized water, have been shown to create stable nanoscale modifications that elevate the

total SFE to 88 mN/m, as shown in Tajti, Berczeli, and Weltsch [51] experimental tests. These superhydrophilic surfaces ensure the liquid polymer completely wets the surface before curing. Other novel surface modification processes such as the ones studied by Saleema and Gallant [45], including atmospheric pressure helium-oxygen (He/O_2) plasma treatments, have proven highly effective on AA6061-T6 alloys. According to their research, a mere 15-second exposure to this plasma enriches the surface with hydroxyl (-OH) groups and reduces the water contact angle from 77º to 13º, resulting in a shear adhesion strength of 24 MPa for epoxy resins. This bond is so strong that the failure becomes cohesive (fracturing within the polymer itself rather than at the interface).

Given that polyester putties reacts poorly with acidic passivation solutions, stabilizing the aluminum surface chemically is a critical step. Historically, Chromate Conversion Coatings (CCC) provided superior corrosion resistance and a "self-healing" barrier, but strict toxicity and environmental regulations have forced the aerospace and automotive industries to adopt chromate-free alternatives, as discussed by Becker [11].

For modern aluminum lines, zirconium/titanium conversion coatings (Zr/TiCC) have reached a high level of commercial maturity. Becker's tecnhical review explains that operating in mildly acidic conditions (pH approximately 4) and requiring short immersion times (2 to 5 minutes), these baths deposit a highly stable, 50–100 nm thick layer composed mainly of hydrated metal oxides (like ZrO_2). Building on this, Peng et al. [41] details how this nanoscale conversion layer begins nucleating around the intermetallic particles of the aluminum matrix and spreads to form a continuous barrier. Zr/TiCC systems improve the adhesion of subsequent organic coatings (such as the applied putties and paints) due to their rough morphology and high -OH content. Other emerging chromate-free passivation methods include rare earth chemical conversion (RECC) using cerium salts. Becker [11] notes that these form stable Ce^{3+}/Ce^{4+} oxides over intermetallic sites, offering excellent cathodic inhibition.

For the thesis' specific application, it is advantageous that the 6xxx series aluminum alloys (alloyed with magnesium and silicon) respond noticeably well to anodizing and chemical conversion treatments, forming a very homogeneous layer. Chromate-free conversion coatings, including those analyzed by Becker and the one currently in the production line, transform the metallic surface into a stable oxide barrier. These passivation lines prevent erratic re-oxidation, significantly improve the wettability of the surface, and greatly enhance the adhesion of subsequent paints, sealants, and putties.

Even with proper mechanical abrasion and passivation, applying a chemical primer is often a key factor in maximizing the interfacial shear strength (IFSS) of the joint. Tajti, Berczeli, and Weltsch [51] support this conclusion, showing that primers act as a chemical and physical bridge, filling micro-irregularities while bonding natively to both the aluminum oxide and the polymeric putty:

- Evaluated 14 different treatments on aluminum, the study by Tajti et al. found that the combination of veil sanding, alcohol cleaning, and a solvent-based polyurethane primer (e.g.,

Sika Primer-207) increased tensile strength by 82% and shear strength by 258% compared to untreated surfaces.

- Specifically for Al-6061-T6 bonded with a room-temperature curing epoxy, Sumaiya et al. [50] documented that the application of high-temperature curing primers (such as 3M's EC3901) directly onto the substrate doubled the IFSS to 13.23 MPa, even when the primer was only allowed to cure at room temperature.

At the same time, and in the context of bicycle frame manufacturing, a highly cross-linked chemical primer can also act as an impermeable chemical shield. This barrier protects softer and porous cosmetic putties from the highly reactive acidic environment of the passivation line, preventing structural degradation prior to powder coating. This will be explored in the next subsection related to coating processes and technologies.

3.2.2 Coating Processes

According to Fotovvati, Namdari, and Dehghanghadikolaei [23], the application of protective and decorative surface finishes involves a sequence of specialized methods designed to shield structures from mechanical and chemical damage, extending their lifespan while reducing long-term maintenance costs. Polymeric materials, whether applied as primers, liquid paints, or powder coatings, function by creating a tangible physical barrier. Chhipa, Sharma, and Kumar Bagha [17] detail how this barrier separates the underlying metal surface from its environment, effectively blocking corrosive substances like moisture, oxygen, and salts from completing an electrochemical corrosion circuit. Driven by stringent environmental regulations and the demand for high-performance durability, Kardar and Amini [31] note that the modern industrial sector is actively transitioning from traditional solvent-borne systems to low-emission, eco-friendly alternatives such as waterborne, high-solids, and powder coatings. Navigating the transition from bare metal substrates to finished topcoats requires a comprehensive understanding of the intermediate bridge layers and the specific curing mechanics of the chosen topcoat.

3.2.2.1 Primers and Putties

Topcoat paints rarely adhere completely to bare aluminum or directly to cosmetic putties. To overcome this, the primer acts as the essential chemical and physical bridge that synchronizes the surface chemistry of dissimilar substrates. As explained by Baby et al. [8], formulations such as epoxy-amine primers are extensively utilized because they introduce polar functionalities—such as secondary hydroxyl groups and tertiary amines—that significantly increase the cohesive and adhesive interactions at the interface.

Beyond adhesion, a properly applied primer acts as an impermeable shield, blocking the diffusion of corrosive species (like water, oxygen, and chlorides) from reaching the substrate. Singh et al. [48] emphasize that the physical thickness and structural uniformity of the primer dictate its capacity to inhibit corrosion; thinner coatings or those with imperfections such as pinholes

and microcracks allow water to infiltrate through microscopic molecular penetration or macroscopic defects. To further optimize this barrier, their research highlights recent advancements involving the dispersion of nanofillers, such as graphene nanoflakes, into the primer matrix. These nanofillers create a "labyrinth effect" that increases the tortuosity of the penetration paths, thereby restricting the ingress of media and protecting the temperature-sensitive underlying layers. In 3.5 this will be explored more extensively.

Putties primarily serve the role of cosmetic leveling over structural welds and joints prior to the coating application. A more in depth comprehensive analysis of putties is detailed in 3.3.

3.2.2.2 Liquid Coating Systems

Liquid paint systems, encompassing both traditional solvent-borne and modern waterborne technologies, function by suspending resins (such as acrylics, epoxies, or polyurethanes) in a liquid medium. Kardar and Amini [31] explain that once applied, these systems form a continuous film through the evaporation of the solvent or water. In waterborne epoxies, for example, curing proceeds via heterogeneous particle coalescence followed by chemical cross-linking between amine and epoxy groups, a process that successfully occurs at room temperature or under low-heat baking conditions.

Because liquid paints cure at low temperatures, they present a distinct compatibility advantage for cosmetically leveled surfaces. The low-heat curing process does not induce the high thermal expansion or accelerated outgassing kinetics bottlenecks that routinely degrade and detach underlying temperature-sensitive putties.

Despite their operational compatibility with putties, the industry is moving away from conventional liquid paints. Both Li et al. [33] and Kardar and Amini [31] point out that traditional solvent-borne systems release high levels of Volatile Organic Compounds (VOC), which are environmentally harmful and hazardous. While waterborne systems successfully lower VOC, Kardar and Amini [31] note that they present their own performance limitations: the hydrophilic functional groups and surfactants required to keep the resins dispersed in water remain in the dried film. These residual hydrophilic domains can generate microdefects and interstitial voids that facilitate the penetration of water and corrosive ions, limiting the coating's long-term barrier performance in harsh environments. Additionally, liquid systems generally require longer drying and curing times compared to powder or radiation-curable systems, slowing down the overall manufacturing takt time.

3.2.2.3 Electrostatic Powder Coating

Powder coating is widely applied through electrostatic spray deposition (ESD), which involves applying a high-voltage potential (e.g., a constant voltage of -35 kV) to the electrode of a corona spray gun while the object to be coated is grounded. As detailed by Li et al. [33] and Rubino and Venettacci [43], this setup generates a non-uniform electric field between the gun and the substrate,

driving the dry powder particles toward the component and causing them to adhere to the surface via electrostatic force.

A major limitation of this electrostatic deposition process is the Faraday cage effect. Rubino and Venettacci [43] describe how, when dealing with complex metallic geometries, deep recesses, or indentations, the electrostatic field prevents the powder from penetrating and depositing evenly. Consequently, the powder tends to accumulate thickly on the outer edges of the recesses, leaving little to no coverage—effectively creating bald spots—inside the deeper crevices. Crucially, in the context of surface repair, this effect is artificially induced and exacerbated because standard polymeric putties are inherent electrical insulators. Their non-conductive nature disrupts the required electric field over the patched welds, causing the charged powder to repel and accumulate thickly on the surrounding conductive aluminum edges, leaving critical bald spots over the repair zone. Furthermore, the accumulation of free ions on these insulating surfaces makes the process highly susceptible to back-ionization, where an opposite electric field is generated that forms micro-craters and ruins the aesthetic finish of the surface.

The final curing phase exposes the greatest incompatibility with underlying materials. Once electrostatically deposited, the powder must be cross-linked by baking the component in a convection oven at high temperatures, typically requiring conditions such as 190°C for 10 minutes. While Rubino and Venettacci [43] emphasize that this high-temperature fusion is necessary to melt the powder into a durable, continuous film, it represents a considerable thermal bottleneck for any heat-sensitive substrates or intermediate layers (such as cosmetic putties). The intense heat required for powder curing can cause notorious degradation, expansion, and significant outgassing of these underlying temperature-sensitive materials, sharply contrasting with liquid coatings that can cure safely at much lower temperatures.

3.2.3 Critical Discussion and Experimental Implications

While the literature establishes that advanced surface treatments (such as plasma and Zr/TiCC) significantly enhance interfacial adhesion, a relevant industrial gap remains unresolved: these treatments are optimized for bare metal substrates, not for heterogeneous surfaces repaired with highly porous, insulating polymeric putties. Furthermore, the literature highlights a contradiction in barrier performance; while highly cross-linked primers successfully inhibit moisture ingress and corrosion, they simultaneously create an impermeable seal. In the context of this study, this presents a noticeable thermodynamic risk. If applied over a thermally unstable cosmetic putty, this impermeable primer will trap expanding volatiles during the 180°C powder coating cycle, possibly leading to hydrostatic rupture. Therefore, the experimental design in Chapter 4 must isolate the impact of intermediate layers (e.g., 2K primers) to empirically determine if they act as a protective chemical shield against the passivation line, or if they exacerbate outgassing failures by creating a thermal confinement.

3.3 Metal Surface Repair and Covering of Welding Seams

3.3.1 Market Trends of Putties

Growth Market Reports [27] shows that the global market for industrial putties is experiencing a period of robust and sustained growth. The broader polyester and epoxy putty market was valued at approximately USD 1.82 billion in 2024 and is projected to reach USD 3.02 billion by 2033, expanding at a compound annual growth rate (CAGR) of 5.7%. Concurrently, Cooper [22] highlights that the specific sheet metal putty segment reached USD 856.4 million in 2025 and is expected to grow to USD 1.2 billion by 2032 with a 4.9% CAGR. This upward trajectory is heavily propelled by changing industrial economics; as the cost of raw metal components fluctuates, industries are increasingly prioritizing the cost-effective refurbishment and structural restoration of existing assets over total replacement. Geographically, the Asia-Pacific region is the absolute leader in putty consumption. It captures over 42% of the general polyester and epoxy putty market, according to Growth Market Reports, and over 38% of the sheet metal putty market, as further detailed by Cooper [22]. This dominance is largely due to rapid urbanization, immense automotive manufacturing hubs, and continuous infrastructure development across the region.

The usage of putties is highly segmented by application needs and the specific chemical properties of the putty formulas. Automotive refinishing remains the dominant sector, accounting for nearly 68% of the sheet metal putty market in 2025, a metric provided by Cooper [22]. In this industry, Growth Market Reports [27] details that putties are indispensable in vehicle body repair, precise surface leveling, dent filling, and structural restoration for both original equipment manufacturers (OEMs) and aftermarket repair shops. The global construction boom also heavily relies on putties for surface smoothing, crack repair, and joint filling in residential, commercial, and green building projects. In industrial and marine maintenance settings, these materials are crucial for machinery repair and defect rectification, helping operators minimize downtime and maintain equipment. The marine sector specifically utilizes epoxy putties for underwater maintenance, hull repairs, and pipe sealing because they offer superior resistance to water and harsh, corrosive environments. Regarding material preferences, Cooper [22] indicates polyester putty is the most widely adopted material, capturing over 58% of the sheet metal putty market. It is favored for its cost-effectiveness, fast-setting characteristics, and excellent sanding properties, making it ideal for automotive and construction surface leveling. Alternatively, the Growth Market Reports [27] analysis shows epoxy putty is selected for heavy-duty and structural applications because it delivers superior mechanical strength, chemical resistance, and the ability to bond to diverse substrates like metals, plastics, and ceramics.

Several key industry trends are actively shaping the future of this market. To address end-user demands for faster handling and material efficiency, Cooper [22] observes that innovation is heavily shifting toward ultra-lightweight formulations. These lighter chemistries provide superior sanding properties and shorter curing times, which are essential for meeting the stringent throughput requirements of modern industrial workflows. Manufacturers and repair shops are also

increasingly adopting UV-curing technology. Moving from laboratory demonstrations into commercial deployments, this technology significantly shortens cycle times and reduces energy and solvent emissions. Additionally, regulatory pressures are forcing a fundamental transformation in putty chemistry. Stringent environmental regulations, such as the EU VOC Directive 2004/42/EC and evolving California mandates, are compelling manufacturers to invest heavily in water-based, low-VOC, and eco-friendly alternatives. Alongside these changes, Growth Market Reports [27] identifies a growing trend toward hybrid putty formulations that combine the best attributes of both polyester and epoxy resins. These hybrids aim to deliver enhanced flexibility, faster curing, and superior environmental resistance, thereby overcoming the traditional limitations of single-resin putties. Finally, while traditional offline hardware stores and authorized distributors still dominate sales, online distribution channels are rapidly gaining momentum. The rise of e-commerce is broadening market access, especially for the growing base of DIY enthusiasts, hobbyists, and small-scale contractors.

3.3.2 The Role of Industrial Putties

As explored by Ghafafian and Nutt [24], industrial putties and polymeric repair patches are fundamental across the automotive, marine, wind energy, and aerospace sectors to extend component service life, cover manufacturing imperfections, and reduce the environmental waste of replacing entire parts. Across these applications, the choice of the polymer matrix is dictated by a strict balance of cost, mechanical properties, and curing speed.

For example, the same study notes that in marine and wind turbine applications, polyester and vinyl ester resins are frequently used because they are easy to laminate and cure quickly at room temperature, but they suffer from high volumetric cure shrinkage of 7% to 10%. In contrast, epoxy resins are heavily favored for high-performance structural bonds because they offer superior moisture resistance, greater tensile strength, and a much lower cure shrinkage of approximately 2%, even though they often require heat blankets or ovens to cure effectively.

In high-volume manufacturing like the automotive industry, the use of industrial putties is closely related to the automated application of polymeric sealers, dampening coats, and primer surfacers. Akafuah et al. [3] detail how after the anti-corrosion electrodeposition (e-coat) stage, polymeric materials such as polyvinyl chloride (PVC) and urethanes are applied to metal joints, hoods, and underbodies. These polymeric layers serve multiple critical functions: they seal out water and air to inhibit rust, provide vital anti-chipping protection against road debris, and act as vibration-deadening layers to prevent mechanical noise from reaching the passenger cabin. Following this, as Akafuah et al. further explain primer surfacers are used specifically to fill and smooth out minor scratches and welding imperfections, acting as a leveling agent to ensure the final topcoat is completely smooth.

Unlike highly automated automotive assembly lines, the application of putty at Triangle's - Cycling Equipments S.A. remains a targeted, manual process. It is selectively applied to specific high-end bicycle frames to achieve a 'seamless' aesthetic by concealing weld seams, or as a localized rework step for surface defects prior to painting. Consequently, this operation introduces

significant variability into the production line, highlighting the critical need to optimize the putty formulation and application parameters to ensure compatibility with subsequent surface treatments and high-temperature curing cycles.

Looking toward the future, the broader industrial context is evolving beyond the manual application of static putties toward smart, self-healing polymer composites, a shift extensively analysed by Bhuvaneswari [13]. Because microscopic internal damage is difficult to detect visually before a considerate failure occurs, researchers are embedding polymer matrices with autonomous repair mechanisms. According to his research, innovations include encapsulating healing agents (like dicyclopentadiene) inside microcapsules that rupture and fill cracks upon impact, or integrating Shape Memory Alloys (SMAs) and carbon nanotubes into the matrix. When activated by heat, UV light, or ultrasound, these smart materials can physically pull delamination gaps closed and autonomously cure, restoring up to 100% of the structure's original mechanical strength without the need for manual putty application.

3.3.3 Current Problems and Bottlenecks

The application of polymeric putties (such as polyester and epoxy-based resins) to aluminum frames AA 6061 presents several industrial challenges that hinder production line efficiency.

3.3.3.1 Application and Incompatibilities with the Substrates

The physical application of the putty must account for the thermal dynamics of ovens depending the field of application. When an aluminum frame and a polymeric putty are heated and subsequently cooled, they undergo a significant thermal expansion mismatch. As detailed by Marques et al. [35], in the case of this project materials, Aluminum has a coefficient of thermal expansion (CTE) of approximately 24×10^{6}/ ºC, whereas epoxies and polyesters generally exhibit CTEs of 60×10^{6}/ ºC or higher. Upon cooling from the temperatures of the oven down to room temperature, the polymer shrinks significantly more than the aluminum, "locking in" residual thermal stresses at the interface.

Because of these inherent stresses, the thickness of the putty applied to the frame is critical. According to Sumaiya et al. [50], experimental testing on AA-6061 bonded with epoxy shows that the IFSS is highly dependent on the thickness of the applied polymer. The strength reaches a maximum at an optimal thickness of 0.08–0.12 mm, but drops noticeably at thicknesses greater than 0.12 mm due to a decrease in the apparent fracture toughness of the bulk polymer. Therefore, when filling deep dents or large welds, the locked-in thermal stresses from the 180ºC oven can easily exceed the joint's strength if the putty is applied too thickly without an optimized, primed, and passivated surface.

In this project's context, these thickness levels are very difficult to be achieved. Putty layers enter the scale of 2 to 3 mm due to the difficulty of covering the welding seam, which aggravates this interaction between the polymer and the substrate.

3.3.3.2 Chemical Degradation and Interfacial Contamination

Borges et al. [14] highlight that a critical issue with polymers in industrial applications is their susceptibility to physical and chemical degradation when exposed to harsh environments, which alters the interfacial regions between the adhesive and the metallic substrate. In the case of polyester putty, its poor reaction with the acidic solutions used in the passivation line can be explained by the infiltration of chemical agents into the interface. The same review notes that contaminants and fluids can diffuse through the joint or remain at the adhesive/substrate interface, producing locally debonded areas that lead to joint failure. Furthermore, the natural appearance of oxide layers on aluminum surfaces can decrease the strength of the joints if the polymer lacks the chemical resistance to withstand pH alterations during surface treatments.

3.3.3.3 Thermal Bottlenecks, Outgassing, and Porosity Formation

The powder coating cycle requires frames to be baked in ovens at 180ºC. While polyester cannot withstand these temperatures, the epoxy putty survives but exhibits significant porosity after the powder primer stage. This phenomenon is directly related to outgassing—the escape of embedded gases, moisture, and volatile compounds from a solid material, a phenomenon extensively studied by Chandrakant Joshi [15]. When porous polymeric materials are subjected to high temperatures, the energy gained causes weakly adhered surface particles to loosen and increases the evolution rate of trapped gas molecules. The majority of mass loss during thermal exposure is typically due to water vapors and organic solvents attempting to escape to the surface. As these gases forcefully exit the putty during the 180ºC baking process, they create voids, blisters, and porosities in the overlying primer layer.

3.3.3.4 Moisture Absorption and *Tg* Depression

During the time that elapses between manufacturing steps, polymeric putties are highly susceptible to moisture absorption, as noted by Borges et al. [14]. The diffusion of water into the adhesive causes plasticization and volumetric expansion (swelling), which introduces stresses near the interface due to the constriction imposed by the rigid aluminum substrate. More critically for the high-temperature powder coating process, moisture uptake causes the glass transition temperature (Tg) of the polymer to decrease. When the oven temperature (180ºC) surpasses the depressed Tg of the moisture-laden putty, the diffusion rate of water increases progressively, accelerating the outgassing effects and degrading the material's structural integrity.

3.3.3.5 Curing Kinetics and the Viscosity Trade-off

Although epoxy is resistant to acids and high temperatures, its major bottleneck is the requirement for batch curing at 160ºC. The formation of the interphase in epoxy-amine systems is highly dependent on complex adsorption reactions of the curing agents (amines) to the metallic substrate, according to Borges et al. [14]. Preferential adsorption of the curing agent to the aluminum oxide

layer is required to form strong chemical connections. Borges et al. also point out that the presence of residual contaminants or environmental moisture can alter the kinetics of the cross-linking process. Because this chemical cross-linking is highly sensitive to temperature and surface conditions, it requires strict, prolonged thermal cycles to complete properly, creating a significant delay in a production line that demands rapid throughput.

3.3.3.6 Surface Conditions and Wettability

As Silva et al. [47] emphasize, for any putty to achieve durable adhesion across both liquid and powder coating lines, the wettability of the aluminum surface is a fundamental factor. Adhesion requires intimate contact, meaning the liquid putty must properly wet the surface of the solid substrate. Poor surface preparation, existing contaminants, or specific oxide layers can lower the surface free energy, preventing the putty from achieving the necessary mechanical or chemical interlocking with the AA 6061 surface.

3.3.3.7 Electrical Conductivity and Electrostatic Deposition Constraints

For the powder coating line, the electrostatic adhesion of paint to the frame relies on the substrate being electrically conductive. However, standard putties, including epoxies and polyesters based ones, lack free electrons and are inherent electrical and thermal insulators, a limitation detailed by Chen et al. [16]. This insulating nature disrupts the electrostatic field, repelling the powder coat and causing uneven paint thickness over the putty-repaired areas. To resolve this, Chen et al. note that conductive fillers—such as silver, copper, or carbon nanotubes (CNTs)—must be incorporated into the putty. However, achieving sufficient electrical and thermal conductivity requires adding enough filler to reach a "percolation threshold," the point where particles form a continuous interconnected network. Reaching this threshold requires high filler loadings depending on the additive used, which may not only drastically worsen the aforementioned viscosity and sanding bottlenecks, but also introduce Kapitza resistance (thermal boundary resistance) at the interfaces between the polymer and the conductive fillers due to mismatched vibrational phonon frequencies.

To overcome these interconnected bottlenecks, ranging from thermal outgassing to electrostatic repulsion, it is imperative to analyze the chemical architecture of the underlying polymer matrices and investigate the integration of advanced functional fillers capable of bridging the gap between cosmetic leveling and high-performance thermomechanical stability.

3.3.4 Critical Discussion and Experimental Implications

The existing literature clearly identifies CTE mismatch, moisture absorption, and the Faraday cage effect as the primary failure mechanisms of polymeric putties in industrial environments. However, current market solutions fail to address the specific characteristic of high-volume e-bike manufacturing: the competing demands of process agility and thermodynamic stability. Most studies focus on low-temperature liquid coating applications or isolated aerospace structural repairs, offering little guidance on surviving a rapid 180°C thermal shock on a high-throughput line. This

gap dictates the core methodological approach of this thesis. Because no single commercial matrix naturally resolves both the temporal bottleneck of epoxy and the thermal outgassing of polyester, an evaluation of commercial baselines against these unalterable manufacturing constraints must be made, before attempting any chemical modification.

(a) Example of outgassing defect.

(b) Close-up of the defect.

Figure 3.1: Outgassing phenomena with the polyester putty underneath the coating.

3.4 Thermosetting Polymer Matrices

3.4.1 Polyester resins

Unsaturated polyester resins are a primary matrix used in the formulation of industrial putties, coatings, and composite materials, as highlighted by Abu-Jdayil [2] and Moujdin et al. [38]. According to the combined research of Kaichang, Renhui, and Wendi [30] and Aldrighetti et al. [4] they are synthesized through the polycondensation of unsaturated bifunctional acids (such as maleic anhydride or fumaric acid), saturated dibasic acids (such as phthalic anhydride), and glycols (such as ethylene or diethylene glycol). Because the base polyester is typically solid at room temperature, it is dissolved in a reactive diluent, most commonly styrene (which can make up to 40 wt% of the mixture), such as in the case of the currently used putty in the company. These authors explained that the styrene serves a dual purpose: it reduces the viscosity of the resin so it can be easily sprayed or applied as a putty, and it actively reacts with the carbon-carbon double bonds (C=C) in the polyester chain to form a highly cross-linked, three-dimensional thermosetting network.

3.4.1.1 Advantages

As Abu-Jdayil [2] exposes, unlike many other thermosetting resins, the curing of UPR does not produce any byproducts (like water or gas), allowing it to be molded and cured at low pressures and ambient temperatures. Moujdin et al. [38] and Aldrighetti et al. [4] detail that the crosslinking is initiated by free radicals, typically generated by adding a hardener such as methyl ethyl ketone

peroxide (MEKP) or benzoyl peroxide (BPO) along with a catalyst like cobalt octoate. Benzoyl peroxide hardener is used coupled with the current polyester-based putty, being added a value of 2 to 3% of the weight of the two component resin.

Abu-Jdayil [2] outlines that these types of resins are very attractive in a large industrial scale:

- **Rapid Processing:** They offer fast, room-temperature curing capabilities, which is highly desirable for manufacturing cycle times.
- **Cost-Effectiveness:** UPRs are widely available and relatively inexpensive compared to high-performance alternatives like epoxy.
- **Good Baseline Properties:** Once cured, they exhibit reasonable mechanical properties, chemical resistance, and can be easily sanded and painted over.

3.4.1.2 Disadvantages

However, disadvantages and processing bottlenecks naturally emerge:

- **High Shrinkage:** Moujdin et al. [38] identify that one of the most critical flaws of UPR is its high volumetric shrinkage during the crosslinking cure, which ranges between 7% and 12%. In putty applications, this high shrinkage rate means that even if a dent or void is completely filled, the putty will contract after curing and painting, leading to the appearance of defects like pinholes.
- **Exothermic Stress & Cracking:** The same study notes that the curing reaction is highly exothermic. If operators increase the amount of hardener/catalyst to speed up the process, the exothermic temperature can rapidly spike to 171°C – 193°C. This considerate heat generates thermal gradients and residual stresses within the putty, leading to cracking, warping, and an even higher shrinkage rate.
- **High Thermal Expansion:** Aldrighetti et al. [4] explain that cured UPR networks contain many unreacted chain ends, known as "dangling chains". These dangling chains retain a high degree of mobility, which causes the UPR to have a high coefficient of thermal expansion. This can cause the putty to expand or contract at a different rate than the underlying aluminum bicycle frame under thermal stress, eventually leading to delamination or paint cracking.
- **Inherent Brittleness and Poor Adhesion:** Standard UPR is rigid, lacks flexibility (low deflection at break), and has poor inherent chemical adhesion, usually relying primarily on mechanical interlocking with the roughened substrate, a limitation corroborated by multiple studies (Rajaee et al. [42], Kaichang, Renhui, and Wendi [30], Yoon et al. [54]).

3.4.2 Epoxy resins

As detailed in the fundamental studies by Wei et al. [52] and Jin, Li, and Park [29], epoxy resins are thermosetting pre-polymers characterized by the presence of one or more oxirane (epoxide) rings in their molecular structure. These authors note that the most widely utilized base for industrial and high-performance applications, accounting for the vast majority of the market, is the diglycidyl ether of bisphenol-A (DGEBA), which is also the case of the epoxy putty used in the manufacture line. Unlike unsaturated polyester resins (UPR) which cure via free-radical polymerization, Jin et al. and Wei et al. explain that epoxy resins cure through nucleophilic addition or catalytic reactions with specific hardeners (curing agents) such as amines (aliphatic, cycloaliphatic, or aromatic), anhydrides, or polyamides. This reaction forms a highly dense, three-dimensional cross-linked network. Consequently, these same researches indicate that the curing process is irreversible and heavily dictates the final glass transition temperature (Tg), mechanical strength, and chemical resistance of the polymer.

3.4.2.1 Advantages

The advantages of epoxy resins are vastly different from the previous ones. Both Wei et al. [52], Jin, Li, and Park [29] emphasize that once fully cross-linked, the 3D network of epoxy provides outstanding stability against chemical attacks (such as the acid solutions used in your passivation line) and high temperatures (like the 180°C required for powder coating). Jin et al. further highlight that high-temperature heat curing significantly elevates the network's Tg and chemical resilience.

According to Yoon et al. [54], a critical advantage of epoxy putties over polyester is their low volumetric shrinkage. While UPR putties can shrink over 7% during cure, optimized DGEBA-based epoxy putties exhibit much lower shrinkage rates (typically 2.8% to 4.2% at elevated temperatures). This dimensional stability prevents the putty from contracting excessively after application, which Yoon points out eliminates the formation of pinholes and structural voids under the paint.

Regarding adhesion, Wei et al. [52] demonstrates that epoxy molecules contain a high concentration of polar hydroxyl (-OH) and ether groups. These polar groups create strong secondary bonds (such as hydrogen bonding and van der Waals forces) with the oxide layer of metal substrates like AA 6061, leading to superior interfacial adhesion that resists delamination and shear forces.

3.4.2.2 Disadvantages

However, as noted by Jin, Li, and Park [29], high-performance epoxy networks generally require elevated temperatures and extended curing cycles to achieve full cross-linking. This directly explains the production bottleneck in the current line, where the epoxy putty requires 20 minutes in a batch oven at 160°C. Furthermore, studies by both Wei et al. [52] and Jin, Li, and Park [29] show that in its pure, highly cross-linked state, an epoxy matrix is stiff and highly brittle, showing poor

resistance to crack initiation and propagation. This high molecular rigidity makes the cured epoxy putty much harder to sand manually compared to polyester putties. Lastly, Moujdin et al. [38] cautions that the exothermic nature of the curing reaction, combined with high oven temperatures, can induce thermal gradients. Additionaly, Moudjin explains that a mismatch in the coefficient of thermal expansion between the rigid epoxy putty and the aluminum frame can lead to the development of internal residual stresses, which may cause microcracking during heating and cooling cycles.

3.4.3 Critical Discussion and Experimental Implications

A critical comparison of unsaturated polyester and epoxy matrices reveals fundamentally opposing limitations for powder coating applications. Unsaturated polyester systems excel in rapid curing and ergonomic workability but suffer volumetric expansion and styrene outgassing at elevated temperatures. Conversely, DGEBA-based epoxies offer superior thermal stability and acid resistance but introduce unacceptable cycle-time bottlenecks due to their curing kinetics. The literature does not currently present a hybrid matrix that universally satisfies both extremes. Consequently, this research hypothesizes that process-level optimization alone is insufficient. The experimental work, must therefore select the most robust baseline matrix from each family and strategically alter its fundamental properties—either by accelerating the epoxy or thermally shielding the polyester—to force the polymer to survive outside its native operational limits and meet the shop floor's demands of continuous production and high quality standards.

3.5 Polymer Modification and Functional Fillers

Composite materials, such as those based on commercial epoxy and unsaturated polyester (UPE) matrices, frequently incorporate various fillers and additives to improve their physical and mechanical characteristics, while optimizing the matrix's response to heat and dimensional changes during curing.

However, polymer modification presents inherent challenges. As Attia-Essaies et al. [6] and Bai et al. [10] note, a primary issue is the structural incompatibility between hydrophilic (polar) inorganic fillers and the hydrophobic (non-polar) polymer matrix. This incompatibility results in large interfacial tension and weak bonding, leading to stress concentration and ultimate material failure. Furthermore, multiple studies (Bai et al. [10], Yeo, Lee, and Hwang [53], Goudarzi et al. [26]) highlight that UPE resins suffer from a major drawback during processing: a high volume shrinkage of 7-9% during polymerization. Yeo et al. and Goudarzi et al. explain that this shrinkage causes noticeable manufacturing defects, such as warpage, sink marks, rough surfaces, and cracks, heavily justifying the need to use highly filled putties and low-profile additives (LPAs) to compensate for volumetric changes and preserve dimensional stability.

A cautious and structured approach is then key to properly modify the base polymer and still obtain the desired results, indepedent of the type of filler used.

3.5.1 Different Filler Approaches

3.5.1.1 Thermally and Electrically Conductive Fillers

As Nayak, Mohanty, and Nayak [40] point out, to combat the low intrinsic thermal and electrical conductivity of standard polymer matrices (e.g., a thermal conductivity of approximately 0.193 W/m.K for epoxy), specialized fillers must be integrated into the composite network. In the context of bicycle frame manufacturing, this conductivity is not just a structural enhancement, but a critical thermodynamic and logistical requirement for the electrostatic powder coating process.

To support the thermal demands of the curing oven and prevent localized outgassing, ceramic fillers like alumina (Al_2O_3) are highly effective. Moreira et al. [37] and Abeer, Raghad, and Nadia [1] note that alumina possesses a high intrinsic thermal conductivity (approximately 30 W/m.K), directly enhancing the heat transfer capabilities of the composite. Abeer's research demonstrates that while adding high volumes of alumina (e.g., up to 20 vol%) continuously increases thermal conductivity and Shore D hardness, it simultaneously causes a sharp decrease in impact strength and elasticity. Furthermore, Moreira et al. [37] indicates that larger micro-particles (e.g., 150 nm to 200 nm) provide a greater thermal conductivity augmentation than smaller nanoparticles (30-40 nm) due to a reduction in interfacial thermal resistance and the formation of conductive agglomerates.

Beyond thermal management, the putty must also facilitate electrostatic attraction. Interestingly, while Nayak, Mohanty, and Nayak [40] observe that increased electrical conductivity is often cited in literature as unsuitable for electronics, in the specific industrial context of bicycle frame manufacturing, this conductivity is a tremendous benefit. When an electrically conductive putty is applied to weld zones, it significantly enhances the electrostatic attraction and adhesion of the powder paint during the electrostatic powder coating process.

For this purpose, carbon-based nanomaterials like expanded graphite (EG) or graphene are highly advantageous due to their low density, high surface area, and superior electron mobility. According to Goudarzi et al. [26], the electrical percolation threshold—the point at which a continuous conductive network is formed—for well-dispersed graphene nanosheets is remarkably low, typically between 0.45 vol% and 0.52 vol%. Adding a volume percentage just above this threshold ensures the necessary semi-conductivity without overloading the resin. Additionally, Karvandian and Hubert [32] highlight that at low concentrations, graphene can act as a curing accelerator due to surface oxygen functionalities. However, they also caution that at higher concentrations, it acts as a radical scavenger, drastically delaying the gelation point of unsaturated polyester resins.

Despite these advantages, the implementation of conductive fillers is not without obstacles. Conventional metallic and ceramic fillers possess a high specific weight, meaning large amounts must be added to achieve the desired thermal conductivity, which adversely affects the mechanical properties of the putty. Additionally, returning to Nayak, Mohanty, and Nayak [40]'s findings, unmodified expanded graphite exhibits poor wettability with resins, leading to patchy dispersion and micro-holes. This poor wettability is the primary cause of trapped free air, resulting in the unwanted bubbles and internal pores often observed inside the applied putty.

3.5.1.2 Reactive Diluents and Functional Modifiers

In heavy industrial chemistry, commercial reactive diluents are incorporated into polymer matrices to reduce viscosity and improve processability. As Jagtap and More [28] explains, unlike traditional solvents that evaporate, reactive diluents chemically participate in the curing process and become an integral part of the final crosslinked network. Their research notes that for epoxy resins, conventional diluents like 1,4-butanediol diglycidyl ether (BDGE) or acrylates are utilized, whereas styrene is the traditional reactive diluent in UPE systems. Following this, Mousa, Heinrich, and Wagenknecht [39] details how functional modifiers, such as silane coupling agents or stearic acid, are then used to chemically or physically bridge the incompatible fillers to the matrix.

However, traditional petroleum-based reactive diluents like styrene are limited by their toxicity, carcinogenicity, and high volatility. Jagtap and More [28] emphasizes that his drives a critical industrial need to seek safer, low-VOC alternatives to protect workers. Yet, the same study reveals that alternative diluents, such as α-methylstyrene, can prolong the exotherm peak time, drastically increase gel time, and decrease the overall rate of polymerization, slowing down the production line. Furthermore, while functional modifiers like silane successfully bridge fillers to the matrix, Nayak, Mohanty, and Nayak [40] cautions that they encapsulate the filler surface with nonconductive inorganic groups. For conductive fillers like graphite, Nayak et al. explain how this insulation prevents electron tunneling and drastically diminishes the electrical conductivity of the composite, which can negatively affect the electrostatic powder coating adhesion.

3.5.1.3 Rheological Modifiers and Bulking Fillers

Finally, bulking fillers, such as calcium carbonate ($CaCO_3$) and industrial slag, are heavily utilized to reduce material costs while enhancing physical properties like stiffness and compressive strength, a practice documented by both Mousa, Heinrich, and Wagenknecht [39] and Bekuma and Nigus [12]. The primary drawback of these additions is the substantial alteration of the uncured resin's rheology. According to Nayak, Mohanty, and Nayak [40], the addition of high-volume bulking fillers shifts the resin from a fluid to a highly viscous, sticky mixture with high internal friction. This creates a critical operational bottleneck: heavily filled putties negatively impact workplace ergonomics, resulting in high application viscosity and increased resistance to mechanical abrasion, thereby reducing operator ergonomic efficiency.

As Attia-Essaies et al. [6] observes, at high loadings (e.g., beyond 20 wt%), these fillers also form agglomerations that act as stress nodes, weakening the matrix interaction and leading to a progressive reduction in flexural strength. Consequently, the incorporation of rigid, unmodified mineral fillers significantly reduces the elasticity of the polymer matrix, which Mousa, Heinrich, and Wagenknecht [39] concludes makes the cured putty more brittle and lowers its impact strength.

Ultimately, the existing literature clearly defines the thermodynamic, chemical, and rheological boundaries of conventional putty formulations. While these studies provide the fundamental theoretical mechanisms behind failures present in the production line, they do not offer a consolidated, process-ready solution for the demanding thermal and chemical constraints of industrial

powder coating. To bridge this gap between chemical theory and factory-floor application, the following chapter 4 details the experimental methodology of this study.

3.5.2 Critical Discussion and Experimental Implications

While the integration of functional fillers is well-documented, the literature frequently highlights contradictory outcomes. For instance, high loadings of alumina effectively increase thermal conductivity and mitigate localized hot spots, but degrade the matrix's elasticity and drastically increase viscosity, crippling manual application. Similarly, while graphene offers exceptional electrical conductivity at low percolation thresholds (resolving the Faraday cage effect), it can act as a radical scavenger, unpredictably delaying the gelation point of polyester resins. For the specific problem addressed in this thesis, these contradictions mean that additives cannot be applied arbitrarily, and small variations may have undesirable impacts. This directly restricts and guides the experimental choices: alumina will be targeted strictly at around 5 vol% to provide physical shielding without having a negative impact on ergonomics, while graphene must be capped near 0.6 vol% to secure electrostatic adhesion without altering the resin's curing kinetics.

3.6 Methodological Foundations for Process Optimization

Much of the existing literature focuses on polymer theory and ideal-state laboratory testing, often neglecting the chaotic variables of active production lines. Industrial coating failures are rarely driven by single-point chemical defects; they are typically the result of systemic, common-cause variations. Factors such as fluctuating ambient humidity, operator application variance, and micro-gradients in industrial oven thermodynamics compound to create latent defects. As manufacturing scales, these defects manifest as non-traceable rework—undocumented, iterative repair loops that artificially inflate FTY metrics while impacting the COPQ. Resolving these bottlenecks requires shifting the analytical focus from isolated material properties to the holistic survivability of the polymer within the manufacturing value stream.

3.6.1 Methodological Foundations for Process Optimization

To transition from theoretical material science to factory-floor implementation, it is necessary to establish a rigorous framework for evaluating process failures and optimizing multi-variable systems.

3.6.1.1 Design of Experiments (DoE)

To systematically address the multivariable nature of industrial polymer processing, a robust statistical framework is essential. Traditional One-Factor-At-A-Time (OFAT) experimentation is widely recognized as inefficient and fundamentally incapable of detecting interactions between competing variables. As established by Montgomery [36] in his foundational text on experimental design,

a factorial DoE is required to accurately map the response surface of a complex system. By utilizing structured experimental arrays, DoE enables the simultaneous evaluation of multiple factors, allowing researchers to isolate both the main effects of individual chemical modifiers (e.g., the addition of graphene) and their respective interaction effects with intermediate layers (e.g., a 2K primer). This mathematical rigor ensures that observed performance deltas are statistically significant and not artifacts of background factory noise, providing a defensible justification for the experimental methodology implemented in this study.

3.6.1.2 Multi-Criteria Decision Making and the AHP

In industrial engineering, the optimization of a formulation often presents competing objectives, where maximizing thermal stability may inadvertently compromise application ergonomics or cycle time. To objectively resolve these multi-objective conflicts, structured multi-criteria decision-making models must be employed. The AHP, originally developed by Thomas L. Saaty, provides a mathematically robust framework for organizing and analyzing complex decisions. AHP utilizes pairwise comparisons based on expert judgments to calculate a principal eigenvector, which subsequently assigns normalized percentage weights to each evaluation criterion. As developed by Saaty [44], a critical strength of the AHP methodology is its ability to quantify and filter out subjective human bias through the calculation of a Consistency Ratio (CR). By maintaining logical transitivity within the pairwise matrix, AHP ensures that the final formulation selection mathematically prioritizes the unalterable thermodynamic limits of the factory over superficial operational gains.

3.6.1.3 Statistical Assumptions and Scale Continuity

A recognized methodological limitation within the application of DoE and subsequent Analysis of Variance (ANOVA) is the statistical treatment of heuristic evaluation metrics. Strictly speaking, heuristic grades represent ordinal data, which theoretically restricts the use of parametric variance analysis. However, non-parametric tests frequently lack the multivariate rigor required to accurately isolate interaction effects in complex polymer blends. To overcome this limitation, the heuristic scales are treated as approximately continuous. This statistical assumption is robustly supported in the methodological literature; seminal works by Churchill Jr and Peter [18], as well as Bagozzi and Baumgartner [9], demonstrate that Likert-type and ordinal rating scales can be validly treated as approximately continuous in structural equation models and hypothesis testing. Consequently, the application of parametric ANOVA to heuristic scores is scientifically justified, provided that residual analyses confirm normal distribution and constant variance across the experimental specimens.

Chapter 4

Methodology and Experimental Work

This chapter details the experimental architecture and protocol developed for this thesis. Transitioning a theoretical framework onto an active shop floor rarely follows a linear trajectory; consequently, this research necessitated a highly iterative, adaptive approach to successfully navigate strict thermodynamic, material, and safety constraints. As illustrated in Figure 4.1, the methodology operated as an evolving pipeline.

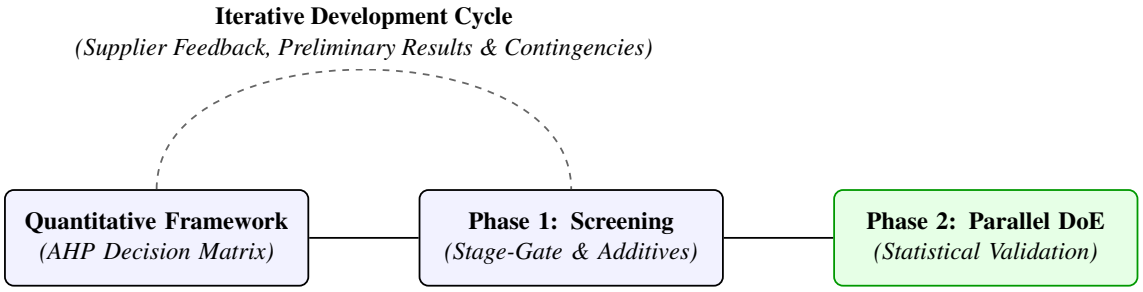

Figure 4.1: Linear progression of the methodology.

To provide immediate clarity on the exact parameters being tested, this chapter is structurally organized to present the destination before the journey. It begins by defining the Final Experimental Methodology in section 4.1. This opening section establishes the strict mathematical rules of the experiment—translating industrial metrics via an AHP framework—and details the definitive setup of the final, statistically controlled Phase 2 DoE.

Following the establishment of the final architecture, the chapter subsequently details the Route Mapping and Iterative Process in section 4.2. This section provides a transparent chronological analysis of the empirical hurdles and logistical contingencies that dictated the final DoE. It explores the expansion of the original 48-specimen theoretical plan following active supplier engagement, and the subsequent elimination of the 1K primer based on critical thermal outgassing failures. Furthermore, it documents the "implementation shock" associated with hazardous commercial e-conductives, the strategic pivot towards graphene and alumina, and the rigorous feasibility analyses that ultimately invalidated the upcycling of circular economy waste streams.

By structuring the chapter in this manner, it is definitively proven that the final methodology was not predefined, but rather forged through a rigorous stage-gate process where every final parameter was strictly justified by empirical evidence and factory reality.

4.1 Experimental Architecture and Protocol

This first section details the methodology followed throughout the experimental part, showcasing the tools, decisions and process step by step.

4.1.1 Evaluation Methodology

To objectively isolate the optimal formulation, the expected results (dependent variables, Y) were evaluated utilizing a Weighted Decision Matrix.

While multiple quality control stations are integrated throughout the production line, the final acceptance criteria rely predominantly on qualitative visual inspection—specifically, evaluating the surface for adequate leveling and the absence of porosity in accordance with established standards. The sole quantitative evaluation of the putty occurs at the final packaging stage. At this point, a randomized sampling of frames undergoes mechanical testing (specifically, cross-cut adhesion and thickness measurements) targeted exclusively at models where putty is systematically applied to conceal structural welds.

However, as extensively detailed in Section 2.3.5, the factory's reliance on batch tracking and the sporadic application of leveling putty creates a traceability constraint for the high-volume models analyzed in this study. Because it is virtually impossible to locate the localized putty patches beneath the final cured coating, conducting precise mechanical evaluations on these specific repaired zones is not viable for standard production models.

To circumvent this systemic traceability limitation, a custom scoring framework was developed specifically for the DoE. Rather than attempting to strip away inherent operational realities, this custom evaluation matrix is explicitly designed as a deterministic tool. It translates discrete industrial requirements and strictly prioritized shop-floor constraints into a standardized mathematical framework, executing the selection through a rigorous, two-tiered elimination protocol.

Phase 1: Non-Compensatory Boundary Elimination (The Hard Gate) The core evaluation logic was formalized through consultations with both the company's technical mentor and external material suppliers. Through these discussions, a unanimous directive was established: the primary objective must be identifying a robust technical solution capable of surviving the unalterable thermodynamic limits of the factory. Consequently, the methodology mathematically penalizes false economies; a putty formulation that offers rapid curing and ergonomic workability, yet ultimately fails during the final high-temperature coating stages, cannot be considered a viable industrial solution.

Because the subsequent AHP matrix is inherently compensatory—theoretically allowing a formulation to offset a critical thermal failure with high scores in secondary metrics—a non-compensatory Boolean "Hard Gate" filter is applied first. Any formulation that fails fundamental thermodynamic or chemical boundary conditions (e.g., structural failure at continuous curing temperatures) is immediately eliminated.

Phase 2: Single-Decider AHP and Intra-Rater Reliability The AHP weighting is applied exclusively to the structurally viable survivors. While each formulation's empirical performance is evaluated on a standardized grading scale from 1 to 5, the relative importance (weight) of each metric is defined as a percentage established through the AHP, following the documented procedure by Saaty [44].

Crucially, the pairwise comparisons within this AHP were established by a single primary decision-maker (the author). While classical AHP literature favors multi-criteria expert panels aggregated via geometric means to establish consensus, this departure from qualitative consensus-building is strictly justified by the deterministic nature of the targeted industrial environment. The relative importance of each metric was not derived from subjective preference, but rather reverse-engineered directly from the non-negotiable physical, chemical, and thermodynamic constraints of the Nave 4 assembly line. By forcing pairwise comparisons via a single decider, the AHP methodology translates these rigid operational realities into a mathematically transitive hierarchy. The complete AHP comparison matrix, computed utilizing an analytical software calculator designed by Goepel [25], and the resulting percentage distribution graphs are detailed in Appendix A.1.2.

Finally, it is acknowledged that several variables within the decision matrix rely on qualitative assessments scored on an ordinal 1-to-5 scale. To protect the methodology against subjective drift, the protocol relies on the principle of Intra-Rater Reliability. Because a single evaluator applies a strict, standardized grading rubric across all samples under identical factory conditions, the relative performance deltas between the formulations remain highly accurate. Within the context of an isolated industrial DoE, this controlled internal consistency guarantees that the selection matrix correctly identifies the optimal relative solution, superseding the need for absolute, multi-operator objectivity.

Table 4.1: Evaluation metrics, assigned weights, and impact levels for the Weighted Decision Matrix.

Metric	Description	Weight (%)	Impact Level
$\mathbf{V_1}$	Application and handling of the putty.	3.000	Low
$\mathbf{V_2}$	Time until final sanding (bottleneck potential).	7.800	Medium
$\mathbf{V_3}$	Resistance to acidic passivation baths.	24.80	High
$\mathbf{V_4}$	Thermal resistance and outgassing during oven cure.	32.90	Critical
$\mathbf{V_5}$	Mechanical adhesion post-sanding.	3.300	Low
$\mathbf{V_6}$	Powder primer adhesion and electrostatic conductivity.	24.80	High
$\mathbf{V_7}$	Surface condition after the first putty application.	3.400	Low

To validate the mathematical integrity of the pairwise comparisons, the CR was calculated. In the AHP methodology, the CR measures the transitivity of the evaluator's judgments—ensuring that if metric A is prioritized over B, and B over C, then A is strictly prioritized over C. The pairwise logic established for this project yielded a CR of 3.0%, well below the universally accepted maximum threshold of 10% (0.10). It must be emphasized that this low ratio does not claim empirical scientific objectivity; rather, it proves that the formalized industrial bias and engineering judgments applied to the model are transitive, structurally consistent, and logically sound.

From Table 4.1, the varying variables can be divided into three major functional groups.

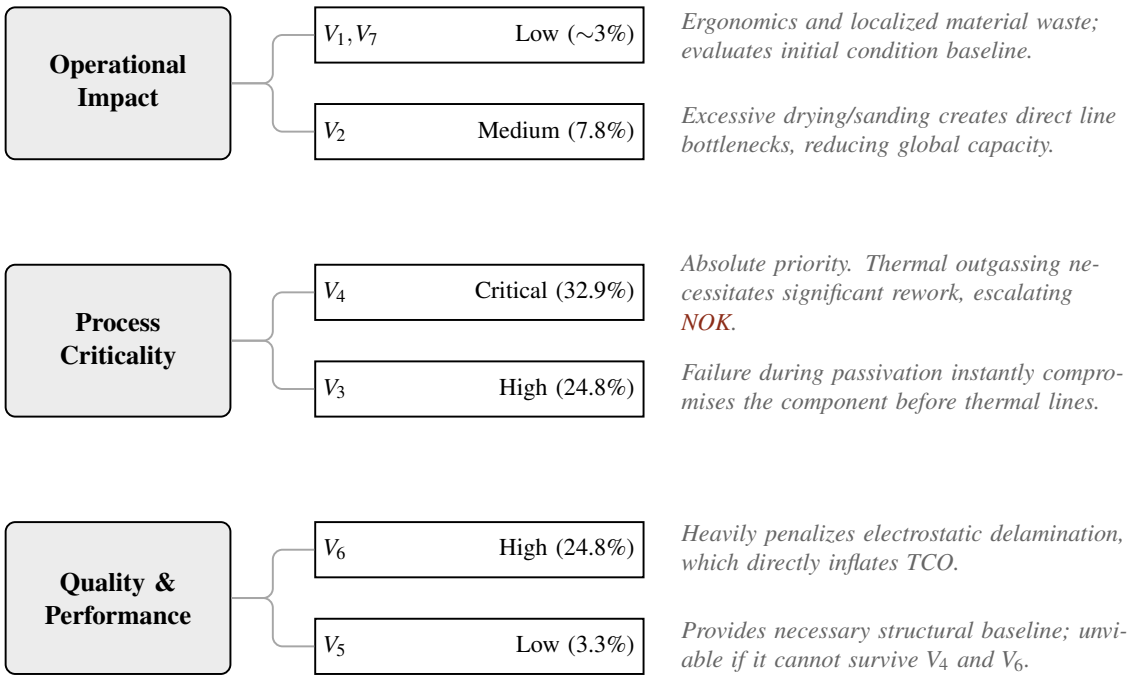

Figure 4.2: Functional mapping, weight assignment, and primary evaluation rationale for process variables.

In the case of V_7, it must be noted that any topcoat should be applied only after the putty reaches its optimal physical state; therefore, the evaluation isolates the initial putty condition rather than the overall first application sequence.

Regarding V_6, it was necessary to formulate a strict mathematical translation of the factory reality into the project framework. The mechanical adhesion of the baseline putties to the primed aluminum substrate was evaluated utilizing the cross-cut tape test, standardized under ISO 2409 (Standard [49]). Within the standard operating procedures of the manufacturing facility, the results of this test are treated as a binary quality control metric: a score of Class 0, Class 1, or Class 2 constitutes a "Pass," while any score of Class 3 or higher results in immediate component rejection.

While this binary classification is sufficient for baseline production quality control, it presents a statistical limitation for the DoE. Grouping Class 0 (maximum adhesion) and Class 1 (minor intersectional flaking) into a singular "Pass" metric mathematically blinds the analysis to subtle thermomechanical improvements generated by the nanomaterial additives. To capture this necessary granularity, and to standardize the entire experimental matrix so that a higher numerical value universally correlates to a superior material property across all tested variables (V_1 through V_7), the raw inverted ISO classifications were translated into a progressive 1-to-5 scoring system.

Statistical Treatment of Ordinal Data The ISO 2409 adhesion classification yields strictly ordinal data (Classes 0–5), where the physical intervals of coating detachment are discrete and not mathematically equidistant. However, to effectively map multifactorial interactions and generate topological optimization models, Response Surface Methodology (RSM) within Minitab's DoE framework is required.

As RSM algorithms operate on continuous variables, the discrete 0–5 classifications are mapped to a continuous axis. This parametric mapping is utilized specifically to extract directional optimization drivers and visualize factor interactions within standard industrial Six Sigma frameworks.

To guarantee that this mapping does not introduce topological distortion or parametric bias, a rigorous Sensitivity and Robustness Analysis protocol is established. The continuous parametric ANOVA outputs are systematically cross-validated against the non-parametric Kruskal-Wallis test, which strictly adheres to ordinal data assumptions. The protocol for this analysis will be defined in section 4.1.3.

The translation matrix was defined as follows:

Table 4.2: Translation matrix of ISO 2409 adhesion classes into the custom quantitative scoring system.

Score	Classification	ISO Class	Description of Flaking
5	Best Scenario	Class 0	The cut edges are completely smooth with 0% lattice detachment.
4	Industrial Pass	Class 1	Minor flaking at the intersections, affecting less than 5% of the cross-cut area.
3	Borderline Pass	Class 2	Flaking along the edges and intersections, affecting between 5% and 15% of the area.
2	Failure	Class 3 or 4	Significant partial or total delamination of the lattice squares.
1	Critical Failure	Class 5	Flaking beyond 65%.

The remaining detailed descriptions of the 1-to-5 scoring criteria for each variable were established to standardize operator evaluation and have been included in Annex A.1.1 for reference.

While fundamental materials science research traditionally relies on analytical characterization techniques such as Differential Scanning Calorimetry (DSC), Thermogravimetric Analysis (TGA), and Dynamic Mechanical Analysis (DMA) to quantify molecular-level kinetics and thermal transitions (e.g., T_g), the scope of this research is strictly defined as an applied industrial process optimization. In a high-volume manufacturing environment, absolute microscopic thermal stability curves are secondary to macroscopic boundary-condition survivability.

For instance, the precise degradation temperature gradient quantified by a TGA is functionally irrelevant if the polymer matrix outgasses at the factory's non-negotiable 180°C curing threshold. Therefore, this methodology deliberately bypasses isolated laboratory characterization in favor of empirical, heuristic scales (V_1 through V_7). These scales are not arbitrary visual approximations; rather, they are calibrated operational metrics designed to map physical material behavior directly to line-side production bottlenecks, rework costs, and pass/fail quality control standards.

By treating the assembly line's actual thermodynamic ovens and acidic passivation baths as the primary testing apparatus, the experimental design guarantees that the resulting optimization is immediately scalable and economically actionable. This macroscopic, boundary-driven approach successfully isolates the optimal industrial formulation without requiring abstract, decoupled laboratory quantification.

Because the assigned weights (W_i) are now normalized percentages derived from the AHP eigenvector ($\sum W_i = 1.0$), the maximum theoretical score (S_{max}) is inherently capped at 5.00. Assuming a maximum empirical evaluation (a score of 5) across all seven dependent variables, the maximum attainable score is defined as:

$$S_{max} = \sum_{i=1}^{7} (W_i \times 5) = 5.000 \text{ points} \tag{4.1}$$

Following the establishment of the maximum theoretical score, the actual performance of each putty formulation is calculated. The achieved score ($S_{achieved}$) is determined by multiplying the assigned empirical shop-floor grade (V_i, evaluated on the 1 to 5 scale) for each metric by its corresponding normalized AHP weight (W_i), and summing the results across all seven variables:

$$S_{achieved} = \sum_{i=1}^{7} (W_i \times V_i) \tag{4.2}$$

To facilitate a clear, standardized comparison across all tested formulations—and to later quantify the precise impact of the experimental graphene and alumina doping—the achieved score is then converted into an overall Efficacy Percentage ($E_{\%}$). Because the maximum theoretical score is mathematically fixed at 5.00, this final metric is calculated as follows:

$$E_{\%} = \left(\frac{S_{achieved}}{5.000} \right) \times 100 \tag{4.3}$$

In addition to the qualitative Efficacy Percentage ($E_{\%}$), the total cross-sectional thickness of the applied layers will be quantitatively measured (in μm) to establish the volumetric failure thresholds of each matrix. For the baseline formulations evaluated without a liquid primer (denoted by the '-0' suffix), this specific measurement comprises the combined thickness of the applied putty and the final powder coating. Conversely, for the experimental variations incorporating the intermediate chemical barrier, the total measured thickness encompasses the base putty, the primer variable, and the final powder coating layer. These quantitative measurements will be correlated directly with the thermal outgassing scores (V_4) to determine the strict physical application limits of each formulation on complex geometries.

4.1.2 Heuristic Stage-Gate Screening Protocol

To rapidly identify the most promising candidates from the expanded experimental pool—which encompassed 32 distinct formulation-primer combinations—an initial heuristic stage-gate screening was implemented, taking into account strict industrial production constraints that govern the factory production line. This preliminary phase utilized a single, worst-case boundary application ($N = 1$) per formulation on discarded structural frames.

It is critical to note that this phase was explicitly designed not as a parametric statistical evaluation, but as a phenomenological culling mechanism. While standard academic protocols dictate $N \geq 3$ to isolate special-cause anomalies from systemic material behavior, applying such metrics to this specific industrial screening would misrepresent the nature of the targeted failure modes.

The criteria for elimination at this stage—specifically chemical dissolution in the passivation bath (V_3) or significant thermodynamic outgassing in the curing oven (V_4)—are binary, macroscopic material failures dictated by fundamental polymer chemistry, not micro-variances induced by random environmental fluctuations. A heavily cross-linked matrix does not completely dissolve in an acidic bath due to a random humidity spike; it dissolves due to inherent chemical incompatibility.

Furthermore, to mitigate the risk of Type II errors (the false elimination of a viable matrix due to operator variability), all $N = 1$ screening applications were executed by a single, senior master-technician, strictly controlling the ergonomic application baseline. Therefore, the $N = 1$ heuristic approach was scientifically justified: it rapidly eliminated chemically non-viable matrices based on absolute thermodynamic and chemical thresholds, successfully isolating the macroscopically viable formulations for the subsequent multi-replicate DoE phase.

While future scalability studies would undoubtedly benefit from Fractional Factorial DoE or Taguchi Orthogonal Arrays to establish statistical power with reduced experimental runs, this $N = 1$ heuristic approach successfully and efficiently isolated the macroscopically viable formulations for subsequent rigorous testing. The workflow followed a strict, sequential evaluation process.

To systematically evaluate the thermomechanical behavior of the formulations, the theoretical experimental space for this screening phase was strictly defined by two primary categorical factors (Table 4.3).

Table 4.3: Experimental Protocol: Factors and levels of the Screening Phase.

Factor	**Type**	**Levels**	**Level Details**
$\mathbf{X_1}$	Categorical	16	8 Unmodified commercial baselines (ES, PD, NT, T8, MP, P70, CH, IM) and 8 corresponding additive-enhanced variants (suffix '1').
$\mathbf{X_2}$	Categorical	2	0: No primer 2: With 2K Primer (Supplier M or R).

Nomenclature Note: To maintain strict traceability throughout the DoE, formulation matrices are designated by their letter ID (e.g., PD, ES). Formulations doped with functional nanomaterials receive the suffix '1' or '2' attached to their base ID (e.g., PD1, PD2). The primer state is separated by a hyphen: **'-0'** denotes an unprimed state, while **'-2R'** denotes the application of the 2K Primer R, for example.

As established in Table 4.3, the evaluation matrix is governed by these two final variables:

- **Factor $\mathbf{X_1}$ (Formulation and Additive State):** A categorical factor defined by 16 theoretical levels. This encompasses the 8 unmodified commercial baseline putties (ES, PD, NT, T8, MP, P70, CH, IM) and their 8 corresponding additive-enhanced variants, denoted with the suffix '1' (ES1, PD1, NT1, T81, MP1, P701, CH1, IM1).

- **Factor $\mathbf{X_2}$ (Primer Interface):** A categorical factor defined by 2 levels to evaluate the impact of an intermediate chemical layer on electrostatic adhesion and outgassing. Level 0 represents the unprimed baseline, and Level 2 represents the application of a 2K Primer, pending the final selection between Supplier M and Supplier R.

Regarding product specifications, it is possible to find them in Table 4.4:

Designation	Material Description & Specifications
PD	Legacy polyester putty.
ES	Legacy epoxy putty.
NT	Experimental epoxy putty utilized for factory testing.
MP	Polyester putty tested for thermal resistance up to 180°C.
T8	Polyester putty tested for thermal resistance up to 160°C.
P70	Polyester putty infused with aluminum powder.
IM	Polyester putty infused with a higher percentage of aluminum powder.
CH	Hybrid polyester/metallic putty tested for thermal resistance at 220°C for 30 minutes. Manufacturer specifications indicate optimal performance for powder coating compatibility and the concealment of weld seams.

Table 4.4: Nomenclature and technical specifications of the base putty matrices utilized in the study.

First, the specimens were applied across the designated frame zones with careful attention to prevent process bias, thereby ensuring valid transferability to standard operations and providing baseline data for application ergonomics and putty state (V_1, V_5, V_7). Following application, the respective curing times were recorded (V_2). The frames were then sent through the production line, where the passivation bath served as a crucial physical Hard Gate (V_3).

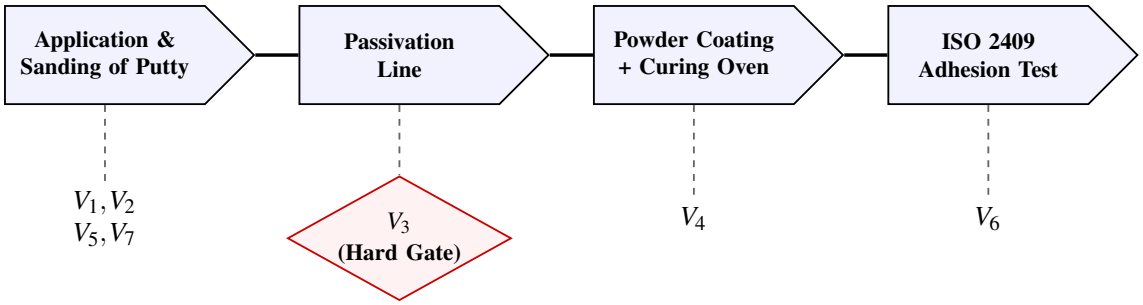

Figure 4.3: Chronological stage-gate screening sequence. Formulations progress horizontally through distinct processing gates, where critical empirical variables (V_1–V_7) are measured.

Although the AHP decision matrix mathematically assigns the absolute highest criticality to thermal resistance (V_4), the physical chronology of the manufacturing line dictates that passivation acts as the primary sequential threshold. A putty formulation cannot realistically be evaluated for high-temperature oven survival if its structural and chemical integrity has already been compromised by acidic degradation. Furthermore, altering the chemical composition of these baths to accommodate a sensitive putty formulation would necessitate a complete halt of the factory's production line—an economically and operationally unfeasible scenario for the time period allocated to the project. Consequently, any formulation exhibiting chemical degradation (an evaluation of

less than 3 in V_3) at this stage was immediately disqualified from being considered a viable industrial solution. The schematic representation can be found in Figure 4.3.

Disqualified putties still progressed through the remainder of the line to undergo full data collection. This ensured a comprehensive Root-Cause Analysis (RCA), providing clear cause-and-effect relationships regarding subsequent thermal and electrostatic failures, and generating valuable empirical feedback for material suppliers. Finally, each specimen was scored against the previously established V_1–V_7 decision matrix, and the three formulations securing the highest cumulative scores advanced to the rigorous multi-replicate DoE phase.

4.1.2.1 Additive Allocation Strategy

To formulate the X_1 enhanced levels (e.g., MP1, PD1) and address the thermodynamic and mechanical stresses anticipated in the curing oven, two specific additives will be considered for integration, following targeted consultations with the suppliers.

Alumina (Al_2O_3) will be utilized for its documented ceramic thermal stability. As established in Section 3.5.1.1, when integrated into a polyester matrix, alumina particles create a dense physical barrier that increases the tortuosity of the outgassing path, effectively shielding the matrix and suppressing the rapid expansion of trapped solvents or unreacted styrene.

Graphene will be integrated for its immense functional surface area and superior thermal conductivity, as explored in Section 3.5.1.1. The platelet structure of graphene provides vast molecular anchoring points to improve interfacial adhesion between the putty and the aluminum substrate, while its thermal conductivity prevents the formation of localized "hot spots" within the putty patch during the oven cycle.

The integration targets were defined as follows:

Additive	**Target (vol%)**	**Primary Functional Rationale**
Alumina	5	Maximizes thermal conductivity and physical shielding during the oven cure without rendering the matrix excessively brittle.
Graphene	0.6	Forms a continuous semi-conductive network for electrostatic powder adhesion.

Table 4.5: Target volumetric concentrations and primary functional rationale for matrix integration.

The volumetric targets summarized in Table 4.5 were established based on strict theoretical and operational constraints. For alumina it targets establishes the optimal “sweet spot” in accordance with the findings of Moreira et al. [37], while the the 0.6 vol% value for graphene was selected because it safely exceeds the theoretical electrical percolation threshold of 0.52 vol% established by Goudarzi et al. [26].

While the theoretical targets for the functional additives are defined by volume percentage (vol%) to ensure proper spatial distribution within the polymer matrix, the physical compounding of the putty on the shop floor must be executed by weight (mass). To achieve this, the theoretical volume fractions are converted into actionable mass measurements utilizing the specific densities of the baseline matrices and their respective fillers.

To determine the exact mass of additive required per batch of putty, the following density-based conversion formula is applied:

$$m_{additive} = \left(\frac{V_{target} \times \rho_{additive}}{(1 - V_{target}) \times \rho_{putty}} \right) \times m_{putty} \tag{4.4}$$

Where $m_{additive}$ is the required mass of the filler, V_{target} is the targeted volume fraction (e.g., 0.05 for alumina), $\rho_{additive}$ is the density of the specific nanomaterial, ρ_{putty} is the baseline density of the unmixed commercial putty, and m_{putty} is the desired total mass of the base putty batch. This rigorous conversion ensures that the thermodynamic and electrostatic properties observed in the literature are accurately replicated within the physical test specimens.

Note on Occupational Health and Safety The decision to allocate graphene nanoplatelets to the matrix—despite the known inhalation hazards associated with airborne carbonaceous nanomaterials—was made following a strict comparative risk assessment against the commercial silver-coated e-conductives. The rejected commercial alternatives were classified as CMR (Reprotoxic) and STOT RE 2 hazards, presenting a systemic chemical toxicity that is inherently difficult to mitigate in an open shop-floor environment. In contrast, graphene nanoplatelets present a physical, particulate hazard strictly localized to the mechanical abrasion (sanding) phase, as the nanomaterial is otherwise fully encapsulated within the cured epoxy matrix. This physical risk does not introduce a new hazard class to the facility; rather, it is fully mitigated by the factory's existing hierarchy of controls. Specifically, the integration relies on established industrial dust-management protocols, mandating the use of localized HEPA-vacuum extraction at all sanding stations and standard FFP3/P3 respiratory protection. Consequently, graphene was selected because its physical risks are manageable via existing engineering controls, whereas the chemical toxicity of the alternatives was not.

4.1.2.2 Additive Choice Criteria

While the X_1 factor defines eight enhanced formulations, the specific additive used to create these upgraded variants will not be executed arbitrarily. Instead, a targeted, conditional application strategy will be employed, dictated entirely by the empirical results obtained during the first screening phase (Mode 0). The specific functional modifier applied to upgrade a baseline formulation will be selected to directly mitigate its most prominent failure mode, governed by strict quantitative thresholds on the 1-to-5 evaluation scale.

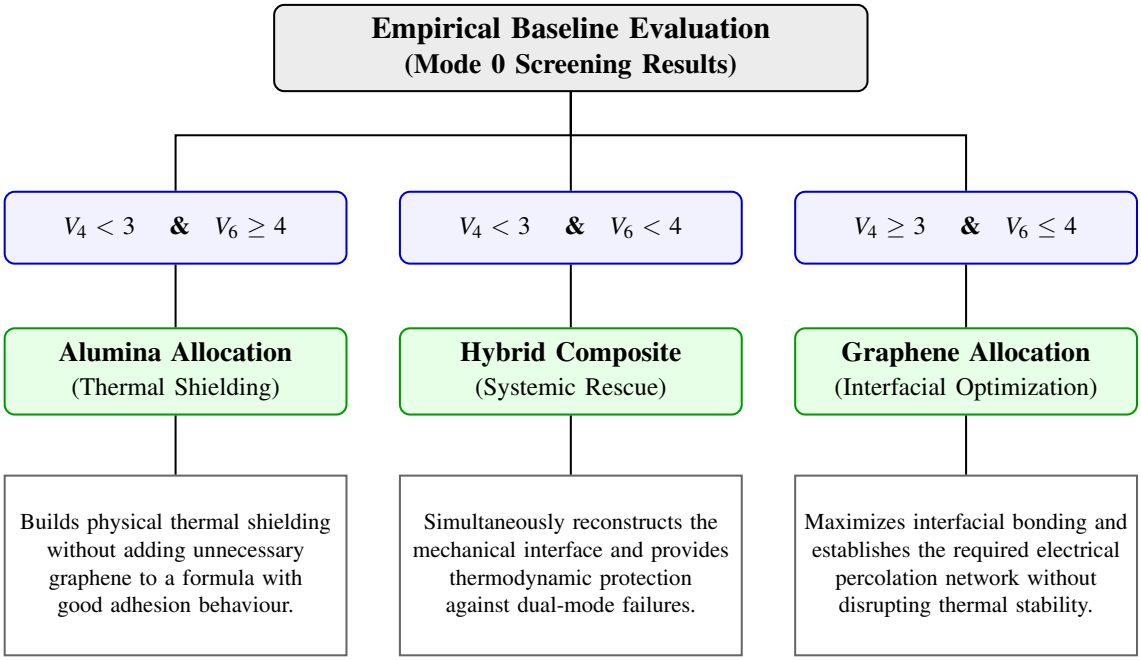

Figure 4.4: Decision-tree logic dictating the strategic allocation of functional modifiers.

This conditional logic guarantees that advanced nanomaterials are utilized strictly as targeted, mathematically justified engineering solutions to the specific empirical defects identified during the initial baseline screening.

4.1.2.3 Nanocomposite Compounding Strategy

The physical integration of high-surface-area nanomaterials into a highly viscous unsaturated polyester matrix presented a significant rheological challenge. Standard low-shear manual compounding methods are inherently insufficient to break down the agglomeration tendencies of graphene nanoplatelets or to ensure the homogenous bulk distribution of alpha-alumina.

To achieve the rigorous dispersion required for reproducible experimental trials, compounding was executed using a planetary centrifugal mixer (Thinky Mixer) located at the University of Aveiro. This equipment resolved the immediate compounding constraints by utilizing dual-axis centrifugal rotation to generate significative internal shear forces without the use of invasive mechanical blades. Initial validation trials confirmed that this protocol successfully dispersed both the bulk alumina and the graphene nanoplatelets within the high-viscosity matrix, effectively breaking down agglomerates while simultaneously degassing trapped macroscopic air voids. Consequently, this planetary centrifugal mixing method was formalized as the standardized compounding protocol to guarantee the structural homogeneity of all subsequent DoE formulations.

Scale of Research and TRL The developmental scope of this thesis is strictly bounded within Phase 1 of the industrial scale-up framework, corresponding to TRL 3 to 4. The foundational

objective is not to replicate final industrial morphology, but to empirically validate the baseline chemical affinity and polymerization kinetics of the nanocomposite matrices.

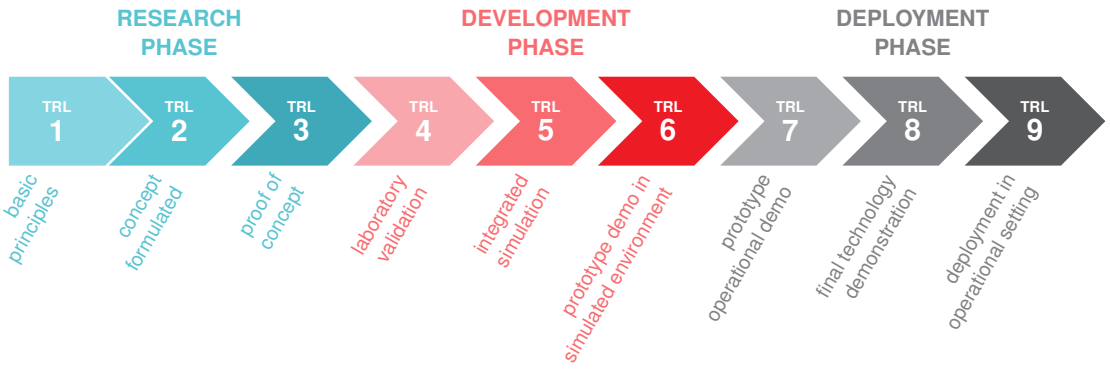

Figure 4.5: TRL denominations. Source: Autohas-waechtershaeuser [7].

While planetary mixing (Thinky mixing) introduces distinct morphological dispersion profiles that do not scale linearly to continuous, high-volume manufacturing, its inclusion was a deliberate methodological control. This highly regulated, high-homogeneity technique isolates the fundamental chemical performance of the nano-additives—specifically verifying the absence of steric hindrance during polymerization—from the unpredictable shear-induced variance inherent to industrial compounding environments.

Consequently, this methodology establishes a validated chemical blueprint. The subsequent transition to TRL 5 and 6—which will require morphological scaling via advanced high-shear dispersion, three-roll milling, or continuous twin-screw extrusion—is defined as out-of-scope for this initial feasibility study. These high-shear scaling protocols are designated as mandatory milestones in the project's future industrial roadmap, to be executed collaboratively with chemical suppliers prior to shop-floor deployment.

4.1.2.4 Stepwise Rheological Compounding Protocol

Based on empirical evidence from the initial compounding trials, reliance on centrifugal forces alone was insufficient for bulk filler integration. Consequently, a three-stage compounding protocol utilizing rigid milling media was standardized.

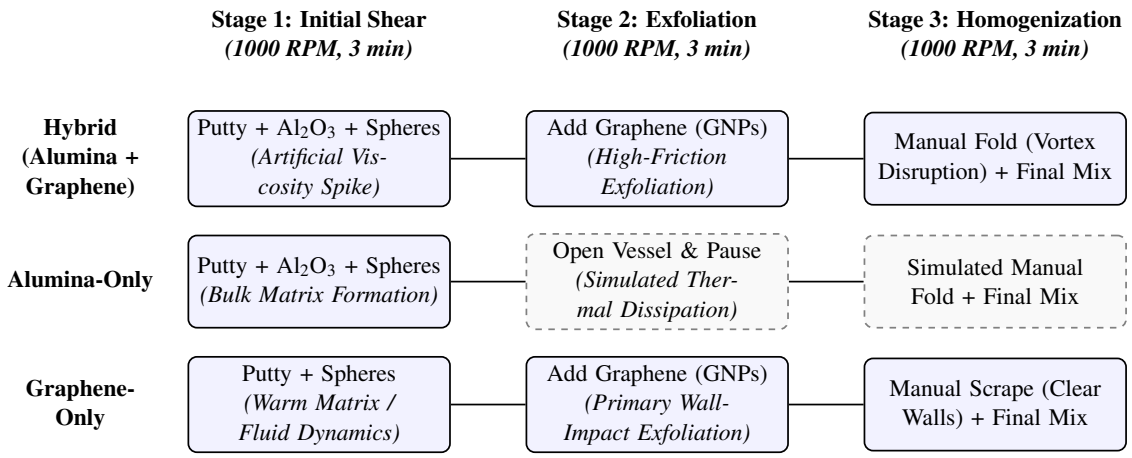

Figure 4.6: The three-stage centrifugal compounding protocol. Dashed boxes indicate carefully simulated procedures designed to maintain an identical shear history and uniform thermal stress.

To maintain statistical validity within the DoE, it was critical to standardize the "shear history", as seen in Figure 4.6 Every formulation, regardless of its specific filler composition, was subjected to an identical cumulative shear duration (9 minutes total at 1000 RPM). This ensured that the polymer chains across all batches experienced uniform thermal and mechanical stress.

4.1.3 Phase 2: Parallel DoE Architecture

The three top-performing formulations identified during the Phase 1 screening will advance to a rigorous, statistically controlled Phase 2 evaluation. To definitively validate these optimal thermo-mechanical solutions and statistically isolate the interactions between the functional nanomaterials and the 2K primer, a Phase 2 Parallel DoE Strategy is implemented.

For each of the three winning formulations, its core chemical matrix is isolated. Rather than evaluating divergent matrices against each other within a single, statistically noisy model, an independent 2×2 General Full Factorial Design is constructed around that specific matrix family to evaluate Factor A (Modification State: Unmodified vs. Modified) against Factor B (Primer State: Unprimed vs. 2K Primer).

Table 4.6: Phase 2 Experimental Design: Rigorous DoE parameters for the top 3 screening candidates.

Variable	Type	Levels	Details
A	Categorical	2	**U:** Unmodified Baseline Formula **M:** Modified (Doped) version of the Putty
B	Categorical	2	**0:** Unprimed baseline **2 (R or M):** Application of the selected 2K Primer
N	Replicates	3	Three distinct samples per combination to ensure statistical validity and reproducibility.

This methodology, as outlined in Table 4.6, ensures that even if a doped variant wins Phase 1, it is rigorously tested alongside its unmodified counterpart in Phase 2. This creates a highly controlled comparative environment across 36 randomized test specimens, allowing the exact performance delta (Δ) of the additive to be mathematically proven.

Throughout this testing cycle—regardless of the activated scenario—the specimens will be rigorously evaluated against the complete spectrum of the seven established response variables (V_1 through V_7). These variables will capture granular quantitative and qualitative data across all operational metrics, ranging from initial application ergonomics (V_1) and curing kinetics (V_2), to high-temperature outgassing (V_4) and final electrostatic adhesion (V_6).

Adaptive Experimental Architecture and Resource Reallocation

Because this research is executed within the constraints of a live, high-volume manufacturing environment, an **Adaptive Experimental Design** is established to mitigate the risk of catastrophic variable failure. Specifically, the execution of the 2×2 factorial model is strictly contingent upon the initial process-compatibility of Factor B (the 2K Primer). Consequently, two distinct execution scenarios are pre-defined for Phase 2:

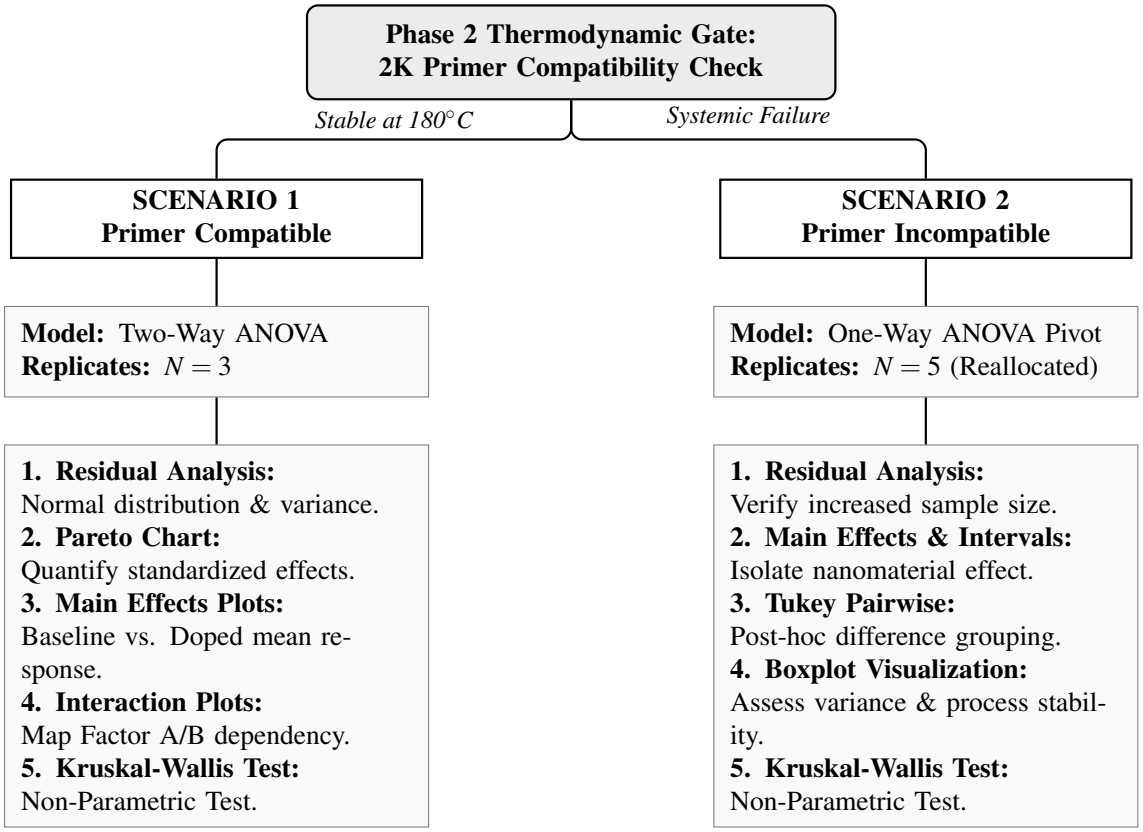

Figure 4.7: Adaptive experimental architecture and active statistical treatments based on Phase 2 primer compatibility.

Statistical Treatment and Comparative Analysis The extracted data will be processed utilizing an adaptive statistical framework dictated by the activated Phase 2 scenario, operating at a standard 95% confidence interval ($\alpha = 0.05$). The statistical software will evaluate both the final aggregated Efficacy Percentage ($E_{\%}$) and execute independent analyses for each individual response variable (V_1 through V_7).

This multi-response separation evaluates the specific performance differences (Δ) induced by the functional additives within each native polymer matrix. Evaluating the variables individually avoids the masking of operational trade-offs (e.g., determining if a specific additive increases cross-linking cure time V_2 to achieve the required thermal stability V_4). The final evaluation will cross-analyze these differences to determine which formulation achieves the highest overall quality score and which chemical matrix responds most favorably to nanoparticle doping.

Interpretation of Statistical Outputs To transition from raw data to analytical conclusions, Minitab outputs will be interpreted through frameworks mapped in Figure 4.7. These frameworks are designed to isolate structural viability and process consistency:

- **Residual Analysis:** Validates foundational ANOVA assumptions (normal distribution and constant variance) to ensure model reliability.
- **Pareto Chart of Standardized Effects:** Quantifies the magnitude of each variable, identifying if Factor A (doping), Factor B (primer), or their interaction meets the critical significance threshold ($\alpha = 0.05$).
- **Main Effects & Interval Plots:** Map mean responses against the baseline, visualizing the directional impact (increase/decrease) of nanomaterial doping.
- **Interaction Plots:** Evaluate whether nanocomposite efficacy operates independently or is statistically dependent on the presence of the 2K primer.
- **Tukey Pairwise Comparisons:** Provides post-hoc groupings to calculate the statistical difference between specific additive formulations, isolating the most favorable combination.
- **Boxplot Visualization:** Assesses process stability by visualizing dispersion, specifically identifying reductions in lower-tail outliers or narrowing of the interquartile range (improved process consistency).
- **Kruskal-Wallis Test:** Serves as the non-parametric fallback to confirm significance in data sets that violate normality assumptions.

Because macroscopic aggregation metrics (such as Global Efficiency) calculate the mathematical mean of multiple variables, they introduce a statistical vulnerability: they can obscure localized boundary-condition failures. In an industrial context, a formulation that achieves exceptional workability but fails in the curing oven may yield the same mean efficiency score as a formulation that performs moderately but reliably across all stations.

Therefore, relying exclusively on an ANOVA to evaluate aggregated efficiency is insufficient for industrial material selection. A failure to reject the null hypothesis ($p \geq 0.05$) at the macroscopic level merely proves that the formulations are equivalent in their average performance; it does not guarantee equivalence in process variance or failure-rate probability. To prevent the erroneous selection of a statistically tied but operationally unstable material, a strict, two-tiered optimization protocol was defined *a priori* for final formulation selection:

- **Tier 1: Macroscopic Statistical Dominance:** Formulations are first evaluated for consistent statistical significance ($p < 0.05$) across both parametric and non-parametric models regarding overall Global Efficiency. If a formulation achieves macroscopic statistical dominance, it is mathematically declared the optimal matrix.

- **Tier 2: Boundary-Condition Resolution (The Variance Filter):** In the event of a macroscopic statistical deadlock—where formulations yield $p \geq 0.05$, strictly indicating a failure to reject the null hypothesis regarding the aggregated mean—classical statistical differentiation reaches its limit. At this point, the optimization protocol systematically cascades to Tier 2. Rather than fabricating a conclusion, Tier 2 breaks the statistical tie by isolating the empirical variance and absolute survivability within the factory's most critical bottlenecks (specifically thermal degradation resistance, V_4, and interfacial adhesion, V_6). A formulation that achieves statistical parity in the macro-metric, but demonstrates a deterministic elimination of probabilistic defects in these critical sub-metrics, is definitively classified as the optimized industrial solution.

4.2 Route Mapping and Iterative Process

Although the finalized methodology culminated in the precise DoE architecture detailed in Section 4.2, this experimental framework was the result of a highly iterative process. The developmental journey was marked by industrial contingencies, necessary methodological adaptations, and the strict implementation of a lean, rigorous engineering mindset.

The initial phase of this project aimed to systematically evaluate the performance of various putty formulations to identify the most viable candidate for the process requirements. To achieve this, a structured DoE was developed to test the formulas, observe the relationships between process variables, and objectively select the optimal putty utilizing the weighted decision matrix.

Seven distinct experimental hypotheses, ranging from 12 to 48 specimens, were initially proposed to account for potential time and resource constraints. These proposals ranged from basic comparative analyses of current market solutions to strictly in-house additive development, alongside the investigation of protective primer interfaces. Ultimately, to ensure maximum statistical rigor and to comprehensively evaluate the multi-variable interactions, the most exhaustive methodology was selected, guaranteeing a full-scope analysis of the available technological pathways.

4.2.1 Independent Variables and the Initial Experimental Matrix

The foundational experimental design was constructed upon two primary independent categorical variables (factors), as detailed in Table 4.7.

Table 4.7: Initial Experimental Design (DoE) factors and categorical levels.

Factor	Type	Levels	Level Details
$\mathbf{X_1}$	Categorical	8	EP, PD, NT, M, and their respective modified versions: EP1, PD1, NT1, and M1.
$\mathbf{X_2}$	Categorical	2	0: No Primer 1k: With Primer

In this scenario, the M formula represents a newly sourced commercial alternative. Combining these factors (8 formulations $\times$ 2 primer states) resulted in 16 unique experimental conditions. To ensure statistical rigor, three replicates ($N = 3$) were mandated per condition, establishing an initial testing batch of 48 individual specimens. To maintain strict traceability, a standardized nomenclature was adopted (e.g., *EP-1k-R1* denoting EP Putty, with primer, Replicate 1). Furthermore, a rigorous randomization protocol was enforced. To prevent external confounding variables—such as diurnal fluctuations in ambient humidity or operator fatigue—from skewing the empirical data, the sequence of the 48 tests was completely randomized. The testing protocol explicitly forbade the consecutive processing of three replicates from the same putty batch.

4.2.2 Logistics Expansion and Supplier Engagement

Following the definition of the initial experimental scope, active market engagement was initiated to source theoretical alternatives. Four distinct putty manufacturers and three chemical additive suppliers were formally consulted. To provide necessary context regarding the facility's thermodynamic and chemical constraints, shop-floor tours were conducted for the respective technical representatives. The industrial response to these consultations was unexpectedly robust, yielding a multitude of proposed solutions that significantly expanded the scope of the project.

4.2.2.1 Supplier Feedback and Material Selection

Supplier engagement and internal R&D yielded diverse technical proposals, necessitating strict evaluation against the facility's production and safety constraints.

Regarding chemical additives, proposed modifiers included aluminum e-conductives (aluminum-coated silver particles) and a specific epoxy diluent engineered to mitigate outgassing during thermal cycles. In contrast, two proposed epoxy modifiers were immediately disqualified prior to testing due to their CMR classifications, which violated the factory's operational safety mandates.

Concurrently, the experimental matrix was expanded to integrate several novel commercial and internally sourced base formulations (MP, T8, P70, IM, and CH). In addition to the bulk

polymer matrices, intermediate chemical layers were introduced into the DoE to evaluate their potential as thermal and chemical barriers during the acidic passivation and high-temperature curing phases—specifically, a 1K solvent-borne epoxy primer and a 2K epoxy primer.

Methodological Note on Empirical Validation of Theoretical Constraints From a strict thermodynamic and polymer science perspective, the application of a 1K solvent-borne primer prior to a rapid, high-ramp electrostatic powder coating oven presents a fundamental structural contradiction. 1K systems dry via solvent evaporation; exposing entrapped volatile solvents to a sudden 180°C shock-cycle inevitably induces flash-boiling, leading to outgassing and film rupture. Despite this known theoretical constraint, the 1K primer was deliberately retained within the experimental screening. This empirical trial was not executed to discover or validate basic chemistry, rather, it was a strictly required commercial qualification gate. In industrial R&D, external chemical suppliers frequently propose "advanced" 1K formulations, claiming proprietary rheological modifications that theoretically resist standard thermal limits.

To officially reject a proposed commercial solution and satisfy the traceability requirements of the procurement department, a theoretical dismissal is insufficient. The candidate material must be subjected to the exact thermodynamic ramp-rate of the factory's physical oven. The resulting physical rupture and flash-boiling did not merely confirm basic thermodynamics; it provided the deterministic, documented failure required to formally close the commercial supplier gate. This empirical documentation was a necessary administrative and engineering prerequisite to justify the financial transition to higher-cost, highly-crosslinked multi-component (2K) systems.

4.2.3 Updated Experimental Matrix and Contingency Execution

Due to the influx of proposed materials, the independent variables were structurally expanded. Factor 1 (X_1) increased to 16 levels, encompassing eight base formulas (ES, PD, NT, T8, MP, P70, CH, IM) and their modified variants. Factor 2 (X_2) expanded to three categorical levels: No Primer (0), 1K Primer (1k), and 2K Primer (2k).

Executing a full factorial design with the original $N = 3$ replication strategy for all combinations became logistically unfeasible. Consequently, the methodology was restructured into the two-phased Stage-Gate approach documented in Section 4.1.1.

To manage varying supplier lead times and maximize testing density, the physical application strategy was also optimized. Initial destructive sampling—cutting discarded frames to extract isolated weld junctions—was abandoned due to high resource consumption. Instead, entire "junk" frames were utilized, with up to four distinct formulations applied to strategically selected, geometrically comparable welded zones. This ensured an impartial geometric baseline while maintaining direct transferability to standard factory scenarios. Detailed mapping of these application zones and nomenclatures (e.g., Frame X1, X2) is provided in Annex A.9.

4.2.4 Thermal Incompatibility and Elimination of the 1K Primer

With the screening methodology firmly established, Phase 1 testing commenced on the initial batch of formulations. This included the baselines (ES, PD, NT), the newly sourced alternatives (MP, T8, P70), and their respective interactions with the 1K epoxy primer. To establish a rigorous control, the specimens were tested both with the 1K primer (suffix "-1") and without any primer (suffix "-0").

Additionally, an exploratory application method (suffix "-A") was introduced for the PD formulation to observe if altering the curing mechanics would impact thermal survivability. Method A consisted of applying a thin base layer, allowing a 10-minute ambient flash-off period, followed by a top layer and a final 20-minute cure prior to sanding.

Upon processing these initial specimens through the continuous production line and evaluating them against the weighted decision matrix, a critical systemic failure emerged during the oven curing stage (evaluated under variable V_4: Thermal Resistance), with the visual evidence in Figure 4.8.

Table 4.8: Comparative Thermal Outgassing Analysis: Baseline vs. 1K Primer Variation.

Formulation Pair	**Baseline V_4 Score**	**"-1" V_4 Score**	ΔV_4
MP-0 $\rightarrow$ MP-1k	1	1	0
T8-0 $\rightarrow$ T8-1k	1	1	0
P70-0 $\rightarrow$ P70-1k	1	1	0
PD-0 $\rightarrow$ PD-1k	3	1	-2
ES-0 $\rightarrow$ ES-1k	4	1	-3
NT-0 $\rightarrow$ NT-1k	4	1	-3

(a) Failure of the 1k primer in the ES putty.

(b) Close-up of the defect.

Figure 4.8: Process incompability with the 1k primer.

4.2.4.1 RCA of 1K Thermal Reactions

The empirical data instantly highlighted a catastrophic failure mode intrinsically linked to the 1K primer. As evidenced in Table 4.8, every single formulation coated with the 1K primer (MP-1k, T8-1k, PD-1k, ES-1k, NT-1k, PD-1k-A, and P70-1k) received a score of 1 in the V_4 metric. This indicated significant outgassing, and a loss of structural integrity upon exposure to the powder coating oven.

As illustrated in the Ishikawa diagram (Figure 4.9), this thermal failure occurred irrespective of the underlying putty's native resistance. Even the epoxy-based formulations (ES and NT), which achieved passing scores of $V_4 = 4$ in their unprimed state, failed ($V_4 = 1$) when the 1K primer was applied. This data pattern isolated the root cause to the 1K primer's inherent chemistry. Because 1K primers dry via solvent evaporation rather than chemical cross-linking, residual solvents become entrapped within the film.

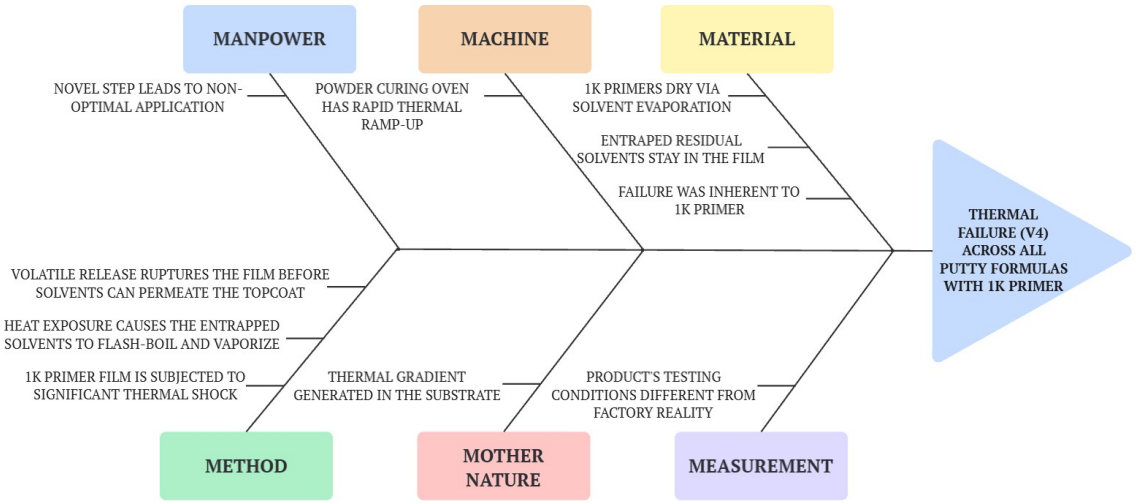

Figure 4.9: RCA of the 1k primer failure.

To validate the physical mechanism behind the outgassing, thermal profiling of the curing oven was executed. Temperature differentials were recorded for both the ambient oven air and the physical surface of the aluminum frame across various welded zones. The resulting data confirmed a rapid thermal ramp-up. Although the nominal target curing temperature for the powder process is 180°C, the frame surface was subjected to a steep thermal gradient in the last 10 minutes due to heat transfer from the oven to the substrate.

This profiling highlighted a discrepancy in measurement: the product's idealized testing conditions differ significantly from the factory's thermal reality. Furthermore, introducing this novel primer layer to the process led to non-optimal manual applications, creating uneven film thicknesses that further hindered standard solvent evaporation.

Ultimately, the immediate exposure to these oven temperatures causes the entrapped solvents within the primer matrix to flash-boil. The volatiles vaporize and physically rupture the protective film before they can safely permeate the topcoat, resulting in the cratering observed across all

1K specimens. Consequently, the 1K primer was eliminated from all subsequent experimental matrices.

4.2.5 Methodological Pivot and Supplier Feedback Loop

Because the 1K primer actively degraded the performance of otherwise viable putties—acting as a catalyst for thermal failure rather than a protective barrier—it was deemed fundamentally incompatible with the thermodynamic reality of the factory. Consequently, any modifications made to the underlying putties via chemical additives would fail to improve the V_4 scores, as the outgassing originated entirely from the primer interface.

Crucially, the experimental methodology functioned as an active feedback loop with the external supply chain. Upon presenting the empirical thermal degradation data to the supplier who originally recommended the 1K system, their technical team officially acknowledged the thermodynamic limitations of solvent evaporation at 180°C. In direct response to this data, the supplier strategically pivoted, replacing their failed 1K sample with a robust two-component (2K) epoxy primer.

This development validated the initial approach suggested by a competing supplier, who had mandated a 2K system from the project's inception. Unlike 1K systems, 2K primers utilize a chemical hardener to initiate a cross-linking cure, creating a denser, highly stable polymer network theoretically capable of surviving the thermal shock without outgassing. Moving forward, the screening process strictly isolated the unprimed formulations (Mode 0) against the 2K primer variations (Mode 2). This decisive stage-gate elimination prevented the unnecessary expenditure of factory resources on the remaining putty formulations.

Following the empirical elimination of the 1K primer (detailed in Section 4.2.4), the methodology pivoted exclusively to 2K (two-component) epoxy primers. To optimize this newly established Factor X_2, the screening process was updated to evaluate two distinct commercial 2K primers (Primer M and Primer R). Figure 4.10 illustrates the comparative curing kinetics utilized for this evaluation.

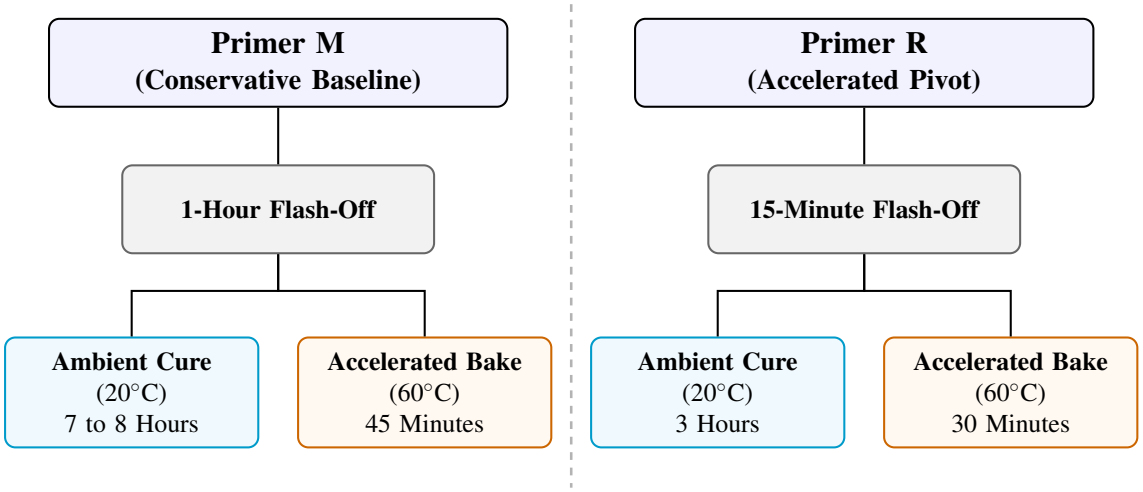

Figure 4.10: Comparative curing kinetics for the Factor X_2 evaluation.

To objectively evaluate the trade-off between curing speed and high-temperature thermal stability, a specific parallel test was deployed. Two identical discarded frames were prepared using the same underlying four putty formulations. Primer M was applied to the first, and Primer R to the second. To ensure curing kinetics remained the sole independent variable, application parameters (pneumatic spray pressure, distance, and pass count) were standardized across both frames to enforce a constant nominal cross-sectional thickness.

The objective was to definitively determine if the highly accelerated cross-linking kinetics of Primer R compromised its ability to resist the powder curing oven temperatures. If successful, Primer R would represent a vastly superior operational solution by significantly reducing the process takt time (V_2).

4.2.5.1 Surface Activation and Interfacial Preparation

Following the thermal curing of the 2K primer, a critical surface activation step was mandatory to ensure optimal interfacial adhesion with the final powder coat. This step overcomes the "glassy" surface tension natively exhibited by fully cross-linked 2K epoxies, which inherently inhibits mechanical anchoring. The activation was executed utilizing a manual sanding technique with P500/P600 grit abrasive media. This specific parameter was governed by two technical constraints:

- **Surface Energy Enhancement:** The fine grit induces a micro-topography that exponentially increases the available surface area for mechanical interlocking without introducing deep lacerations capable of propagating through the thin powder topcoat.

- **Coating Integrity:** Manual abrasion provides precise tactile feedback to the operator, ensuring that the activation process does not compromise the Dry Film Thickness (DFT) of the primer layer, thereby preserving its function as an impermeable chemical barrier against the passivation baths.

4.2.6 Engineering Contingencies and Circular Economy Limitations

While the stage-gate screening successfully managed the influx of commercial formulations, the parallel investigation into custom functional additives introduced unforeseen contingencies. Transitioning theoretical material science directly onto an active shop floor often triggers an "implementation shock"—a stark reality where materials that excel in isolated laboratory environments violently clash with the strict safety protocols and environmental realities of industrial production.

4.2.6.1 Implementation Shock of Commercial E-Conductives

The initial strategy to resolve thermal and electrostatic deficiencies relied on aluminum-coated silver particles. However, a Safety Data Sheet (SDS) analysis revealed catastrophic incompatibilities with the factory's operational mandates; the material is classified as a high-risk CMR hazard (Reprotoxicity, Repr. 2, H361f) with Specific Target Organ Toxicity (STOT RE 2, H373). Furthermore, the powder presented reactivity risks if exposed to the acidic environment of the continuous passivation line.

Given that manual compounding and mechanical sanding generate fine, airborne particulate dust, introducing systemically hazardous substances to the shop floor constituted an unacceptable operator health risk, leading to the immediate termination of these conductives prior to physical trials.

Following this rejection, the methodology pivoted to multi-layer graphene nanoplatelets. Scientific review confirmed that graphene acts as both a conductive thermal dissipation network and satisfies the electrical percolation threshold, fulfilling the project's thermodynamic and electrostatic requirements without introducing CMR hazards to the workforce.

4.2.6.2 Feasibility Analysis of Circular Economy Byproducts

To mitigate supply chain and safety limitations, a feasibility analysis evaluated upcycling internal factory waste streams into putty additives.

The first hypothesis investigated utilizing discarded spherical aluminum powder from 3D sintering machines to perfectly align the putty's Coefficient of Thermal Expansion (CTE) with the frames. This was rejected on safety grounds: manual high-shear compounding of fine metallic powder presents ATEX (Explosive Atmospheres) hazards. Furthermore, sanding would expose unpassivated aluminum particles, creating a risk of rapid hydrogen outgassing when submerged in the wet passivation line.

The second hypothesis proposed calcining residual sludge—primarily aluminum hydroxide ($Al(OH)_3$) from the chemical cleaning baths—to extract pure alumina (Al_2O_3) for use as the ceramic filler. However, chemical analysis of the desiccated sludge via HCl dissolution (10 g/L) revealed heavy contamination from machining lubricants, polymeric fibers, and a significative phosphate concentration:

- **Aluminum Content:** 0.7 g per 10 g of sample (7 wt%).

- **Phosphate Content:** 3.3 g per 10 g of sample (33 wt%).

This contamination conclusively invalidated the upcycling hypothesis. Isolating pure aluminum hydroxide from this toxic, phosphate-heavy matrix would require a hazardous, energy-intensive solvent extraction process, completely negating its economic and logistical viability. Consequently, this justified the final strategic decision to source pristine, commercially synthesized functional nanomaterials for the final DoE.

4.2.6.3 Equipment Sourcing

The initial sourcing strategy targeted external composite research institutes. Contact was established with the Institute of Science and Innovation in Mechanical and Industrial Engineering (INEGI) to utilize their 3-roll milling equipment. However, bureaucratic bottlenecks and prolonged communication delays regarding facility access rendered this option incompatible with the strict temporal constraints of the project timeline. Concurrently, inquiries made to INEGI's planetary ball milling unit, as well as to the Instituto Superior de Engenharia do Porto (ISEP), were met with either scheduling conflicts or a lack of response, necessitating a strategic pivot to internal university resources.

An evaluation of the internal departments yielded mixed logistical results but critical material support. The Mechanical Engineering department, while lacking high-shear mixing apparatuses, supplied the requisite alumina (Al_2O_3) bulk filler utilized in the formulations. The Materials Department possessed a standard ball mill; however, this method was ultimately rejected. The inherently high viscosity and adhesive nature of the polyester putties would have resulted in an unacceptably high percentage of material loss on the milling media and chamber walls, alongside operational bottlenecks regarding equipment decontamination between formulation batches.

To bypass the lack of mechanical high-shear equipment, an intermediate chemical dispersion strategy was initially developed utilizing the Chemistry Department's ultrasonic processor (sonicator). The preliminary methodology proposed utilizing pure styrene monomer—the native reactive diluent of the polyester matrix—as a liquid dispersion vehicle for the graphene. This low-viscosity masterbatch was to be subsequently folded into the bulk putty and alumina via manual flat-plate shearing.

Ultimately, the possibility of using the Thinky Mixer at the University of Aveiro allowed the correct mixture of the base putties with the additives. The result of this will be presented and discussed in the following chapter 5.

Chapter 5

Results and Discussion

This chapter presents the empirical data and technical interpretations derived from the physical execution of the DoE methodology established in Chapter 4. To ensure a logical progression from qualitative observation to quantitative statistical validation, the discussion is systematically structured into three primary phases, mirroring the established Stage-Gate protocol.

5.1 Initial Screening Phase

This first section details the execution of the heuristic 1-to-5 evaluation matrix. The analysis begins by establishing the thermomechanical baselines for the legacy and commercial putty formulations. It then evaluates the impact of introducing the 2K primer interface to these baselines. Following this, the performance of the custom-modified formulations is analyzed, both with and without the 2K primer. The section concludes with a comprehensive discussion of the overall scores and a sensitivity analysis to mathematically stress-test the decision matrix.

5.1.1 Performance of Baseline Putties

The initial phase of the screening protocol evaluated the raw, unmodified commercial and legacy formulations (denoted by the suffix "-0"). The objective of this phase was to establish a baseline performance metric for each polymeric matrix prior to the introduction of any intermediate primer interfaces or functional additives.The formulations were evaluated against the Weighted Decision Matrix, with the final weighted scores and Efficacy Percentages ($E_{\%}$) detailed in Table 5.1.

Table 5.1: Baseline Screening Results for Unmodified Putty Formulations (-0).

ID	MP-0	T8-0	PD-0	PD-0-A	ES-0	NT-0	P70-0	CH-0	IM-0
V_1	5	5	4	4	3	2	5	3	4
V_2	5	5	5	4	3	3	5	5	5
V_3	**2**	**2**	3	3	4	4	3	3	3
V_4	1	1	3	3	4	4	1	1	1
V_5	4	4	4	4	4	4	4	4	4
V_6	3	2	4	4	3	3	4	3	3
V_7	4	4	3	3	3	3	4	3	4
Score	2.377	2.129	3.467	3.355	3.610	3.580	2.873	2.531	2.595
$E_{\%}$	47.54	42.58	**69.34**	67.10	**72.20**	**71.60**	57.46	50.62	51.90
Status	**Rejected**	**Rejected**	Approved	Approved	Approved	Approved	Approved	Approved	Approved

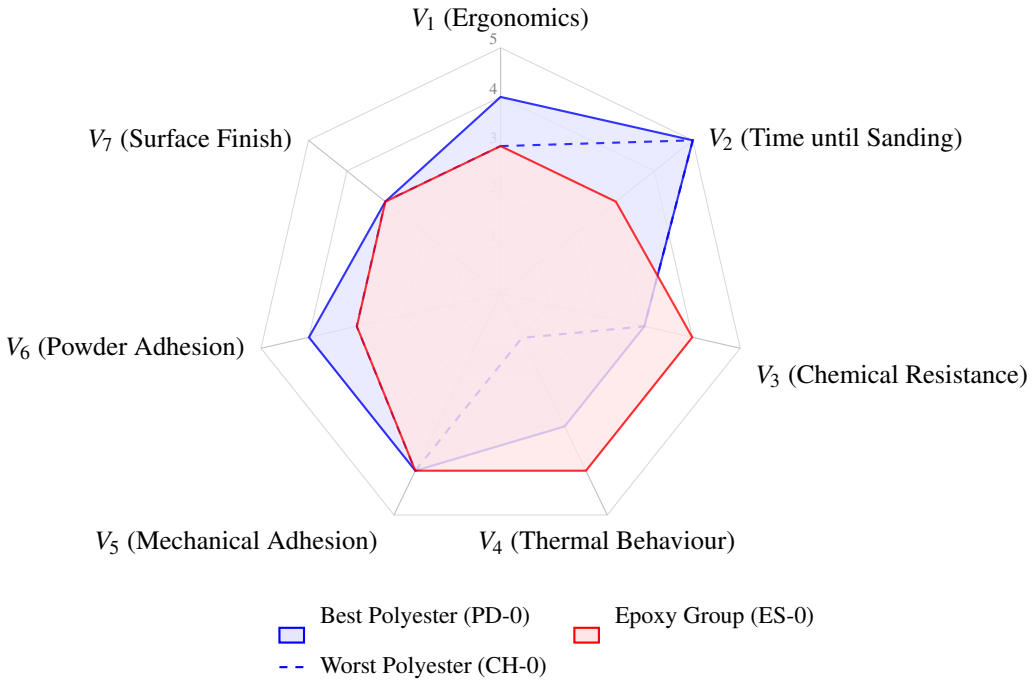

Figure 5.1: Baseline Performance Envelope: Isolating the highest and lowest scoring formulations of the standard polyester family against the baseline epoxy matrix.

Diagnostic Analysis of the Baseline Paradox As illustrated by the radar envelope, the baseline performance of the unmodified putties dictates the necessity of the Phase 2 nanomaterial intervention. While mechanical adhesion to the prepared aluminum substrate (V_5) was uniformly robust across all nine formulations (scoring a universal 4), the specific failure modes of the matrices can be chemically and volumetrically isolated.

- **Ergonomics vs. Curing Constraints (V_1, V_2, V_7):** The standard polyester matrices, originally formulated for the high-throughput automotive refinishing industry, dominate shop-floor handling. They are rheologically optimized for rapid cross-linking ($V_2 = 5$) and supe-

rior manual workability, yielding excellent surface finishes. Conversely, the epoxy formulations (ES-0, NT-0) represent a manufacturing bottleneck. Their reliance on an extended thermal curing cycle ($V_2 = 3$) disrupts the continuous flow of the production line and inherently requires more physical effort to abrade.

- **The Passivation Hard Gate (V_3):** The chemical passivation stage served as the primary filter. A comparative safety data sheet (SDS) analysis revealed that the failure of formulations MP-0 and T8-0 ($V_3 = 2$) was caused by the presence of specific acetates and glycols. In the low-pH and heated environment of the continuous passivation line, these solvents undergo rapid hydrolysis, leading to the macroscopic degradation of the putty. Conversely, the legacy PD-0 formulation survived using inert mineral fillers (talc and barium sulfate) which do not react with the conversion acids. The densely crosslinked oxirane networks of the epoxies natively resisted acidic attack ($V_3 = 4$). *Note: Due to its chemical redundancy with MP-0 and immediate passivation failure, T8-0 was removed from subsequent experimental matrices to optimize resources.*

- **Electrostatic Matrix Synergy (V_6):** Experimental results revealed an anomaly in dielectric properties. Despite the insulating nature of unsaturated polyesters, formulations PD-0 and P70-0 demonstrated electrostatic attraction equivalent to or exceeding the epoxies. This variance is likely attributed to the differing charge accumulation capacities (dielectric permittivity) of each specific paste. Paradoxically, P70-0 exhibited superior powder attraction compared to IM-0 and CH-0, despite containing a lower weight percentage of aluminum powder. This establishes that electrostatic efficacy is not dictated strictly by raw metallic loading, but rather by the synergistic interaction between secondary fillers and the primary resin matrix's capacity to accumulate and hold the applied electrostatic charge.

Thermal Outgassing and Volumetric Limits (V_4) The most critical disparity between theoretical supplier specifications and industrial reality occurred during the curing cycle. Supplier testing is traditionally conducted at 600µm over steel using a gradual pre-bake; the factory line imposes an immediate thermal shock over passivated aluminum. To quantify the impact of application geometry on this thermal failure, cross-sectional thickness measurements were recorded (Table 5.2). The average was calculated with a sample size of N=3 across the board.

A cross-analysis of this volumetric data reveals a matrix-dependent tolerance to outgassing:

- **Epoxy Stability:** Lacking volatile reactive diluents like styrene, the epoxies (ES-0, NT-0) maintained structural integrity even at high application depths (e.g., 897 μm for NT-0).

- **Competitor Polyester Failure:** Formulations P70-0, CH-0, and IM-0 suffered styrene outgassing and micro-porosity ($V_4 = 1$) when applied at the thicknesses required to conceal complex weld seams (>1000 μm). MP-0 exhibited failure even below 500 μm.

- **The PD-0 Outlier:** The baseline formulation, PD-0, emerged as the sole polyester capable of surviving high-build applications (up to 1300 μm) without total structural collapse

Table 5.2: Thickness Results for Unmodified Putty Formulations (-0).

Formula	**Layers**	**Thickness interval (μm)**	**Average (μm)**
MP-0	Putty + PP[1]	[252, 420]	325
T8-0	Putty + PP	[409, 464]	442,7
PD-0	Putty + PP	[603, 1300]	921
ES-0	Putty + PP	[422, 561]	481,7
NT-0	Putty + PP	[343, 897]	634,7
P70-0	Putty + PP	[542, 1238]	845,3
CH-0	Putty + PP	[682, 1091]	846
IM-0	Putty + PP	[555, 1377]	1068,3

[1] PP stands for Powder Primer.

($V_4 = 3$). As established in the prior RCA (Section 2.3.4), this unexpectedly superior performance is not indicative of superior chemistry, but is instead the result of operational adjustments. The survival is attributed to a divergence in application geometry (localized thicker layers on the weld zone versus thinner layers on the tube of Model C) combined with a critical optimization in the Work Instruction (IT). Specifically, abandoning the legacy protocol of sanding immediately when the putty is "dry to the touch" ensures adequate polymer cross-linking prior to oven entry. However, because the total recorded thickness uniformly encompasses a standard 160 μm powder topcoat, the effective depth of the putty matrix is significantly lower. This mathematical subtraction confirms that while PD-0 survives due to these operational protocols, it operates at its absolute thermodynamic limit, leaving the operator with virtually no margin for error during application.

5.1.1.1 Baseline Evaluation

Analysis of the baseline screening results (suffix -0) demonstrates that PD-0, ES-0, and NT-0 represent the most robust formulations in their original state. These three matrices achieved the highest efficacy percentages (69.34%, 72.20%, and 71.60%, respectively) while exhibiting the most favorable balance between electrostatic attraction and interfacial anchoring. While the polyester system (PD-0) excels in manual workability and rapid curing, the epoxy matrice (ES-0, NT-0) provides the necessary chemical and thermal resistance required for the powder coating environment.

Based on this comparative evaluation, these three candidates establish the performance benchmarks in the case of comparing strictly the market solutions. Having defined the baseline behavior of the raw matrices, the following section evaluates the impact of introducing a 2K epoxy primer interface to all the formulations to determine the introduction of this variable manages to upgrade overall the score of the different putties.

5.1.2 Addition of the 2k Primer

5.1.2.1 Primer R vs. Primer M Performance

As presented in section 4.2.5, before analysing the overall scores of the putty formulas with 2k primer, it was first necessary to establish which primer would be used and subjected to evaluation across the board: primer R or primer M.

The empirical results, detailed in Table 5.3, demonstrate that the performance of the two primers was highly competitive until the final variable V_6 was graded on the production line.

Table 5.3: Comparative Screening Results: 2K Primer M vs. 2K Primer R.

ID	**CH-2M**	**CH-2R**	**IM-2M**	**IM-2R**	**PD-2M**	**PD-2R**	**MP-2M**	**MP-2R**
V_1	3	3	4	4	4	4	5	5
V_2	2	3	2	3	2	3	2	3
V_3	5	4	5	4	5	4	5	4
V_4	1	1	1	1	1	1	1	1
V_5	4	4	4	4	4	4	4	4
V_7	3	3	4	4	3	3	4	4
Score	2.049	1.879	2.113	1.943	2.079	1.909	2.143	1.973
$E_{\%}$	40.98	37.58	42.26	38.86	41.58	38.18	42.86	39.46
Score Δ ($E_{\%R}$ - $E_{\%M}$)	**-3.400**		**-3.400**		**-3.400**		**-3.400**	

The empirical results, detailed in Table 5.3, demonstrate that the performance of the two primers was highly competitive until the final variable V_6 was graded on the production line. Before the final adhesion test, Primer M was leading by a margin of 3.4% due to its superior passivation resistance.

Table 5.4: Decisive Tie-Breaking Metrics: V_6 Score and Final Efficacy.

ID	**CH-2M**	**CH-2R**	**IM-2M**	**IM-2R**	**PD-2M**	**PD-2R**	**MP-2M**	**MP-2R**
V_6	4	**5**	3	**5**	4	**5**	4	**5**
Total Score	3.041	3.119	2.857	3.183	3.071	3.149	3.135	3.213
$E_{\%}$	60.82	62.38	57.14	63.66	61.42	62.98	62.70	64.26
Score Δ ($E_{\%R}$ - $E_{\%M}$)	**+1.560**		**+6.520**		**+1.560**		**+1.560**	

However, upon grading the final variable (V_6), Primer R achieved a perfect score of 5 across all matrices. Because the AHP model correctly weights the critical impact of mechanical adhesion, this late-stage dominance mathematically eclipsed Primer M's early lead, resulting in a definitive AHP victory for Primer R (positive Δ across all formulations, peaking at a +7 point advantage on the IM matrix.).

Moving forward, all subsequent analyses regarding the impact of the 2K primer on the putty matrices will refer exclusively to formulations utilizing Primer R (suffix -2R).

Volumetric Profiling within Industrial Tolerances To ensure the observed performance advantages of Primer R were inherently chemical, a comparative thickness analysis was conducted. As detailed in Table B.1, the cross-sectional measurements confirm that both liquid primer systems were successfully applied within standard, universal industrial tolerances.

However, due to inherent differences in the rheological properties and volumetric solids of the two systems, Primer R naturally established a higher average film build ($\Delta = 104.7\ \mu m$) than Primer M when applied under these universal parameters. In coating mechanics, even within acceptable industrial limits, a thicker polymer film inherently elevates the risk of solvent entrapment and internal shrinkage stress during crosslinking. Therefore, Primer R's ability to completely dominate the mechanical adhesion metrics despite operating at a thicker nominal film build definitively validates its chemical superiority as an interfacial binder.

Discussion of the Outcome In polymer chemistry and coating mechanics, standard theoretical models generally dictate that slower-curing polymer systems (such as Primer M) provide superior adhesion. This is typically due to an extended surface wetting time, allowing for optimal molecular contact, combined with reduced internal shrinkage stress during crosslinking. However, the empirical V_6 data directly contradicted this paradigm, demonstrating the indisputable superiority of the fast-curing Primer R. This mechanical anomaly can be attributed to two primary physicochemical factors:

- **Formation of an interpenetrating polymer network:** Fast-curing 2K primers require highly volatile solvent packages (e.g., fast-flashing acetates or ketones) to accelerate the evaporation phase. When applied over the polyester substrates, these solvents promote the formation of an Interpenetrating Polymer Network (IPN) at the boundary layer. Before the flash-off phase concludes, the primer's unreacted resins penetrate the uppermost layer of the putty. As the primer rapidly crosslinks, it effectively creates a hybrid chemical-mechanical weld, resulting in the superior adhesion scores observed.
- **Cohesive Film Toughness vs. Shear Stress:** The ISO 2409 Cross-Cut standard is a rigorous measurement of a coating's resistance to multi-directional shear and tensile stress. A fast-curing matrix rapidly achieves a high crosslink density, resulting in a mechanically rigid and tough film interface. When the multi-blade cutter sections the lattice, Primer R possessed the internal cohesive strength necessary to resist tearing and edge-flaking. Primer M, curing at a slower rate, may have remained microscopically "green" or softer during the testing window, making it more susceptible to the localized shear forces of the blade and the subsequent adhesive tape pull, leading to the micro-flaking observed at the lattice intersections.

5.1.2.2 The Epoxy Control Group

Following the integration of Primer R, the empirical data revealed a critical systemic failure: all polyester-based assemblies recorded the lowest possible score in thermal resistance ($V_4 = 1$). This

outgassing and surface blistering mirrored the outcomes previously observed during the 1K primer trials, in section 4.2.4.

To rigorously conduct a RCA, the established methodological logic was reapplied. Primer R was applied to the two baseline matrices that had previously demonstrated innate thermal stability: the experimental epoxies (ES and NT). In this diagnostic phase, the epoxy matrices serve as a thermodynamic control group. The objective is to determine whether the outgassing is fundamentally driven by the high volatility of the polyester matrices (e.g., rapid styrene evaporation), if the 2K primer itself acts as an impermeable boundary layer that traps ambient expansion and induces blistering regardless of the underlying substrate, or if the appearance of the porosities is a result of the diluent present in the liquid 2k primer.

The resulting V_4 performance of these epoxy-primer assemblies (ES-2R and NT-2R) acts as a definitive Go/No-Go decision gate for the primer architecture:

Scenario A (Polyester Volatility): If the epoxy assemblies maintain their high baseline thermal scores, it proves the 2K primer is structurally sound and the outgassing is exclusively an intrinsic failure of the polyester matrices.

Scenario B (Primer Incompatibility): If the addition of Primer R degrades the V_4 score of both epoxy matrices, it empirically demonstrates that the 2K primer film is thermodynamically incompatible with the factory's oven cycle. Such an outcome would justify the complete elimination of the 2K primer system from the remainder of the project.

Having this logic in mind, Table 5.5 shows the results of this control group.

Table 5.5: hermal Performance of Epoxy Control Group.

ID	**ES-2R**	**NT-2R**
V_1	3	2
V_2	1	1
V_3	4	4
V_4	**2**	**4**
V_5	4	4
V_6	5	5
V_7	3	3
Score	3.292	3.920
$E_{\%}$	65.64%	78.40%

The empirical data from the epoxy control group (Table 5.5) yielded a split outcome, failing to trigger a definitive Go/No-Go decision based on the predefined scenarios. While formulation NT-2R successfully survived the thermal cycle without exhibiting surface blistering ($V_4 = 4$), formulation ES-2R suffered a significant thermal degradation ($V_4 = 2$).

It was considered that further testing needed to be done (with the modified versions of the putties) to draw a conclusion on the impact of the 2k primer.

5.1.2.3 Impact Analysis of the 2K Primer

With the validity of the primer R not reached, the direct impact on the base formulations can still be quantified.

Polyester Baselines A comparative analysis was conducted between the unprimed baselines (suffix *-0*) and their respective primed counterparts (suffix *-2R*) for formulations MP, PD, CH, IM, and P70. Formulation T8 was excluded from this phase due to its prior definitive elimination.

Table 5.6: Comparative Analysis: Unprimed Baselines (-0) vs. 2K Primer R (-2R) on Polyester Matrices.

ID	**MP-0**	**MP-2R**	**PD-0**	**PD-2R**	**CH-0**	**CH-2R**	**IM-0**	**IM-2R**	**P70-0**	**P70-2R**
V_1	5	5	4	4	3	3	4	4	5	5
V_2	5	**3**	5	**3**	5	**3**	5	**3**	5	**3**
V_3	2	**4**	3	**4**	3	**4**	3	**4**	3	**4**
V_4	1	1	3	**1**	1	1	1	1	1	1
V_5	4	4	4	4	4	4	4	4	4	4
V_6	3	**5**	4	**5**	3	**5**	3	**5**	4	**5**
V_7	4	4	3	3	3	3	4	4	4	4
Total Score	2.377	3.212	3.467	3.149	2.531	3.119	2.595	3.183	2.873	3.213
$E_{\%}$	47.54	64.26	69.34	62.98	50.62	62.38	51.90	63.66	57.46	64.26
Score Δ ($E_{\%R}$ - $E_{\%0}$)	**+16.72**		**-6.36**		**+11.76**		**+11.76**		**+6.8**	

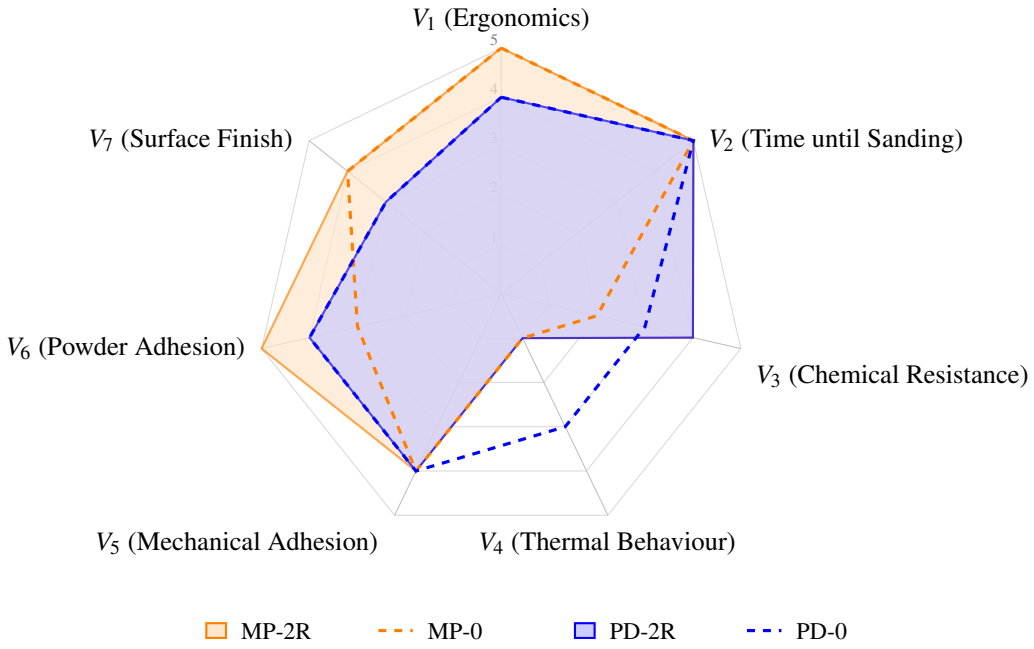

Figure 5.2: The Interfacial Paradox: Comparing the unprimed (dashed) versus primed (solid) states of the polyesters that suffered the biggest impact.

The application of Primer R yielded significant systemic improvements in the chemical and mechanical interfaces of the completed polyester putties.

- **Interfacial Optimization (V_3, V_6):** The cross-linked 2K epoxy primer acts as a highly effective, impermeable shield against the acidic conversion baths. Formulation MP recovered from a baseline Hard Gate failure to a passing $V_3 = 4$, while PD, CH, and IM similarly improved from 3 to 4. Additionally, the primer unified the surface energy of all formulations, maximizing electrostatic powder adhesion to a universal $V_6 = 5$.

- **Operational Curing Penalty (V_2):** The integration of a 2K liquid system inherently penalizes factory throughput. Across all completed formulations, the curing kinetics score (V_2) uniformly dropped from a rapid 5 to a 3, reflecting the unavoidable manufacturing bottleneck caused by the primer's mandatory flash-off and cross-linking times.

- **The "Sealed Pot" (V_4):** The most critical consequence of the primer is the universal crash in thermal resistance ($V_4 = 1$). While CH, IM, MP, and P70 already failed this metric in their raw states, the legacy PD matrix suffered a regression, dropping from a passing 3 down to a 1. In its unprimed state, the PD matrix possesses sufficient natural porosity for internal volatiles (expanding air and unreacted styrene) to "breathe" and escape during the thermal ramp-up. By encapsulating the putty with the impermeable Primer R to solve the passivation issue, these volatiles are forcefully trapped. Upon exposure to the 195°C oven, the expanding gases hydraulically rupture the primer layer, resulting in surface cratering.

Epoxy Baselines Following the evaluation of the polyester matrices, an identical comparative framework was applied to the epoxy control group. Table 5.7 delineates the performance deltas between the unprimed epoxy baselines (-0) and their Primer R encapsulated counterparts (-2R), revealing significant matrix-specific trade-offs.

Table 5.7: Comparative Analysis: Unprimed Baselines (-0) vs. 2K Primer R (-2R) on Epoxy Matrices

ID	**ES-0**	**ES-2R**	**NT-0**	**NT-2R**
V_1	3	3	2	2
V_2	3	**1**	3	**1**
V_3	4	4	4	4
V_4	4	**2**	4	4
V_5	4	4	4	4
V_6	3	**5**	3	**5**
V_7	3	3	3	3
Total Score	3.610	3.292	3.580	3.920
$E_{\%}$	72.20	65.84	71.60	78.40
Score Δ ($E_{\%R}$ - $E_{\%0}$)	**-6.36**		**+6.80**	

The most immediate negative consequence of the Primer R application was the degradation of the process cycle time, specifically the time required until final sanding (V_2). Both the ES-0 and NT-0 baselines maintained a functional processing window (Score = 3). However, the subsequent application of the liquid primer over these matrices introduced a temporal bottleneck, dropping the V_2 scores to a uniform Critical Failure (Score = 1). This is a direct result of the primer's curing kinetics. The 2K Primer requires extended flash-off and cross-linking periods before it can be mechanically abraded. Attempting to sand the interfacial layer prematurely results in abrasive clogging, forcing extended wait times that fundamentally disrupt the continuous flow of the production line.

Conversely, the mechanical adhesion data (V_6) empirically justifies why the interfacial primer is attempted despite the time penalty. In their unprimed state (-0), both epoxy matrices achieved a borderline pass (Score = 3) under the ISO 2409 cross-cut test, indicating localized flaking. The introduction of Primer R completely resolved this vulnerability. Both ES-2R and NT-2R achieved a Class 0 adhesion rating (Score = 5). This proves that Primer R functions as a chemical link, successfully bridging the surface energies of the rigid epoxy matrix and the powder topcoat to establish an impenetrable structural bond.

Ultimately, the aggregate scores reflect a distinct industrial trade-off between manufacturing cycle time (V_2) and electrostatic powder adhesion (V_6). Because powder adhesion is established as a critical variable (carrying a 24.8% AHP weight) compared to the 'Medium' impact of sanding time (7.8%), exchanging cycle speed for a Class 0 adhesion rating ($V_6 = 5$) yields a net positive mathematical outcome. This theoretical advantage is demonstrated by the NT matrix, which

absorbed the temporal bottleneck ($V_2 = 1$) but maximized adhesion, resulting in a positive performance delta ($\Delta = +6.80$ %).

Conversely, the ES matrix suffered a negative performance delta (%) despite gaining the exact same adhesion benefits. Under the application of Primer R, the ES formulation experienced a critical drop in thermal resistance ($V_4 = 2$), with the analysis explored in section 5.1.2.2. Given that outgassing behavior (V_4) occupies the highest tier in the metric hierarchy (32.9%), this thermal penalty mathematically eradicated any gains achieved in adhesion.

5.1.3 Phase 1 Conclusion: The Operational Paradox and the Limit of Commercial Baselines

A macro-level cross-examination of the polyester matrices (Table 5.6) and epoxy control groups (Table 5.7) reveals a systemic, chemically driven trend governing the application of the 2K liquid primer (Primer R). The integration of this interfacial layer does not act uniformly across differing polymer networks; rather, its performance is strictly bound by the baseline thermodynamic capabilities of the underlying matrix.

For the standard market polyesters (MP, CH, IM and P70), the application of Primer R yielded a consistent positive performance delta ($\Delta = +6.8\%$ to $+16.72\%$). Because these baseline polyesters inherently suffered from critically low thermal outgassing scores ($V_4 = 1$), the localized outgassing issues introduced by the primer film did not fundamentally alter their already failing thermal ranking. Instead, the primer successfully mitigated their interface vulnerability, upgrading all formulations to the maximum cross-cut adhesion rating ($V_6 = 5$). Given the high AHP priority of adhesion (24.8%), this masking effect dictated a net positive mathematical score.Conversely, a mathematical inversion was observed in the top-tier formulations. The baseline polyester (PD-0) and the baseline epoxy (ES-0) registered identical, sharp declines of $\Delta = -6.36\%$. Because these specific matrices possessed superior independent thermal resistance in their unprimed states, they proved uniquely sensitive to the application of an interfacial barrier. The primer film actively acted as an impermeable skin that trapped expanding volatiles within these high-volume matrices, triggering localized hydrostatic ruptures (V_4 dropping to 1 for PD-2R and 2 for ES-2R). Because V_4 holds the ultimate mathematical priority (32.9%), this thermal penalty mathematically erased any adhesion benefits the primer provided.

Justification for Matrix Modification Ultimately, the cross-analysis of the consolidated baseline data dictates that an acceptable industrial outcome cannot be achieved using standard commercial putties paired with subsequent inter-layers. The known operational paradox between the two polymer families resurfaces empirically:

- **Polyester Matrices** offer attractive operator ergonomics and rapid cycle times (V_1, V_2), but fundamentally lack the thermal stability (V_4) required to endure the processing environment.
- **Epoxy Matrices** provide superior baseline thermal resistance, but require an intermediate 2K primer to secure electrostatic adhesion, which has shown non-consistent results. This

primer introduces a temporal bottleneck ($V_2 = 1$) that disrupts the continuous flow of the production line and acts as a highly sensitive, volatile boundary layer over complex geometries.

Because external coating modifications and dual-layer strategies fail to resolve these competing variables, it is empirically established that process-level adjustments using off-the-shelf chemistry have reached their structural limit. Therefore, the direct chemical alteration and synthesis of a custom, doped baseline putty represents the only viable methodology to simultaneously satisfy the mechanical, thermal, and temporal constraints of the manufacturing line.

5.1.4 Performance of Modified Formulas

5.1.4.1 Additive Allocation and Logistical Constraints

Following the conclusive evaluation of the unmodified baselines, the experimental matrix transitioned to the synthesis and evaluation of the doped putties. Initially, the integration of functional modifiers (X_1) was intended to follow a strict conditional application strategy based purely on the specific failure modes observed during the baseline results, as established in section 4.1.2.2.

However, translating this theoretical framework into physical synthesis at the University of Aveiro (UA) laboratories exposed a logistical inventory constraint. This constraint unfolded chronologically across two distinct synthesis sessions, necessitating a real-time strategic pivot in material allocation.

Day 1: The Validation Session To ensure the integrity of the main experimental matrix, an initial validation session was conducted. A single pilot batch, **PD2**, was formulated as a hybrid composite (Graphene + Alumina), the scenario that consumes more additive material. The objective of this session was strictly to empirically validate the high-shear mixing protocol, verify the dispersion capabilities of the laboratory equipment, and establish a repeatable operational standard without risking the limited supply of experimental epoxies. The successful synthesis of PD2 validated the methodology for the subsequent production run.

Day 2: The Production Sequence and Inventory Triage During the primary synthesis session for the remaining matrix, the production sequence commenced with the facility's legacy formulation (PD), which was doped with strictly graphene to create variant **PD1**. Following this, formulation MP was processed and dosed as a hybrid composite to create variant **MP1**.

Immediately after the completion of the MP1 batch, an inventory audit revealed a constraint: the remaining volume of high-purity graphene was low and strictly insufficient to complete the remainder of the experimental matrix as originally designed.

To preserve the industrial value of the project's most promising formulations, a real-time strategic triage was executed. The remaining graphene inventory was locked and strictly reserved for the leading experimental epoxies (NT and ES), as these represented the highest potential for

immediate factory integration. Consequently, the remaining commercial polyesters, having lost access to the graphene supply, were modified utilizing solely the available alumina inventory.

As a result of this chronological synthesis sequence and logistical pivot, the final functional modifiers applied to the variants were established (according to the logic in section 4.1.2.2) as follows in Figure 5.3.

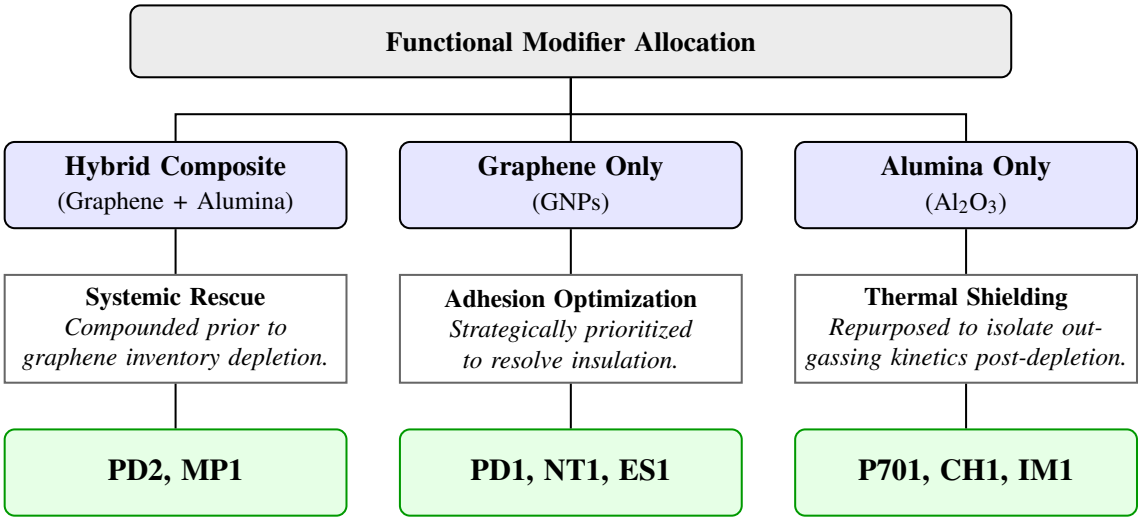

Figure 5.3: Strategic allocation of functional nanomaterials for the variants.

The Analytical Advantage of the Pivot While necessitated by a material constraint, this allocation pivot—combined with the successful retention of the Day 1 PD2 validation batch—inadvertently engineered a highly targeted analytical advantage. By advancing the legacy polyester (PD) in three distinct states (the unmodified PD baseline, the purely graphene-doped PD1, and the hybrid-doped PD2), the resulting data structure allows for a rigorous evaluation of additive synergy. Specifically, should the PD formulation advance to the final DoE, this configuration will explicitly quantify the systemic synergy achieved by combining alumina and graphene (PD2), directly comparing it against the isolated interfacial optimization provided by graphene alone (PD1).

5.1.4.2 Experimental Results

Following the logistical triage and successful synthesis of the doped variants, the complete battery of screening tests was executed. To maintain the comparative integrity of the methodology established in Phase 1, each of the eight modified formulations was tested in both its unprimed state (suffix *-0*) and its primed state utilizing the 2K interfacial layer (suffix *-2R*).

Evaluation of Unprimed Modified Matrices Table 5.8 presents the comprehensive empirical dataset for all modified matrices. To systematically isolate the effects of the functional additives from the compounding variables of the liquid primer, the data analysis is divided into two distinct sequential phases: the unprimed modified matrices, followed by the primed assemblies.

Table 5.8: Baseline Screening Results for Modified Putty Formulations (-0).

ID	**MP1-0**	**PD1-0**	**PD2-0**	**P701-0**	**CH1-0**	**IM1-0**	**ES1-0**	**NT1-0**
V_1	5	4	3	5	4	4	3	2
V_2	4	4	4	4	4	4	3	3
V_3	4	4	4	4	3	4	3	3
V_4	1	1	1	1	1	1	4	4
V_5	4	4	4	4	4	4	4	4
V_6	5	4	5	4	4	3	5	5
V_7	4	4	4	4	3	4	2	3
Score	3.291	3.013	3.231	3.043	2.731	2.765	3.824	3.828
$E_{\%}$	65.82	60.26	64.62	60.86	54.62	55.30	76.48	76.56
Status	Approved	Approved	Approved	Approved	Approved	Approved	Approved	Approved

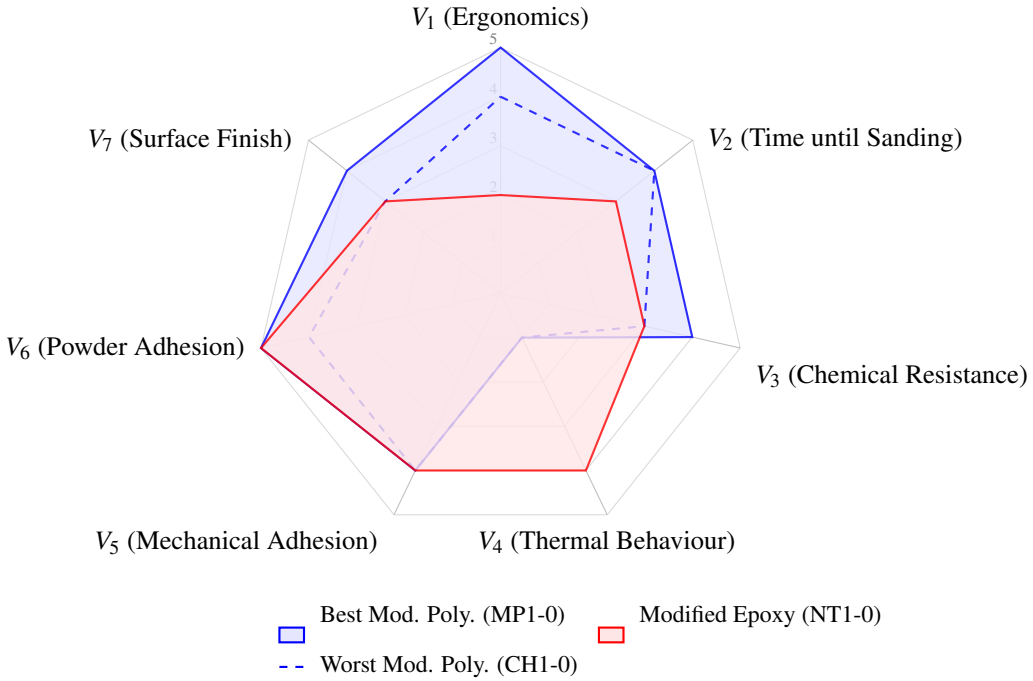

Figure 5.4: Modified Performance Envelope: Isolating the highest and lowest scoring unprimed modified polyesters against the modified epoxy matrix.

As illustrated by the modified performance envelope (Figure 5.4), integrating functional nanomaterials successfully isolated and resolved specific chemical and electrostatic vulnerabilities, but ultimately confirmed the unalterable thermodynamic limitations of the polyester family.

The Polyester Matrices While the solid nanomaterials successfully optimized handling and chemical barriers, they actively destabilized the internal thermodynamics of the matrices under curing temperatures.

- **Rheology and Mixing Validation (V_1, V_7):** The additives functioned as highly effective micro-fillers and positive rheological modifiers, increasing yield stress to prevent sagging while improving physical machinability (PD improved in V_7, CH in V_1). This homogenous dispersion natively validates the efficacy of the Thinky high-shear centrifugal mixing protocol.

- **Interfacial Optimization and Hybrid Synergy (V_3, V_6):** The dispersed particulate network successfully reconstructed the chemical barrier, elevating failing formulations (MP, P70, IM) to a passing $V_3 = 4$. Crucially, electrostatic powder adhesion (V_6) revealed a strict hybrid synergy: formulations doped with *both* alumina and graphene (MP1-0, PD2-0) achieved a perfect Class 0 adhesion rating ($V_6 = 5$). Conversely, isolated additives proved inadequate, with standalone graphene (PD1-0) and standalone alumina (CH1-0, IM1-0) yielding stagnant or inconsistent mechanical anchoring.

- **Thermodynamic Regression (V_2, V_4):** Despite the physical improvements, the operational wait time (V_2) was downgraded from 5 to 4. The high-volume additives absorb exothermic heat, introducing kinetic uncertainty; although Goudarzi et al. [26] notes graphene accelerates curing, a conservative safety factor was enforced pending DSC/DMA validation. More critically, the additives exacerbated thermal outgassing (V_4). While the baseline PD-0 survived the oven ($V_4 = 3$), the highly conductive graphene network in PD1-0 and PD2-0 rapidly accelerated heat transfer, flash-vaporizing the trapped styrene and crashing the modified scores to a fatal $V_4 = 1$.

The Epoxy Matrices The direct integration of graphene yielded outcomes that perfectly support the Phase 2 hypothesis, establishing the required electrostatic and thermal parameters while identifying precise rheological boundaries.

- **Electrostatic and Thermal Dominance (V_4, V_6):** The graphene percolated network successfully resolved the fundamental insulating flaw of the epoxies, instantly elevating powder attraction from a baseline failure to a maximum $V_6 = 5$. Because the epoxies completely lack volatile reactive diluents (styrene), they safely absorbed the accelerated thermal transfer without inducing sub-surface outgassing during the curing cycle ($V_4 = 4$).

- **Rheological Divergence and Thermal Sag (V_1, V_7):** The low-volume (0.6%) graphene matrix (ES1-0) initially succumbed to thermal sag as dynamic viscosity dropped precipitously before cross-linking. Rather than definitively classifying this as an intrinsic chemical failure, this physical vulnerability highlighted the ambient pre-cure rest period (flash-off time) as a highly influential process variable. Consequently, flash-off time was flagged as a potential Critical-to-Quality (CTQ) parameter, requiring strict monitoring and systematic evaluation in subsequent experimental stages to determine if the rheological instability persists under controlled application intervals.

- **Calculated Operational Trade-offs (V_2, V_3):** The integration of graphene introduced microscopic capillary pathways along the carbon interfaces, slightly reducing chemical resistance to a $V_3 = 3$, which remains an acceptable industrial pass. Furthermore, while Goudarzi et al. [26] suggests enhanced internal thermal transport accelerates epoxy kinetics, the V_2 score was conservatively locked at 3. The mandatory 1-hour factory curing cycle remains strictly enforced until empirical validation via advanced thermal characterization (DSC, TGA) can definitively map the shifted cross-linking timeline.

Evaluation of the Primed Formulas and Final Elimination To complete the comparative matrix and definitively validate the single-step processing hypothesis, the modified formulations were subsequently evaluated utilizing the legacy 2K liquid primer. Table 5.9 presents the empirical dataset for the primed variants.

Table 5.9: Baseline Screening Results for Modified Putty Formulations (-2R).

ID	**MP1-2R**	**PD1-2R**	**PD2-2R**	**P701-2R**	**CH1-2R**	**IM1-2R**	**ES1-2R**	**NT1-2R**
V_1	5	4	3	5	4	4	3	2
V_2	3	3	3	3	3	3	1	1
V_3	4	4	4	4	4	4	4	4
V_4	1	1	1	1	1	1	3	2
V_5	4	4	4	4	4	4	4	4
V_6	5	4	5	3	5	3	5	5
V_7	4	4	4	4	3	4	2	3
Score	3.213	2.935	3.153	2.717	3.149	2.687	3.587	3.262
$E_{\%}$	64.26	58.70	63.06	54.34	62.98	53.74	71.74	65.24
Status	Approved	Approved	Approved	Approved	Approved	Approved	Approved	Approved

The application of the 2K primer over the modified matrices revealed a thermodynamic incompatibility, definitively proving that the primer acts as a compounding variable rather than a protective layer. The Ishikawa diagram was once again utilized to conduct a RCA, considering the multitude of variables present.

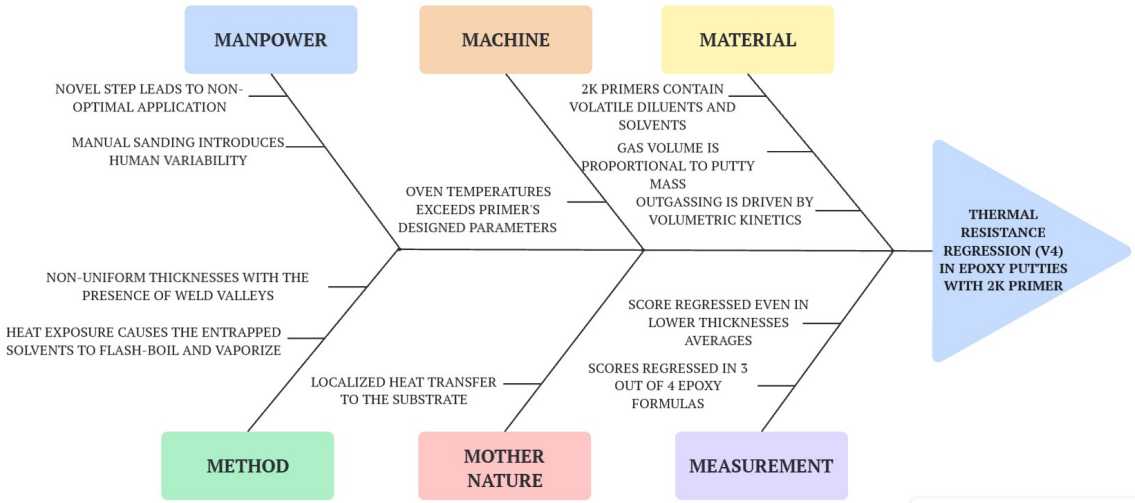

Figure 5.5: RCA of the epoxies' V4 results with the 2k primer.

While the Ishikawa diagram (Figure 5.5) maps the primary causal categories, specific spatial and volumetric nuances confirm the precise failure mechanism across the specimens. The result on the ES-2R in 5.1.2.2 sample exhibited a targeted spatial pattern, clustering heavily along the weld toes while the area directly over the weld bead peak remained intact. Because the 2K primer was applied via pneumatic spray—ensuring a constant cross-sectional thickness across the frame—this variance is attributable exclusively to the underlying putty mass. Over the weld peak, where the putty is sanded to approximately 0.1 mm, the minimal polymer mass contained negligible trapped gas, allowing the primer to remain stable. In the adjacent valleys, where the putty reached localized depths of up to 870 µm to level the geometric drop-off, the proportional expansion of trapped gas generated localized hydrostatic pressure, inducing microscopic ruptures through the boundary layer.

Upon application of the 2K primer, the scores regressed of NT1-2R and ES1-2R regressed (to 2 and 3 respectively). Because this regression occurred even in the modified NT formulation—which maintained a lower thickness average of approximately 460 µm—it confirms the primer's independent failure. The trapped diluents within the liquid interfacial layer flash-boil at high temperatures prior to complete cross-linking, rendering the 2K primer thermodynamically incompatible with the powder coating process regardless of the underlying putty geometry.

5.1.5 Stage-Gate Synthesis: Declaration of the Top 3

The comprehensive screening of both unprimed and primed matrices established a clear demarcation in thermodynamic stability and interfacial viability. The empirical data dictates the elimination of the standard unsaturated polyesters due to high-heat outgassing, alongside the elimination of the 2K liquid primer due to diluent flash-boiling. Consequently, the field of viable candidates is narrowed to the three most strategically significant base formulations for final statistical validation. Table 5.10 presents the finalized comparative scores for these selected matrices: the factory's

legacy production baseline (PD-0) and the two optimized experimental epoxies (ES1-0 and NT1-0).

Table 5.10: Final Stage-Gate Screening Scores for the Selected DoE Candidates.

ID	PD-0	ES1-0	NT1-0
V_1	4	3	2
V_2	5	3	3
V_3	3	3	3
V_4	3	4	4
V_5	4	4	4
V_6	4	5	5
V_7	3	2	3
Score	3.467	3.824	3.828
$E_{\%}$	69.34	76.48	76.56

Based on the stage-gate scoring criteria, these three base matrices are officially advanced to the final parallel DoE. The documented thermal incompatibility of the liquid interfacial layer dictates that Scenario 2 in 4.1.3 is triggered. Phase 2 will be compromised of 3 Parallel One-Way ANOVA utilizing the software Minitab.

5.1.6 Sensitivity Analysis

To validate the robustness of the established AHP model, a mathematical sensitivity analysis was conducted. In industrial decision-making, the prioritization of metrics can shift depending on management objectives (e.g., a sudden push for volume versus a strict mandate for quality). To simulate these shifting factory priorities, the AHP eigenvector was temporarily overridden, and three distinct bias scenarios were modeled. To ensure mathematical consistency and eliminate variable-intensity bias, all scenarios utilized a standardized 60/40 split: the two targeted metrics were artificially elevated to 30% each, while the remaining five metrics evenly divided the remaining 40% (8.0% each).

Scenario A (The Throughput Bias): This scenario models a production environment where factory management prioritizes cycle time and immediate visual leveling above all else, attempting to maximize daily frame output. The mathematical bias was heavily weighted toward the time until final sanding ($V_2 = 30\%$) and the surface condition after the first application ($V_7 = 30\%$).

Scenario B (Ergonomics Approach): This scenario shifts the focus entirely to the shop floor, prioritizing the physical handling and manual labor of the operators. The mathematical bias was applied to the initial application handling ($V_1 = 30\%$) and the mechanical ease of sanding ($V_5 = 30\%$)

Scenario C (Pure Final Quality): This scenario represents a strict quality-control mandate, where management demands high-quality final paint finishes and zero thermal outgassing scrap, removing the weight of the passivation line, V_3. The bias was strictly applied to the factory's final output variables: thermal resistance ($V_4 = 30\%$) and electrostatic powder adhesion ($V_6 = 30\%$).

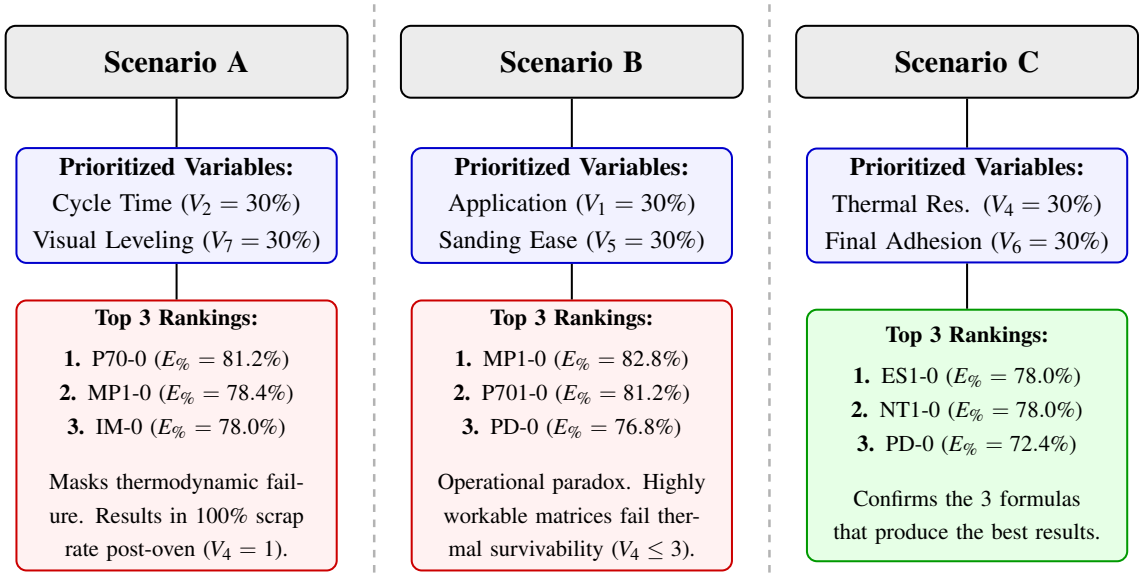

Figure 5.6: Sensitivity Analysis to stress-test the formulation selection algorithm.

Shifting the mathematical bias heavily toward speed and intermediate leveling exclusively isolates the unsaturated polyester chemistries. However, this scenario reveals a vulnerability in relying strictly on weighted averages without boundary limits. By heavily rewarding cycle time, the algorithm completely masks the thermodynamic failure of the selected matrices($V_4 = 1$). Consequently, while this approach would theoretically maximize daily throughput prior to the oven, it would result in a 100% scrap rate upon exiting the curing cycle.

When the evaluation criteria prioritize human factors and physical workability, the model strongly favors the rheologically optimized matrices. However, similar to Scenario A, this bias creates an operational paradox. While MP1-0 and P701-0 optimize the operator's physical labor, they fail to survive the required thermal cycle ($V_4 = 1$). Only the legacy baseline (PD-0) manages to balance ergonomic workability ($V_1 = 4, V_5 = 4$) with acceptable thermal survival ($V_4 = 3$).

By shifting the mathematical bias away from intermediate cycle speeds and strictly toward the quality and structural integrity of the final interface, the model accurately isolates the precise matrices selected for the final DoE stage. Formulations ES1-0 and NT1-0 present the best result in this scenario due to their complete immunity to styrene outgassing ($V_4 = 4$) and their optimized electrostatic conductive networks ($V_6 = 5$). The legacy baseline (PD-0) emerges as the only viable polyester control due to its baseline porosity allowing adequate thermal survival ($V_4 = 3$). This scenario mathematically validates the core engineering logic of the thesis: to achieve a successful

single-step powder coating process, intermediate conveniences (such as rapid sanding times) must be subordinated to the strict thermodynamic constraints of the curing oven.

5.2 Phase 2: DoE on Selected Matrices

Following the formal elimination of the thermodynamically unstable 2K primer during the Phase 1 screening gate, the surviving polymer matrices (PD, ES and NT) advanced to Phase 2 validation. As defined by the adaptive experimental architecture in section 4.1.3, the statistical treatment was executed as a series of independent One-Way ANOVAs, utilizing the reallocated factory resources to achieve an increased replicate size of $N = 5$.

5.2.1 The Legacy Polyester

Operational Handling and Curing Kinetics The initial validation of the PD matrix evaluated its fundamental compatibility with manual factory operations, specifically analyzing application ergonomics (V_1) and operational wait time (V_2).

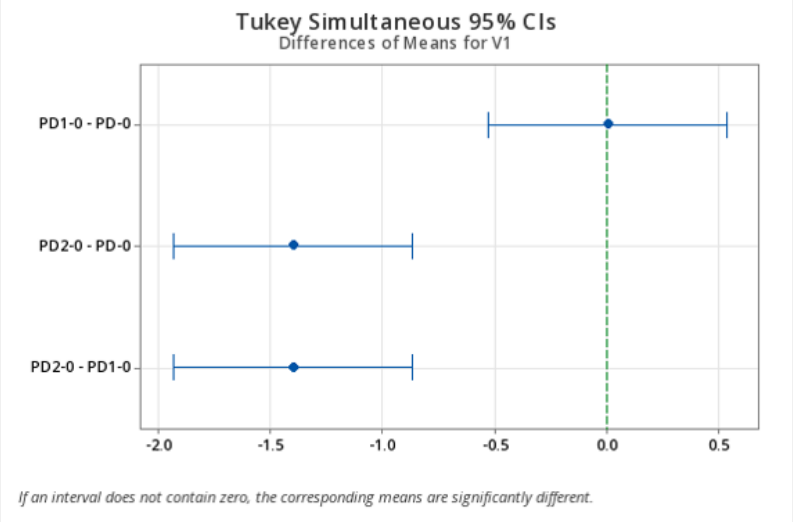

Figure 5.7: Tukey Pairwise Comparisons for V_1.

The One-Way ANOVA for variable V_1 yielded a highly significant effect ($p_{ANOVA} = 0.000$), a result strictly confirmed by the non-parametric Kruskal-Wallis validation ($p_{KW} = 0.001$). This dual-validation indicates a pronounced, mathematically robust shift in the handling characteristics of the polymer putty.

As detailed in the Tukey Pairwise Comparisons for V_1 (Figure 5.7), the statistical analysis mathematically isolated the specific additive responsible for ergonomic degradation. The comparative interval between the graphene-doped formulation (PD1-0) and the unmodified baseline (PD-0) crosses zero, indicating no statistically significant difference in mean performance. This

confirms that the 2D planar structure of the graphene nanoplatelets maintained the baseline spreadability. Conversely, intervals involving the dual-doped formulation (PD2-0)—containing both alumina and graphene—fall entirely below zero. This statistically significant degradation in handling confirms that the integration of granular Al_2O_3 increased the dynamic viscosity and yield stress of the polymer paste, rendering it resistant to manual application.

Concurrent with these rheological shifts, the modified formulations introduced observable variances in the curing kinetics (V_2). Consistent with preliminary Phase 1 screening observations, the operational wait time for both modified PD matrices was downgraded from a baseline score of 5 to a 4. Because the high-volume solid additives absorb exothermic heat during the polymerization process, they introduce kinetic uncertainty. Although Goudarzi et al. [26] notes that graphene can accelerate curing in specific polymer configurations, a conservative safety factor was enforced for this factory-floor evaluation, pending formal quantitative validation via advanced thermomechanical analysis (e.g., DSC/DMA).

Chemical Resistance (V_3) and Surface Integrity (V_7) Following the rheological analysis, the formulations were evaluated for chemical survivability during acidic passivation (V_3) and final surface porosity (V_7).

The One-Way ANOVA for V_3 yielded a significant effect ($p_{ANOVA} = 0.006$), a result strictly confirmed by the non-parametric Kruskal-Wallis validation ($p_{KW} = 0.018$). This dual-validation indicates a mathematically robust shift in the chemical resistance of the PD matrix.

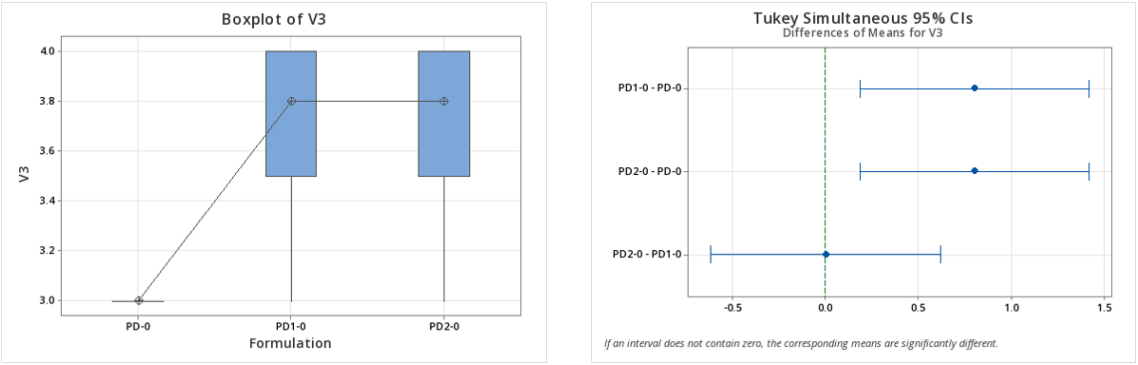

(a) Boxplot detailing data spread and limits.

(b) Tukey Simultaneous 95% CIs.

Figure 5.8: Comparative analysis of Chemical Resistance.

As illustrated in the comparative analysis, the Boxplot (Figure 5.8a) demonstrates a positive mean shift for both the graphene-doped (PD1-0) and dual-doped (PD2-0) formulations compared to the baseline. This aligns with the theoretical mechanism where the dispersion of 2D graphene nanoplatelets creates a physical barrier against acidic pre-treatment solutions. However, the accompanying Tukey Pairwise Comparisons (Figure 5.10b) show that the interval comparing the dual-doped matrix to the graphene-only matrix crosses zero. This confirms that the addition of granular alumina (Al_2O_3) provides no supplementary chemical barrier effect, supporting its removal from the formulation.

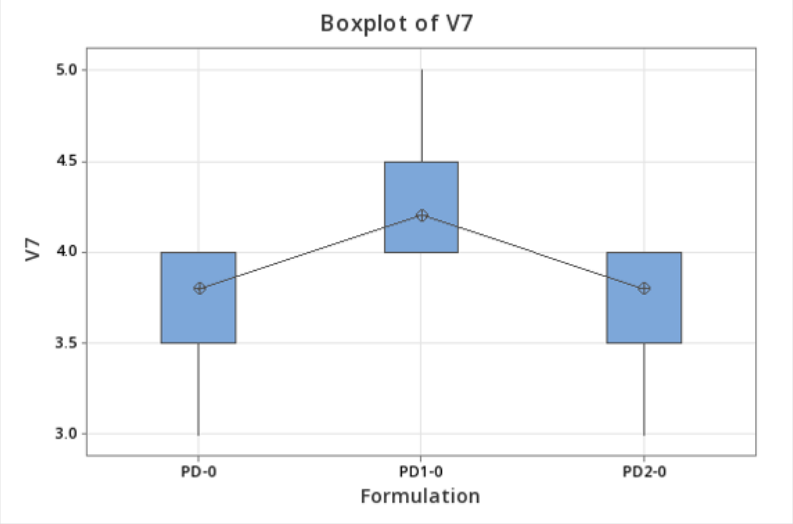

Figure 5.9: Boxplot of V_7 for the PD family.

Regarding final surface integrity, the ANOVA yielded a non-significant effect ($p_{ANOVA} = 0.300$), a result strictly confirmed by the non-parametric Kruskal-Wallis validation ($p_{KW} = 0.288$). This dual-validation indicates no statistically significant difference among the formulations. As visually represented in the Boxplot of V_7 (Figure 5.9), the interquartile ranges exhibit substantial overlap. This suggests that the integration of the nanocomposites did not alter the baseline surface porosity or defect rate prior to the continuation in the process line.

Thermodynamic Stability (V_4) and Electrostatic Adhesion (V_6) The final evaluation of the PD matrix focused on the primary failure modes targeted by this research: thermal stability and electrostatic powder deposition.

For thermodynamic stability (V_4), all evaluated PD formulations—including the baseline and nanocomposite variants—recorded the lowest possible structural integrity scores (value of 1). The integration of thermally conductive networks (graphene and alumina) did not mitigate the inherent outgassing of the polyester backbone under high-temperature curing conditions.

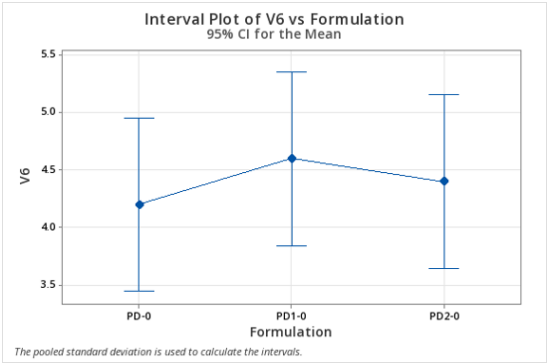

(a) Interval plot detailing data spread and limits.

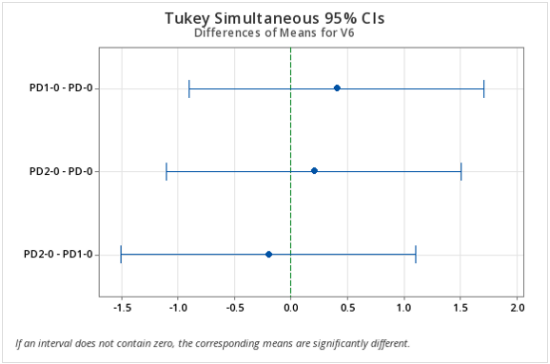

(b) Tukey Simultaneous 95% CIs.

Figure 5.10: Comparative analysis of Electrostatic Adhesion.

Regarding electrostatic adhesion, the One-Way ANOVA yielded a non-significant effect ($p_{ANOVA} = 0.723$), a macroscopic deadlock confirmed by the non-parametric Kruskal-Wallis evaluation ($p_{KW} = 0.573$). This confirms there is no statistically significant difference among the formulations.

As confirmed by the Tukey Pairwise Comparisons (Figure 5.10), all comparative intervals cross zero. This demonstrates that the targeted conductive pathways did not sufficiently alter the matrix's electrical resistance to resolve the Faraday Cage effect or improve the baseline defect rate. (Assumptions of the ANOVA model, including normality and homoscedasticity, were verified via residual analysis; see Appendix B).

5.2.2 The Legacy Epoxy (ES)

The primary objective for the evaluation of the ES matrix was to determine if the integration of conductive graphene nanoplatelets could resolve probabilistic electrostatic defects without compromising the baseline process stability and thermodynamic limits.

Process Compatibility and Zero-Variance Metrics (V_1, V_2, V_4, V_5, V_7) Prior to evaluating targeted optimizations, the modified formulation (ES1-0) was assessed for baseline operational compatibility. Across variables V_1 (Application Ergonomics), V_2 (Curing Kinetics), V_4 (Thermodynamic Stability), V_5 (Mechanical adhesion to the substrate), and V_7 (Condition after first sanding), the empirical data recorded absolute zero variance ($S = 0.000$) between the unmodified baseline and the graphene-doped formulation (with scores of 3, 3, 4, 4, 3, respectively).

All standard replicates for both ES-0 and ES1-0 achieved identical scores for these metrics. This confirms that the integration of the 2D graphene network at the defined volume fraction maintained the structural and rheological equilibrium of the epoxy matrix. Crucially, the modified putty sustained maximum structural integrity during the 180°C curing cycle (V_4), successfully clearing the thermal threshold that previously disqualified the polyester formulations.

Note regarding Zero Variance Results The empirical data for several optimized formulations yielded an absolute zero mathematical variance ($S = 0.000$) across multiple discrete metrics over the $N = 5$ replicate cycles. From a purely statistical perspective, zero variance in a 1-to-5 ordinal scale is occasionally misinterpreted as a measurement defect or "ceiling effect" caused by subjective grading.

However, this assumption fundamentally mischaracterizes the methodology of this DoE. The 1-to-5 evaluation criteria established in Section A.1.1 are not arbitrary, subjective heuristics; the majority are discrete operational mappings of continuous physical phenomena. Specifically, V_2 is strictly quantified by chronometric curing time, V_3 and V_4 are defined by absolute macroscopic pore counts, and V_6 is a direct translation of the international ISO 2409 adhesion standard. Therefore, an $S = 0.000$ in these variables does not indicate a lack of measurement granularity; it physically proves that the formulation consistently yielded the exact same number of defects (zero) or fell into the exact same chronometric window across all five replicates.

For the strictly qualitative operational metrics (V_1 Ergonomics and V_7 Initial Porosity), the 1-to-5 scale functions as a calibrated Go/No-Go tolerance band. A score of '5' does not imply that the material is physically identical at the molecular level across all five applications; rather, it indicates that any microscopic physical variance remained entirely confined within the acceptable upper-specification limit. Thus, the metric correctly ignores invisible physical noise, confirming deterministic line-side capability.

Chemical Resistance (V_3) With core process parameters stabilized, the matrix was evaluated for its resistance to the acidic pre-treatment baths of the passivation line. The One-Way ANOVA for V_3 yielded a non-significant effect ($p_{ANOVA} = 0.347$), which was mathematically corroborated by the Kruskal-Wallis validation ($p_{KW} = 0.317$), indicating no statistically significant difference at the 95% confidence level.

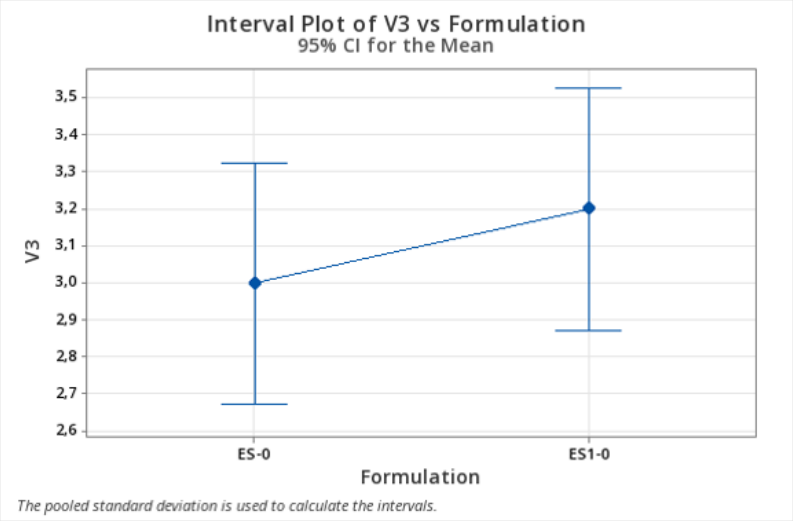

Figure 5.11: Interval Plot for the Chemical Resistance Scores.

However, the empirical data demonstrates a slight positive trend. As illustrated in the Interval Plot (5.11), the mean survivability score increased from 3.00 for the unmodified baseline (ES-0) to 3.20 for the graphene-doped formulation (ES1-0). While the overlapping confidence intervals mathematically confirm the non-significant p-value, the directional improvement aligns with theoretical composite models. The integration of impermeable, 2D graphene nanoplatelets functions as a physical barrier, slightly increasing the tortuosity of the diffusion path and retarding the ingress of corrosive aqueous solutions into the cross-linked epoxy bulk.

Electrostatic Adhesion (V_6) The critical operational requirement for the ES matrix was the optimization of powder deposition (V_6). During Phase 1 screening, the baseline epoxy achieved a Class 2 adhesion rating ($V_6 = 3$). While Class 2 falls within acceptable manufacturing tolerances, it represents a borderline process capability that remains susceptible to the Faraday Cage effect. The integration of the graphene network was specifically targeted to pull the matrix away from this operational limit and ensure absolute process stability.

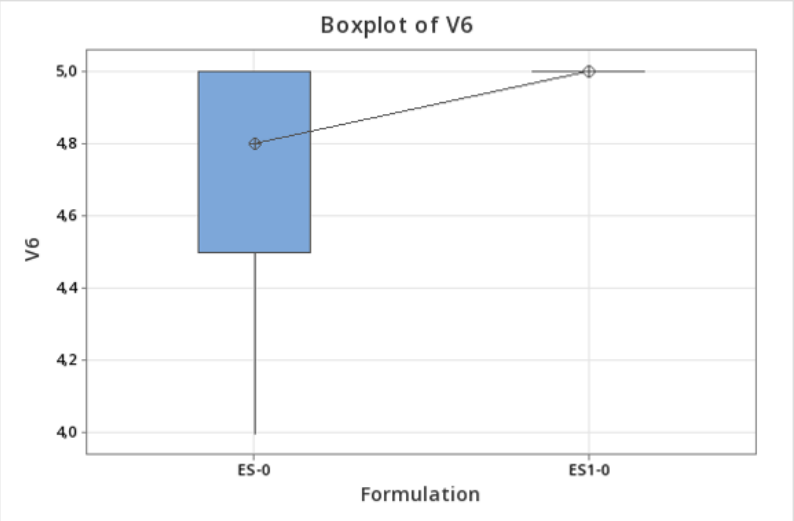

Figure 5.12: Boxplot graph for Electrostatic Adhesion (ES matrix).

The Phase 2 evaluation ($N = 5$) demonstrated a clear transition from probabilistic variance to deterministic stability. The One-Way ANOVA yielded a non-significant effect ($p_{ANOVA} = 0.347$), a result strictly verified by the non-parametric Kruskal-Wallis validation ($p_{KW} = 0.317$). This dual-validation confirms no statistically significant difference in the mean adhesion scores between the formulations. However, the critical engineering improvement lies in the elimination of operational variance.

As visually represented in the Boxplot (Figure 5.12), the unmodified baseline (ES-0) recorded a mean score of 4.80 ($S = 0.447$). Although all replicates achieved a passing grade (ranging between Class 0 and Class 1), this variance indicates that the baseline matrix does not ensure absolute stability under dynamic industrial conditions. Conversely, the graphene-doped formulation (ES1-0) recorded a Class 0 adhesion score (5.00) across all standard replicates, resulting in zero variance ($S = 0.000$).

This empirical data confirms that the targeted conductive pathways established by the graphene network successfully stabilized the matrix's dielectric properties. By insulating the powder application process from factory-floor variability, the nanocomposite eliminates adhesion variance and establishes a highly reliable, zero-deviation operational standard.

5.2.3 Evaluation of the NT Matrix

The formula of the experimental design to be evaluated was the NT matrix. Given the successful stabilization achieved in the ES matrix, it is important to see if this alternative epoxy putty can produce superior results to the ones obtained from the ES matrix.

5.2.3.1 Process Compatibility and Zero-Variance Metrics (V_1, V_2, V_4, V_5)

Prior to evaluating targeted chemical and electrostatic capabilities, the modified formulation (NT1-0) was assessed for baseline operational compatibility. Consistent with the results observed in

the epoxy matrix, the empirical data for the NT recorded zero variance ($S = 0.000$) between the unmodified baseline and the graphene-doped formulation across variables V_1 (Application Ergonomics), V_2 (Curing Kinetics), V_4 (Thermodynamic Stability), and V_5 (Adhesion to the substrate).

All standard replicates for both NT-0 and NT1-0 achieved identical optimal scores for these metrics. This confirms that the integration of the 2D graphene network at the defined volume fraction successfully maintained the structural and rheological equilibrium of the rigid novolac matrix. Most importantly, the formulation sustained structural integrity during the 180°C curing cycle ($V_4 = 4$).

5.2.3.2 Surface Porosity (V_7)

The One-Way ANOVA yielded a non-significant effect ($p_{ANOVA} = 0.580$), a result confirmed across both parametric and non-parametric models ($p_{KW} = 0.549$). This indicates no statistically significant difference in the mean porosity scores at the 95% confidence level. Furthermore, the empirical data demonstrates that the integration of the nanocomposite did not alter the operational variance for this specific metric.

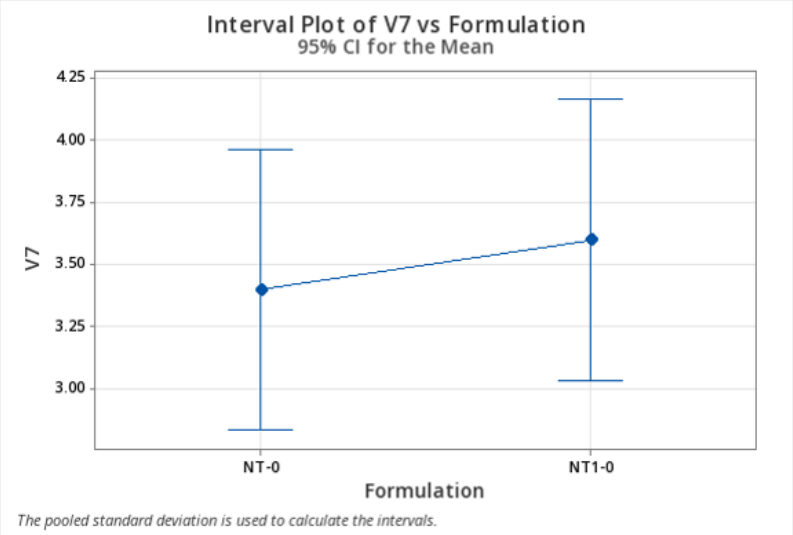

Figure 5.13: Interval Plot regarding Condition after First Sanding.

As illustrated in the Interval Plot (Figure 5.13), the mean score experienced a marginal increase from 3.400 for the unmodified baseline (NT-0) to 3.600 for the graphene-doped formulation (NT1-0). However, the standard deviation remained identical across both formulations ($S = 0.548$).

This indicates that while the high-aspect-ratio graphene nanoplatelets may act as a minor micro-structural filler—slightly improving the average surface density—they are insufficient to completely overcome the inherent curing dynamics of the highly cross-linked novolac network. Unlike the electrostatic properties (V_6), the formulation remains susceptible to intermittent interstitial micro-voids, maintaining a probabilistic surface finish rather than achieving absolute zero-deviation stability.

Chemical Resistance (V_3) Following the confirmation of baseline process stability, the matrix was evaluated for its resistance to the acidic pre-treatment baths of the passivation line (V_3).

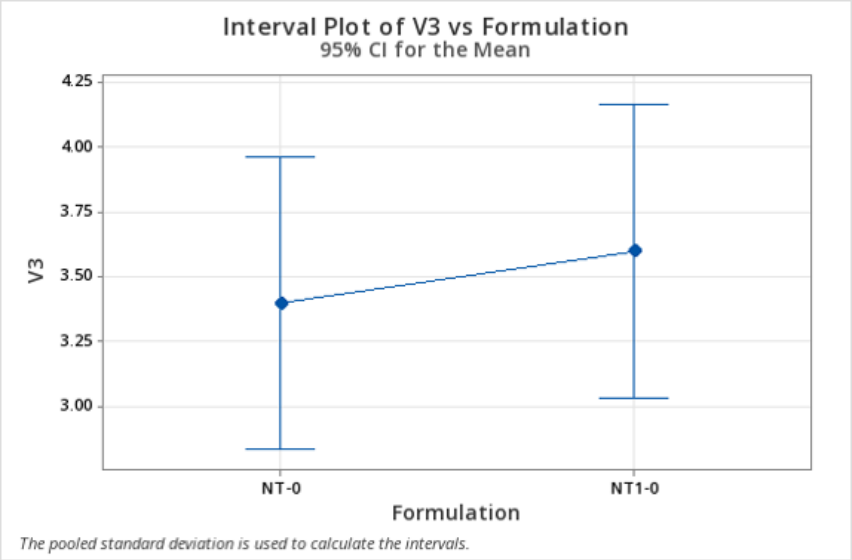

Figure 5.14: Interval Plot of Chemical Resistance Scores (NT Matrix).

The One-Way ANOVA for V_3 yielded a non-significant effect ($p_{ANOVA} = 0.580$), a result mathematically anchored by the Kruskal-Wallis validation ($p_{KW} = 0.549$). This dual-validation indicates no statistically significant difference at the 95% confidence level. However, consistent with the behavior observed in the epoxy matrix, the empirical data demonstrates a slight positive trend. As illustrated in the Interval Plot (Figure 5.14), the mean survivability score increased from 3.40 for the unmodified baseline (NT-0) to 3.60 for the graphene-doped formulation (NT1-0).

While the overlapping confidence intervals mathematically confirm the non-significant p-value, this directional improvement aligns with the theoretical nanocomposite models. The integration of impermeable, 2D graphene nanoplatelets functions as a physical barrier, increasing the tortuosity of the diffusion path and retarding the ingress of corrosive aqueous solutions.

5.2.3.3 Electrostatic Adhesion (V_6)

The critical requirement for the NT matrix during the powder coating phase (V_6) was the optimization and stabilization of electrostatic deposition. During the Phase 1 screening trials, the baseline formula achieved a Class 2 adhesion rating. While formally classified as a passing grade, this borderline process capability indicated that the raw matrix remained susceptible to the Faraday Cage effect under varying operational conditions. The integration of the graphene network was specifically targeted to eliminate this vulnerability and ensure zero-deviation process stability.

The empirical data from the Phase 2 trials ($N = 5$) demonstrates the successful achievement of optimal process capability. As detailed in Table 5.11, both the unmodified baseline (NT-0) and the graphene-doped formulation (NT1-0) achieved perfect Class 0 adhesion scores across all replicates, resulting in a mean score of 5.000 with absolute zero variance ($S = 0.000$).

Table 5.11: Descriptive statistics for Electrostatic Adhesion (V_6) of the NT formulas.

Formulation	N	Mean Score	StDev (S)	Minimum	Maximum
NT-0	5	5.000	0.000	5.000	5.000
NT1-0	5	5.000	0.000	5.000	5.000

While the Phase 2 baseline (NT-0) performed optimally under controlled trial conditions, the integration of the graphene network (NT1-0) served as the critical engineered safeguard. This data confirms that the highly conductive nanocomposite successfully preserved the Class 0 adhesion capability, definitively resolving the Class 2 vulnerability observed in the screening phase and guaranteeing absolute, zero-deviation stability on the electrostatic line.

5.3 Cross-Matrix Synthesis and Final Operational Capability

To establish a definitive conclusion for the experimental design, the empirical results from the three evaluated polymer families—Polyester (PD), and Epoxy (ES, NT)—are synthesized cohesively.

5.3.1 Visualizing the Performance Envelopes

The overall operational footprint of each matrix family is evaluated using multi-variable performance envelopes. These radar charts map the empirical mean scores across all seven primary variables (V_1 through V_7), establishing a visual representation of material capability relative to the maximum operational limit (Score: 5.0).

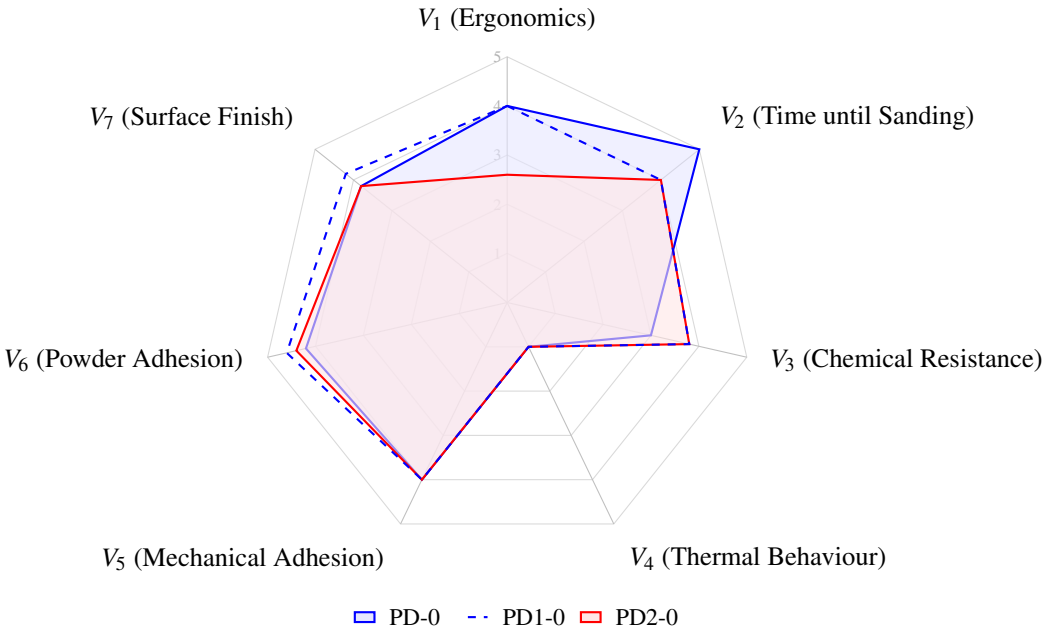

Figure 5.15: Radar chart evaluating PD family mean performance across the variables.

As seen in Figure 5.15, while the polyester family demonstrated capable baseline performance across ambient parameters—including application ergonomics (V_1) and mechanical adhesion (V_5)—the performance envelope illustrates a systematic structural failure along the V_4 axis (Thermal Behavior). All three formulations recorded a score of 1.0, failing to survive the 180°C powder coating curing cycle. This thermodynamic limitation validates the immediate elimination of the polyester family from further optimization.

Conversely, Figure 5.16 contrasts the high-performance thermosetting families (ES and NT) in both their unmodified and graphene-doped states. The visualization demonstrates that both matrix families occupy a consistent, high-capability envelope approaching the maximum operational limits. The visual tracking of the dashed lines (ES1-0 and NT1-0) highlights the specific, incremental advancements achieved via the 2D graphene network, notably the directional shifts outward along the V_3 (Chemical Resistance) and V_7 (Surface Finish) axes, while preserving core baseline competencies.

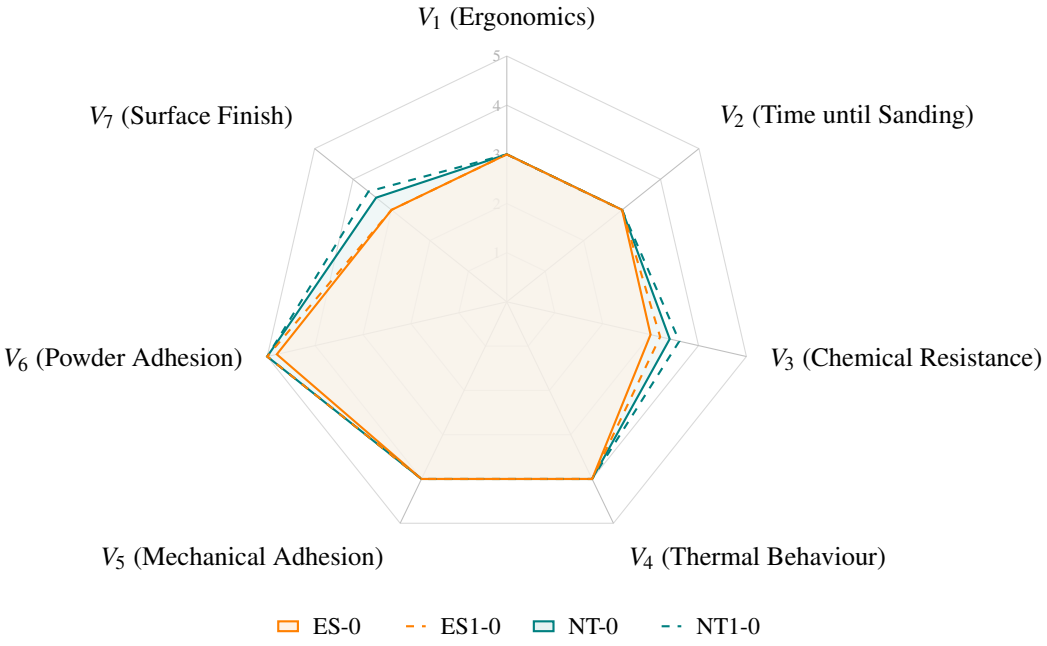

Figure 5.16: Comparative performance envelope showcasing the operational footprint of the ES and NT matrices and the incremental shifts of the nanocomposite formulations.

5.3.2 Consolidated Operational Metrics and Global Efficiency

While the radar charts map the empirical trends, the final industrial validation relies on the aggregated Global Efficiency metric ($E_{\%}$). Table 5.12 presents the statistical summary of the experimental design, pairing the empirical capability shifts with their respective inferential analysis.

The synthesis of the inferential and descriptive data yields a definitive conclusion for this experimental design.

Table 5.12: Final operational capability, statistical significance, and global efficiency profiles.

Matrix Family	**Formula**	**Mean $E_{\%}$ (%)**	**StDev (S)**	**ANOVA p-value**	**K-W p-value**
PD (Polyester)	PD-0	57.72	4.20	0.179	0.226
	PD1-0	62.38	4.17		
	PD2-0	60.28	2.44		
ES (Epoxy)	ES-0	76.17	2.218	0.147	0.095
	ES1-0	78.29	2.162		
NT (Epoxy)	NT-0	79.39	2.630	0.617	0.504
	NT1-0	**80.18**	2.760		

As detailed in Table 5.12, the inferential calculations for all three matrix families yielded p-values greater than the significance threshold ($\alpha = 0.05$) across both the parametric (ANOVA) and non-parametric (Kruskal-Wallis) models. This dual-validation mathematically confirms a macroscopic deadlock: the internal shifts in mean global efficiency between the baselines and their respective modified versions are not statistically significant. Consequently, per the predefined optimization methodology, the selection protocol formally cascades to Tier 2: Sub-Metric Resolution and Variance Control.

Under Tier 2 constraints, the empirical data immediately invalidates the Polyester (PD) family for this specific industrial application. While the formulations recorded moderate mean global efficiencies (57.72% to 62.38%), these aggregate scores obscure a critical boundary-condition failure: systematic thermal degradation (V_4) observed during the 180°C curing cycle.

In contrast, the Epoxy (ES, NT) formulations demonstrated highly capable operational stability and successfully survived the thermal boundary conditions. Within the ES family, the integration of the graphene network (ES1-0) achieved a mean efficiency of 78.29% and successfully stabilized electrostatic powder adhesion (V_6) at a constant Class 0 performance. This effectively eliminated the probabilistic variance observed in the baseline, establishing a reliable, deterministic material for the standard assembly line.

Ultimately, NT1-0 demonstrated the superior empirical trend required to win the Tier 2 evaluation. Building upon a highly capable baseline, the graphene-doped NT1-0 achieved the absolute highest final mean global efficiency of **80.18%**. While it retained minor operational variance in its surface finish (V_7), it successfully minimized critical boundary-condition failures on the factory floor, becoming the only formulation evaluated to surpass the 80% efficiency threshold while maintaining strict stability across all thermal, mechanical, and ergonomic sub-metrics.

Accordingly, the NT1-0 graphene-doped formulation is formally selected as the optimized material specification for this industrial application.

Chapter 6

Conclusions and Future Works

This final chapter synthesizes the primary findings of the research conducted to resolve the thermodynamic and electrostatic bottlenecks inherent to the surface finishing of dual-matrix assemblies. Through the application of RCA and empirical material evaluation, a functional industrial solution was developed and validated within the strict operational constraints of a high-throughput manufacturing environment.

The following sections outline the definitive technical conclusions regarding polymeric thermal stability, the limitations of intermediate interfacial primers, and the efficacy of targeted nanomaterial doping. Furthermore, this chapter contextualizes the methodological decisions required to balance academic rigor with industrial pragmatism. Finally, it outlines actionable recommendations for future analytical characterization, statistical process control, and continuous manufacturing optimization as the project scales toward mass production.

6.1 Industrial Pragmatism vs. Academic Evaluation

The core methodology of this research was defined by the strict necessity to deliver a production-ready solution within an active industrial value stream, bounded by TRL 3 and 4. Consequently, a deliberate decision was made to prioritize empirical, line-side process validation over traditional laboratory-based instrumental characterization. It is fully acknowledged that the absence of analytical tools—such as DSC, TGA, and Scanning Electron Microscopy (SEM)—leaves the precise molecular mechanisms governing the nanomaterial integrations as unquantified hypotheses. However, this limitation was consciously accepted. In a high-throughput manufacturing environment, macroscopic process survival is of greater immediate utility than microscopic characterization. The factory's 180°C powder coating oven served as a high-fidelity, unalterable testing apparatus, providing a definitive pass/fail boundary condition that no laboratory simulation could adequately replace.

6.2 Methodological Constraints and Statistical Limitations

The initial experimental matrix yielded 32 distinct formulation-primer combinations. To manage this volume within the facility's temporal constraints, a heuristic stage-gate screening protocol was implemented utilizing a single-replicate ($N = 1$) boundary application. It is recognized that an $N = 1$ sample size lacks statistical power and is inherently vulnerable to common-cause factory noise, such as localized substrate contamination or pneumatic variance. This risk of Type II errors (falsely eliminating a viable material) was accepted as a necessary trade-off to maintain project velocity. To mitigate the risk of factory noise skewing the data, this lean approach relied strictly on post-failure RCA. Materials were only eliminated when the physical failure mode (e.g., solvent flash-boiling) was definitively linked to the material's chemical architecture rather than an operational anomaly. This allowed for the rapid and justified elimination of non-viable materials, conserving critical production resources for the subsequent phases.

During the Phase 2 DoE, the sample size was increased to $N = 5$ to evaluate the functional nanomaterials. The data confirmed a known limitation of industrial research: small-sample parametric models, such as ANOVA, struggle to achieve mathematical significance when the signal is heavily diluted by the high background variance of a live assembly line. Consequently, the macroscopic global efficiency metrics resulted in a statistical deadlock. This limitation was accounted for in the evaluation framework. Because aggregate means frequently obscure critical local improvements, the final selection of the graphene-doped epoxy matrix (NT1-0) was not based on a statistically significant shift in overall efficiency. Instead, the decision was justified by deterministic variance elimination; the NT1-0 formulation completely stabilized electrostatic powder adhesion, achieving a zero-deviation Class 0 performance that standard efficiency averages fail to adequately weight.

The reliance on the ISO 2409 cross-cut adhesion standard introduced a definitive statistical ceiling to the evaluation. Because the ordinal scale is mathematically capped at Class 0 (translated to a maximum score of 5.0), it restricted the ability to quantify the true magnitude of the adhesion improvement induced by the graphene doping. It is acknowledged that this metric proves macroscopic industrial compliance but fails to define the absolute interfacial shear strength of the modified matrix. This metrological limitation was accepted for the current TRL phase to ensure rapid quality-control compliance, with the understanding that continuous-scale testing is required for future mechanical validation. Consequently, relying solely on the ISO visual classification provides only a macroscopic threshold of success. Determining the exact structural limits and true mechanical bonding capacity of the graphene-enhanced interface will require direct quantitative methods, such as pneumatic pull-off adhesion testing (e.g., ISO 4624), to capture the physical limits beyond the Class 0 visual ceiling.

6.3 The Operational Trade-off and Process-Driven Problem Solving

The empirical data confirmed an inherent trade-off between application ergonomics and thermodynamic stability. Fast-curing, operator-friendly formulations, such as the standard unsaturated polyesters, lacked the structural integrity to withstand the 180°C conditions of the powder coating curing cycle. The results indicate that to secure a reliable surface finishing solution, the optimization of takt time must be subordinated to the strict thermal and chemical requirements of the manufacturing process.

An alternative approach to this industrial bottleneck would have been the primary research and development of a novel polymeric solution from scratch. However, by prioritizing a RCA of the existing manufacturing process, the overall development timeline was significantly reduced. Identifying specific failure mechanisms within the value stream—such as the thermal outgassing induced by intermediate primer layers and the specific variables affecting electrostatic adhesion—allowed for the targeted, time-efficient modification of existing commercial baselines.

6.4 Efficacy of Nanomaterial Doping and Interfacial Primers

The experimental results demonstrated that functional additives yield highly divergent operational impacts depending on their morphology and volume fraction. The integration of graphene nanoplatelets at a low volumetric target (0.6 vol%) successfully established the required semiconductive network, resolving the electrostatic Faraday Cage effect (V_6) without degrading the baseline application ergonomics (V_1) of the epoxy matrix. Conversely, the integration of granular alumina, intended to provide physical thermal shielding, significantly increased the dynamic viscosity and yield stress of the formulations. This negatively impacted manual workability without providing sufficient thermodynamic protection to prevent the outgassing of the polyester matrices.

Intermediate chemical layers (1K and 2K liquid primers) were evaluated to determine if a surface coating could shield a thermally sensitive substrate. The exclusive selection of liquid primers for this experimental phase was dictated by strict facility kinematics: while manual application of powder primer is physically possible in one specific zone, it occurs exclusively on a continuous, moving conveyor line. This continuous flow prevents the precise, localized, and time-intensive application required for off-line putty rework. Consequently, liquid primers represented the only viable method for intermediate manual application at the dedicated rework stations.

However, the empirical data did not support the hypothesis of liquid interfacial shielding. While the 2K epoxy primer improved interfacial mechanical adhesion at ambient temperatures, it acted as a barrier during the 180°C oven cycle. This trapped expanding volatiles within the underlying polyester matrices, resulting in hydrostatic ruptures. This outcome indicates that superficial liquid barriers are insufficient to compensate for the intrinsic thermodynamic incompatibilities of a base polymer exposed to high-temperature curing.

6.5 Validation of the Weighted Evaluation Framework

The application of the AHP to weight the evaluation criteria successfully aligned the material selection process with the facility's absolute operational limits. By mathematically prioritizing high-temperature thermal resistance (V_4) and electrostatic powder adhesion (V_6) over rapid cycle times (V_2) and initial application ergonomics (V_1), the decision matrix filtered out "false economy" materials. This framework proved that relying on unweighted averages would have artificially favored formulations that maximize early-stage throughput but ultimately result in a 100% scrap rate during the final curing phase.

6.6 Future Works

The doping of the NT epoxy matrix with graphene addressed the electrostatic deposition issues and withstood the 180°C powder coating curing cycle without significant outgassing, fulfilling the macro-objective of the research. To build upon this baseline, future works should focus on the following:

- **Analytical Material Characterization:** Instrumental characterization (DSC, TGA, and surface resistivity) must be conducted to map the shift in cross-linking kinetics and define the thermal degradation thresholds with molecular precision
- **Long-Term Statistical Validation:** The observed adhesion improvement trend requires continuous statistical validation. Transitioning from controlled batch testing ($N = 5$) to active SPC across a larger volume of production frames is necessary to calculate the Process Capability Index (C_{pk}) and verify the long-term stability of the modified matrix.
- **Compounding Scalability:** As the project scales toward TRL 5 and 6, the planetary centrifugal mixing protocol utilized in this study should be transitioned to continuous industrial-scale dispersion methods, such as three-roll milling or twin-screw extrusion, to ensure morphological homogeneity in mass production.
- **Quantitative Mechanical Testing:** Future validation must replace the ISO 2409 visual scoring system with pneumatic pull-off testing (e.g., ISO 4624) to establish a continuous scale for measuring the physical bond strength of the graphene-matrix interface.
- **Passivation Line Optimization:** The initial two stages of the continuous chemical passivation line rely on highly acidic solutions ($pH < 1$) designed strictly for bare aluminum. These baths exhibit chemical incompatibility with porous polymeric materials. For future process optimization, it is recommended to evaluate the replacement of these acidic stages with a non-aggressive degreasing agent. This modification would preserve the structural integrity of the applied putties while maintaining adequate surface cleaning prior to the conversion coating.

Ultimately, this research navigated the inherent friction between laboratory-standard characterization and industrial reality. By defining the thermodynamic boundaries of the dual-matrix assembly and engineering a targeted nanocomposite solution, a viable proof of concept was successfully validated. Although the facility-level production bottleneck remains active pending large-scale implementation, the empirical baseline established in this study provides the definitive technical blueprint required for its resolution. Combined with the execution of the recommended process optimizations, this framework equips the facility with the exact data-driven pathway needed to transition this surface finishing protocol from a validated TRL 4 prototype into a mass-production standard.

References

[1] F. Abbas Abeer, U. Abbas Raghad, and A. Betti Nadia. *Study Thermomechanical Properties of Unsaturated Polyester Composite Reinforced by Ceramic Particles (Al 2 O 3)*. en. IJISET - International Journal of Innovative Science, Engineering & Technology, June 2015. URL: https://www.researchgate.net/publication/311844332_Study_Thermomechanical_Properties_of_Unsaturated_Polyester_Composite_Reinforced_by_Ceramic_Particles_Al_2_O_3 (visited on 04/29/2026).

[2] Basim Abu-Jdayil. "Unsaturated Polyester Microcomposites". en-US. In: *Unsaturated Polyester Resins*. Elsevier, Jan. 2019, pp. 67–100. DOI: 10.1016/B978-0-12-816129-6.00003-X. URL: https://www.sciencedirect.com/science/chapter/edited-volume/pii/B978012816129600003X (visited on 04/29/2026).

[3] Nelson K. Akafuah et al. "Evolution of the Automotive Body Coating Process—A Review". en. In: *Coatings* 6.2 (June 2016), p. 24. ISSN: 2079-6412. DOI: 10.3390/coatings6020024. URL: https://www.mdpi.com/2079-6412/6/2/24 (visited on 04/28/2026).

[4] Claudia Aldrighetti et al. "Reduction of the thermal expansion of unsaturated polyesters by chain-end modification". In: *Polymer Degradation and Stability*. Special Issue on Chemical Modification of Polymers 90.2 (Nov. 2005), pp. 346–353. ISSN: 0141-3910. DOI: 10.1016/j.polymdegradstab.2005.01.042. URL: https://www.sciencedirect.com/science/article/pii/S0141391005002594 (visited on 04/29/2026).

[5] M Ardelean et al. "Surface treatments for aluminium alloys". In: IOP Publishing Ltd, 2018. DOI: 10.1088/1757-899X/294/1/012042. URL: https://iopscience.iop.org/article/10.1088/1757-899X/294/1/012042/pdf.

[6] Sameh Attia-Essaies et al. "Thermal and Mechanical Performances of Unsaturated Polyester Composites Reinforced by Natural Fillers". en. In: *Chemistry Africa* 7.3 (Apr. 2024), pp. 1523–1533. ISSN: 2522-5766. DOI: 10.1007/s42250-023-00839-5. URL: https://doi.org/10.1007/s42250-023-00839-5 (visited on 04/29/2026).

[7] Autohas-waechtershaeuser. *trl scale*. pt. Aug. 2025. URL: https://www.bing.com/images/search?view=detailV2&ccid=OIC0An%2bi&id=0B0F7CA2447C88C4046BCF0F3C9D&thid=OIP.OIC0An-i-zZ70WBUiBR0FwHaDy&mediaurl=https%3a%2f%2fcoanda.ca%2fwp-content%2fuploads%2f2017%2f01%2fTechnology-Readiness-Levels-1200x613.png&cdnurl=https%3a%2f%2fth.bing.com%2fth%2fid%2fR.3880b4027fa2fb367bd1605488147417%3frik%3dnHeI3BNhnTwPzw%26pid%3dImgRaw%26r%3d0&exph=613&expw=1200&q=trl+scale&FORM=IRPRST&ck=11A5BFD3C5BA116EE58B53270E954504&selectedIndex=25&itb=0&ajaxhist=0&ajaxserp=0 (visited on 07/03/2026).

[8] Monisha Baby et al. “Universal adhesion promoters for enhanced adhesion on metal and polymeric substrates”. In: *International Journal of Adhesion and Adhesives* 140 (June 2025), p. 104013. ISSN: 0143-7496. DOI: 10.1016/j.ijadhadh.2025.104013. URL: https://www.sciencedirect.com/science/article/pii/S0143749625000806 (visited on 04/29/2026).

[9] Richard P Bagozzi and Hans Baumgartner. “The evaluation of structural equation models and hypothesis testing”. In: *Principles of Marketing Research*. Ed. by Richard P Bagozzi. Cambridge, MA: Blackwell Publishers, 1994, pp. 386–422.

[10] Xingjia Bai et al. *A discrete element method study on the effect of interfacial bond strength on the performance and damage behavior of highly filled CaCO3/unsaturated polyester resin composites*. 2025. DOI: 10.13801/j.cnki.fhclxb.20250217.010. URL: https://fhclxb.buaa.edu.cn/en/article/id/79079db3-8fe2-4225-b7d9-9f429b74067c (visited on 04/29/2026).

[11] Markus Becker. “Chromate-free chemical conversion coatings for aluminum alloys”. en. In: *Corrosion Reviews* 37.4 (Aug. 2019), pp. 321–342. ISSN: 2191-0316. DOI: 10.1515/corrrev-2019-0032. URL: https://www.degruyterbrill.com/document/doi/10.1515/corrrev-2019-0032/html?srsltid=AfmBOooSesNPG-ESFCGBhD7nE3fvNDbnoeb0t lang=en (visited on 04/28/2026).

[12] Negesa Bekuma and Hailemariam Nigus. “Experimental analysis of glass fiber reinforced epoxy composite with calcium carbonate (CaCO3) as filler for automobile body panel application using multi-objective optimization”. en. In: *Discover Materials* 6.1 (Feb. 2026), p. 87. ISSN: 2730-7727. DOI: 10.1007/s43939-026-00568-9. URL: https://doi.org/10.1007/s43939-026-00568-9 (visited on 04/29/2026).

[13] V Bhuvaneswari. “Recent advancements in polymer composites for damage repair applications”. en-US. In: *Polymer Composite Systems in Pipeline Repair*. Gulf Professional Publishing, Jan. 2023, pp. 1–26. DOI: 10.1016/B978-0-323-99340-1.00001-0. URL: https://www.sciencedirect.com/science/chapter/edited-volume/pii/B9780323993401000010 (visited on 04/28/2026).

[14] CSP Borges et al. “Review on the effect of moisture and contamination on the interfacial properties of adhesive joints”. EN. In: *Proceedings of the Institution of Mechanical Engineers, Part C: Journal of Mechanical Engineering Science* 235.3 (Feb. 2021), pp. 527–549. ISSN: 0954-4062. DOI: 10.1177/0954406220944208. URL: https://doi.org/10.1177/0954406220944208 (visited on 04/29/2026).

[15] Sunil Chandrakant Joshi. “Outgassing studies on thermal control coatings for micro-satellites”. en. In: *Aircraft Engineering and Aerospace Technology* 83.2 (Mar. 2011), pp. 69–74. ISSN: 0002-2667. DOI: 10.1108/00022661111120953. URL: http://www.emerald.com/aeat/article/83/2/69-74/58823 (visited on 04/29/2026).

[16] Hongyu Chen et al. “Thermal conductivity of polymer-based composites: Fundamentals and applications”. In: *Progress in Polymer Science*. Topical Volume Hybrids 59 (Aug. 2016), pp. 41–85. ISSN: 0079-6700. DOI: 10.1016/j.progpolymsci.2016.03.001. URL: https://www.sciencedirect.com/science/article/pii/S0079670016000216 (visited on 04/29/2026).

[17] Sajid Mohammad Chhipa, Sumit Sharma, and Ashok Kumar Bagha. "Recent development in polymer coating to prevent corrosion in metals: A review". In: *Materials Today: Proceedings* (Oct. 2024). ISSN: 2214-7853. DOI: 10.1016/j.matpr.2024.09.001. URL: https://www.sciencedirect.com/science/article/pii/S2214785324004851 (visited on 04/29/2026).

[18] Gilbert A Churchill Jr and J Paul Peter. "Research design effects on the reliability of rating scales: A meta-analysis". In: *Journal of Marketing Research* 21.4 (1984), pp. 360–375. DOI: 10.1177/002224378402100402.

[19] CONEBI. *Bicycle and E-Bike Sales continue to grow, reaching record levels – CONEBI*. en-US. July 2022. URL: https://www.conebi.eu/bicycle-and-e-bike-sales-continue-to-grow-reaching-record-levels/ (visited on 04/28/2026).

[20] CONEBI. *European Bicycle Industry remains strong in 2024, navigating market adjustments – CONEBI*. en-US. July 2025. URL: https://www.conebi.eu/european-bicycle-industry-remains-strong-in-2024-navigating-market-adjustments/ (visited on 04/28/2026).

[21] CONEBI. *European Bicycle Industry shows resilience and growth potential despite 2023 economic challenges – CONEBI*. en-US. June 2024. URL: https://www.conebi.eu/pr-conebi-bimp-2024/ (visited on 04/28/2026).

[22] Roger Cooper. *Global Sheet Metal Putty Market 2026 – PW Consulting Chemical & Energy Research Center*. en-US. Feb. 2026. URL: https://pmarketresearch.com/chemi/sheet-metal-putty-market/ (visited on 04/28/2026).

[23] Behzad Fotovvati, Navid Namdari, and Amir Dehghanghadikolaei. "On Coating Techniques for Surface Protection: A Review". en. In: *Journal of Manufacturing and Materials Processing* 3.1 (Mar. 2019), p. 28. ISSN: 2504-4494. DOI: 10.3390/jmmp3010028. URL: https://www.mdpi.com/2504-4494/3/1/28 (visited on 04/29/2026).

[24] Carineh Ghafafian and Steven Nutt. "A Multi-Industry Perspective to Composite Repairs". en. In: *Applied Composite Materials* 32.4 (Aug. 2025), pp. 1197–1235. ISSN: 1573-4897. DOI: 10.1007/s10443-025-10351-3. URL: https://doi.org/10.1007/s10443-025-10351-3 (visited on 04/28/2026).

[25] Klaus D. Goepel. *AHP calculator - AHP-OS*. Feb. 2022. URL: https://bpmsg.com/ahp/ahp-calc.php?n=7&t=AHP+priorities&c%5B0%5D=V1&c%5B1%5D=V2&c%5B2%5D=V3&c%5B3%5D=V4&c%5B4%5D=V5&c%5B5%5D=V6&c%5B6%5D=V7.

[26] R. Goudarzi et al. "Graphite Nanosheet as Low Shrinkage Additive, Curing Accelerator, and Conducting Filler for Unsaturated Polyester Resin". In: *Polymer-Plastics Technology and Engineering* 55.12 (Aug. 2016), pp. 1231–1239. ISSN: 0360-2559. DOI: 10.1080/03602559.2015.1132468. URL: https://doi.org/10.1080/03602559.2015.1132468 (visited on 04/29/2026).

[27] Growth Market Reports. *Polyester Putty and Epoxy Putty Market Research Report 2033*. en. 2026. URL: https://growthmarketreports.com/report/polyester-putty-and-epoxy-putty-market-global-industry-analysis (visited on 04/28/2026).

[28] Ameya Rajendra Jagtap and Aarti More. "Developments in reactive diluents: a review". en. In: *Polymer Bulletin* 79.8 (Aug. 2022), pp. 5667–5708. ISSN: 1436-2449. DOI: 10.1007/s00289-021-03808-5. URL: https://doi.org/10.1007/s00289-021-03808-5 (visited on 04/29/2026).

[29] Fan-Long Jin, Xiang Li, and Soo-Jin Park. “Synthesis and application of epoxy resins: A review”. In: *Journal of Industrial and Engineering Chemistry* 29 (Sept. 2015), pp. 1–11. ISSN: 1226-086X. DOI: 10.1016/j.jiec.2015.03.026. URL: https://www.sciencedirect.com/science/article/pii/S1226086X15001033 (visited on 04/29/2026).

[30] Li Kaichang, Qiu Renhui, and Liu Wendi. “Improvement of Interfacial Adhesion in Natural Plant Fiber-reinforced Unsaturated Polyester Composites: A Critical Review”. en. In: *ResearchGate* 3.1 (Mar. 2015), pp. 98–113. DOI: 10.7569/RAA.2015.097301. URL: https://www.researchgate.net/publication/276284367_Improvement_of_Interfacial_Adhesion_in_Natural_Plant_Fiber-reinforced_Unsaturated_Polyester_Composites_A_Critical_Review (visited on 04/29/2026).

[31] Pooneh Kardar and Reza Amini. “Advances and future directions in eco-friendly coatings: From chemistry to industrial applications”. In: *Progress in Organic Coatings* 214 (May 2026), p. 110068. ISSN: 0300-9440. DOI: 10.1016/j.porgcoat.2026.110068. URL: https://www.sciencedirect.com/science/article/pii/S0300944026001244 (visited on 04/29/2026).

[32] Farnaz Mazaheri Karvandian and Pascal Hubert. “Quantitative assessment of dispersion stability and processing parameters in graphene-enhanced unsaturated polyester resins: Effect of mixing techniques”. en. In: *Polymer Engineering & Science* 65.4 (2025), pp. 2133–2145. ISSN: 1548-2634. DOI: 10.1002/pen.27145. URL: https://onlinelibrary.wiley.com/doi/abs/10.1002/pen.27145 (visited on 04/29/2026).

[33] Lang Li et al. *A Novel Method to Formulate Pigmented Powder Coatings by Ultrafine Powders*. Sept. 2022. DOI: 10.3390/powders1040015. URL: https://www.mdpi.com/2674-0516/1/4/15 (visited on 04/29/2026).

[34] Market Research Intellect. *Aluminum Bicycle Frame Market Size | Industry Report 2035*. en. 2026. URL: https://www.marketresearchintellect.com/product/aluminum-bicycle-frame-market/ (visited on 04/28/2026).

[35] E. A. S. Marques et al. “Adhesive Joints for Low- and High-Temperature Use: An Overview, The Journal of Adhesion”. en. In: *ResearchGate* (Dec. 2014), pp. 556–585. ISSN: 0021-8464. DOI: 10.1080/00218464.2014.943395. URL: https://www.researchgate.net/publication/271933349_Adhesive_Joints_for_Low-_and_High-Temperature_Use_An_Overview (visited on 04/29/2026).

[36] Douglas C. Montgomery. *Introduction to Statistical Quality Control*. en. Google-Books-ID: oh7zDwAAQBAJ. John Wiley & Sons, June 2020. ISBN: 978-1-119-72309-7.

[37] Debora C. Moreira et al. *Size effect on the thermal intensification of alumina-filled nanocomposites - Debora C Moreira, Nelson R Braga, Leandro A Sphaier, Luiz CS Nunes, 2016*. 2016. DOI: 10.1177/0021998315624253. URL: https://journals.sagepub.com/doi/10.1177/0021998315624253 (visited on 04/29/2026).

[38] Iqbal Ahmed Moujdin et al. “Development of Low Shrinkage Curing Techniques for Unsaturated Polyester and Vinyl Ester Reinforced Composites”. en. In: *Materials* 15.9 (Jan. 2022), p. 2972. ISSN: 1996-1944. DOI: 10.3390/ma15092972. URL: https://www.mdpi.com/1996-1944/15/9/2972 (visited on 04/29/2026).

[39] Ahmad Mousa, Gert Heinrich, and Udo Wagenknecht. "Toughened Unsaturated Polyester Composites Reinforced with Slag Material". In: *Polymer-Plastics Technology and Engineering* 56.15 (Oct. 2017), pp. 1657–1664. ISSN: 0360-2559. DOI: 10.1080/03602559.2017.1289394. URL: https://doi.org/10.1080/03602559.2017.1289394 (visited on 04/29/2026).

[40] Sagar Kumar Nayak, Smita Mohanty, and Sanjay K Nayak. "A new way synthesis of expanded graphite as a thermal filler to enhance the thermal conductivity of DGEBA resin as thermal interface material". EN. In: *High Performance Polymers* 32.5 (June 2020), pp. 506–523. ISSN: 0954-0083. DOI: 10.1177/0954008319884616. URL: https://doi.org/10.1177/0954008319884616 (visited on 04/29/2026).

[41] Dongdong Peng et al. "The formation and corrosion behavior of a zirconium-based conversion coating on the aluminum alloy AA6061". en. In: *Journal of Coatings Technology and Research* 13.5 (Sept. 2016), pp. 837–850. ISSN: 1935-3804. DOI: 10.1007/s11998-016-9789-1. URL: https://doi.org/10.1007/s11998-016-9789-1 (visited on 04/28/2026).

[42] Pouya Rajaee et al. "Experimental Analysis and Optimization of Mechanical and Physical Properties of Light-Weight Bulk Molding Compound by Design of Experiment". In: *Journal of Macromolecular Science, Part B* 60.4 (Nov. 2020), pp. 237–256. ISSN: 0022-2348. DOI: 10.1080/00222348.2020.1844409. URL: https://doi.org/10.1080/00222348.2020.1844409 (visited on 04/29/2026).

[43] Gianluca Rubino and Simone Venettacci. "Advances in powder coating of metal components: A case study for wire die springs". In: *Journal of Manufacturing Processes* 101 (Sept. 2023), pp. 1257–1274. ISSN: 1526-6125. DOI: 10.1016/j.jmapro.2023.06.067. URL: https://www.sciencedirect.com/science/article/pii/S1526612523006886 (visited on 04/29/2026).

[44] R. W. Saaty. "The analytic hierarchy process—what it is and how it is used". In: *Mathematical Modelling* 9.3 (Jan. 1987), pp. 161–176. ISSN: 0270-0255. DOI: 10.1016/0270-0255(87)90473-8. URL: https://www.sciencedirect.com/science/article/pii/0270025587904738 (visited on 05/21/2026).

[45] N. Saleema and D. Gallant. "Atmospheric pressure plasma oxidation of AA6061-T6 aluminum alloy surface for strong and durable adhesive bonding applications". In: *Applied Surface Science* 282 (Oct. 2013), pp. 98–104. ISSN: 0169-4332. DOI: 10.1016/j.apsusc.2013.05.064. URL: https://www.sciencedirect.com/science/article/pii/S0169433213009914 (visited on 04/28/2026).

[46] L. F. M da Silva et al. "A review on the temperature and moisture degradation of adhesive joints". EN. In: *Proceedings of the Institution of Mechanical Engineers, Part L: Journal of Materials: Design and Applications* 231.5 (Aug. 2017), pp. 488–501. ISSN: 1464-4207. DOI: 10.1177/1464420716671503. URL: https://doi.org/10.1177/1464420716671503 (visited on 04/28/2026).

[47] L. F. M da Silva et al. "An updated review of adhesively bonded joints in composite materials". In: *International Journal of Adhesion and Adhesives* 72 (Jan. 2017), pp. 30–42. ISSN: 0143-7496. DOI: 10.1016/j.ijadhadh.2016.10.010. URL: https://www.sciencedirect.com/science/article/pii/S0143749616302068 (visited on 04/28/2026).

[48] Reetik Singh et al. “Enhancing primer performance: A study of graphene blending percentage and its effects on corrosion resistance, mechanical strength, and wettability”. In: *Journal of Alloys and Compounds* 1020 (Mar. 2025), p. 179359. ISSN: 0925-8388. DOI: 10.1016/j.jallcom.2025.179359. URL: https://www.sciencedirect.com/science/article/pii/S092583882500917X (visited on 04/29/2026).

[49] International Organization for Standard. *Paints and varnishes - Cross-cut test*. 2020.

[50] Syeda Noor E Sumaiya et al. “Effect of Surface Treatment on Interfacial Strength of Metal-Polymer Composite Bond”. en. In: *ResearchGate*. Society for theAdvancement of Material and Process Engineering, June 2016. URL: https://www.researchgate.net/publication/308882044_Effect_of_Surface_Treatment_on_Interfacial_Strength_of_Metal-Polymer_Composite_Bond (visited on 04/28/2026).

[51] Ferenc Tajti, Miklós Berczeli, and Zoltan Weltsch. *Optimizing Adhesion in Aluminum Alloys: A Cross-Disciplinary Approach to Surface Treatment and Bond Strength*. en. 2024. DOI: 10.2139/ssrn.4767278. URL: https://www.ssrn.com/abstract=4767278 (visited on 04/28/2026).

[52] Hongyu Wei et al. “Adhesion and cohesion of epoxy-based industrial composite coatings”. In: *Composites Part B: Engineering* 193 (July 2020), p. 108035. ISSN: 1359-8368. DOI: 10.1016/j.compositesb.2020.108035. URL: https://www.sciencedirect.com/science/article/pii/S1359836819369951 (visited on 04/29/2026).

[53] Jun-Seok Yeo, Ji-Hoon Lee, and Seok-Ho Hwang. “Effects of lignin on the volume shrinkage and mechanical properties of a styrene/unsaturated polyester/lignin ternary composite system”. In: *Composites Part B: Engineering* 130 (Dec. 2017), pp. 167–173. ISSN: 1359-8368. DOI: 10.1016/j.compositesb.2017.07.084. URL: https://www.sciencedirect.com/science/article/pii/S1359836817303268 (visited on 04/29/2026).

[54] Manseok Yoon et al. “Development of Low-Shrink Epoxy Putty to Solve Appearance-Quality Defects of Carbon-Fiber-Reinforced Plastic Automotive Exterior Parts”. en. In: *Materials* 14.21 (Jan. 2021), p. 6419. ISSN: 1996-1944. DOI: 10.3390/ma14216419. URL: https://www.mdpi.com/1996-1944/14/21/6419 (visited on 04/29/2026).

Appendix A

Methodology and Experimental Work

A.1 Methodology Tools

A.1.1 Variable Definitions for the Weighted Decision Matrix

Score	Evaluation Criteria for V_1 (Ergonomics & Workability)
1	Too hard or crumbles easily. Impossible to achieve a smooth surface finish.
2	Requires high downward pressure on the pneumatic sander, causing RPM drop. Sanding cycle takes noticeably longer than standard production limits.
3	Standard application. Sanding requires standard baseline time and pressure to achieve the required smoothness.
4	Spreads seamlessly without tearing. Sands consistently and rapidly using only the dead-weight of the pneumatic sander.
5	Exceptionally smooth application. Sands effortlessly, heavily optimizing the process takt time.

Table A.1: Qualitative evaluation scale for variable V_1.

Score	Evaluation Criteria for V_2 (Curing Time until Sanding is possible)
1	$x >$ 1h20 min: Halts production and creates operational bottlenecks on the line.
2	1h $< x \leq$ 1h20 min: Requires an excessive buffer (waiting) area for the frames to dry.
3	40 min $< x \leq$ 1h: Sub-optimal, but macroscopically viable for analysis.
4	20 min $< x \leq$ 40 min: Integrates well into the standard production workflow.
5	0 to 20 min: Rapid curing. The frame is coated, sanded, and immediately progresses down the line.

Table A.2: Qualitative evaluation scale for variable V_2.

Score	Evaluation Criteria for V_3 (Chemical Resistance / Passivation)
1	Increase of ≥ 7 porosities. The matrix dissolves, crumbles, completely delaminates. Distinct darkening is observed due to acid absorption.
2	Increased porosity (5 to 6 pores) is clearly visible to the naked eye.
3	Structurally stable. Formation of isolated micropores (increase of 3–4).
4	Minimal morphological alteration. Only minor isolated microporosity increase (1–2 pores).
5	Zero increase in porosity. The matrix emerges from the acidic passivation bath in the exact morphological state it entered.

Table A.3: Qualitative evaluation scale for variable V_3. Porosity counts were evaluated strictly within a standardized localized zone of approximately 5–7 cm $\times$ 2–3 cm directly over the primary weld.

Score	Evaluation Criteria for V_4 (Thermal Resistance / Oven Outgassing)
1	Significant pinholing across the entire layer, resulting in a sandpaper-like roughness ($\geq$ 10 pores).
2	Visible, scattered microporosity (7–9 pores), distributed non-uniformly.
3	4–6 pores or slight visible shrinkage.
4	1–3 visible pores to the naked eye. A slight alteration in the paint's surface tension is noticeable only under direct light.
5	"Mirror" or Carbon-look effect. Undetectable beneath the topcoat. Zero porosity.

Table A.4: Qualitative evaluation scale for variable V_4. Porosity counts were evaluated strictly within a standardized localized zone of approximately 5–7 cm $\times$ 2–3 cm directly over the primary weld.

Score	Evaluation Criteria for V_5 (Mechanical Adhesion Post-Sanding)
1	Detaches from the aluminum substrate at the slightest touch of a sander or fingernail.
2	Chips easily at the edges during sanding, leaving distinct step-offs.
3	Remains firmly bonded during standard processing, but requires operator care to avoid tearing the edges.
4	Strong physical bond to the substrate. Permits edge sanding without chipping.
5	Optimal structural bond. The adhesive strength at the interface exceeds the internal cohesive strength of the matrix; forced mechanical removal results in cohesive failure of the putty rather than adhesive detachment from the substrate.

Table A.5: Qualitative evaluation scale for variable V_5.

Score	Evaluation Criteria for V_7 (Initial Surface Porosity)
1	Significant porosity ($\geq$ 10 pores). The affected zone must be ground completely down to bare aluminum and reworked from scratch.
2	High porosity (7–9 pores). Forces the inspector to intercept the frame, apply a new global layer of putty, and repeat the drying and sanding cycle.
3	Moderate porosity (4–6 pores). Requires minor, localized touch-ups with correction putty (epoxy) or the original putty (polyester).
4	Highly residual microporosity (1–3 pores). Passes standard visual inspection after targeted sanding.
5	Zero porosity following the initial sanding sequence. The frame can proceed directly to the passivation line.

Table A.6: Qualitative evaluation scale for variable V_7. Porosity counts were evaluated strictly within a standardized localized zone of approximately 5–7 cm $\times$ 2–3 cm directly over the primary weld.

A.1.2 AHP Tools

Note: AHP Scale: 1- Equal Importance, 3- Moderate importance, 5- Strong importance, 7- Very strong importance, 9- Extreme importance (2,4,6,8 values in-between).

Table A.7: AHP Pairwise Comparison Relations.

No.	Option A	Option B	Preference	Intensity Value
1	V1	V2	V2	4
2	V1	V3	V3	8
3	V1	V4	V4	9
4	V1	V5	Equal	1
5	V1	V6	V6	8
6	V1	V7	Equal	1
7	V2	V3	V3	5
8	V2	V4	V4	5
9	V2	V5	V2	3
10	V2	V6	V6	5
11	V2	V7	V2	3
12	V3	V4	V4	2
13	V3	V5	V3	8
14	V3	V6	Equal	1
15	V3	V7	V3	7
16	V4	V5	V4	6
17	V4	V6	V4	2
18	V4	V7	V4	6
19	V5	V6	V6	8
20	V5	V7	Equal	1
21	V6	V7	V6	7

Table A.8: Priorities and Weight Intervals.

Variable	Priority	Rank	(+)	(-)
V1	3,0%	7	0,6%	0,6%
V2	7,8%	4	2,5%	2,5%
V3	24,8%	2	8,6%	8,6%
V4	32,9%	1	11,1%	11,1%
V5	3,3%	6	0,9%	0,9%
V6	24,8%	2	7,2%	7,2%
V7	3,4%	5	0,8%	0,8%

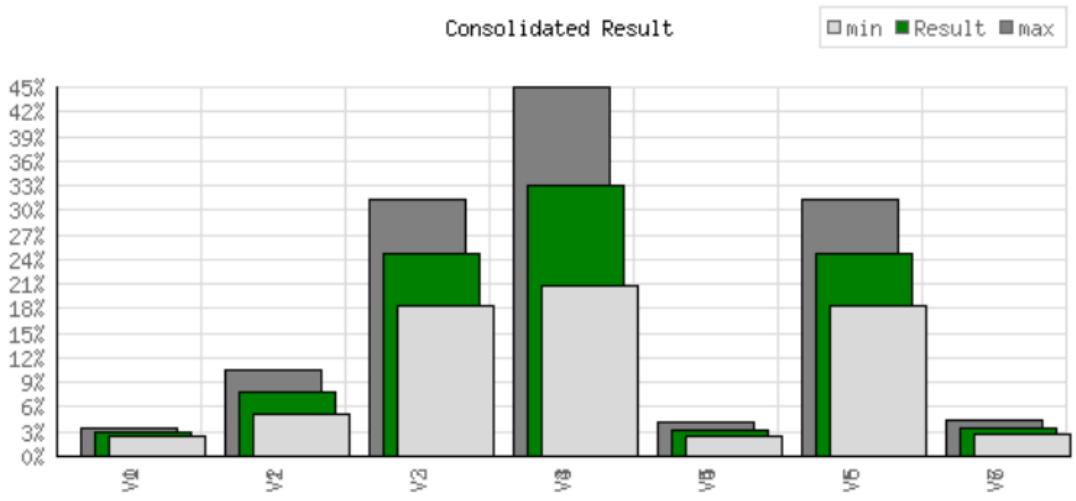

Figure A.2: Weight Intervals of the AHP Process.

	1	2	3	4	5	6	7
1	1	0.25	0.12	0.11	1.00	0.12	1.00
2	4.00	1	0.20	0.20	3.00	0.20	3.00
3	8.00	5.00	1	0.50	8.00	1.00	7.00
4	9.00	5.00	2.00	1	6.00	2.00	6.00
5	1.00	0.33	0.12	0.17	1	0.12	1.00
6	8.00	5.00	1.00	0.50	8.00	1	7.00
7	1.00	0.33	0.14	0.17	1.00	0.14	1

Figure A.1: Principal eigen value = 7.240; Eigenvector solution: 5 iterations, delta = 8.6E-8.

A.1.3 Mapping of the samples

Group / Identifier	Experimental Formulations
Test Specimens	T8-0, T8-1, MP-0, MP-1
X1	NT-0, NT-1, ES-0, ES-1
X2	PD-0, PD-1, PD-A-0, PD-A-1
X3	CH-2M, IM-2M, PD-2M, MP-2M
X4	P70-2R
X5	CH-0, IM-0
X9	CH-2R, IM-2R, PD-2R, MP-2R
Y1	ES-2R, NT-2R
Y2	PD1-0, PD1-2R, P701-0, P701-2R, IM1-0, IM1-2R, MP1-0, MP1-2R, CH1-0, CH1-2R, PD2-0, PD2-2R
Y3	ES1-0, ES1-2R, NT1-0, NT1-2R
Y5	NT-0 (3 replicates), NT1-0 (3 replicates), ES-0 (2 replicates), ES1-0 (2 replicates)
Y6	PD-0 (5 replicates), PD1-0 (5 replicates), PD2-0 (5 replicates)
Y7	ES-0 (3 replicates), ES1-0 (3 replicates), NT-0 (2 replicates), NT1-0 (2 replicates)

Table A.9: Mapping matrix of sample group identifiers to their corresponding chemical formulations and replicate distributions.

Appendix B

Results and Software Data

Table B.1: Thickness Measurements: Primer Head-2-Head.

Formula	Layers	Thickness interval (μm)	Average (μm)	Delta (2M-2R)
MP-2M	Putty + Primer M + PP	[575, 1072]	764,3	14,7
MP-2R	Putty + Primer R + PP	[386, 1364]	749,7	
PD-2M	Putty + Primer M + PP	[366, 1244]	855,7	-104,7
PD-2R	Putty + Primer R + PP	[752, 1187]	960,3	
CH-2M	Putty + Primer M + PP	[224, 1282]	769,3	108
CH-2R	Putty + Primer R + PP	[296, 1084]	661,3	
IM-2M	Putty + Primer M + PP	[675, 1282]	916,7	256
IM-2R	Putty + Primer R + PP	[323, 1011]	660,7	

B.1 PD Data

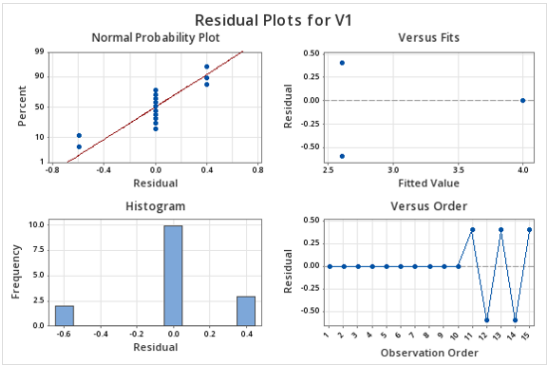

(a) Residual V_1 PD family.

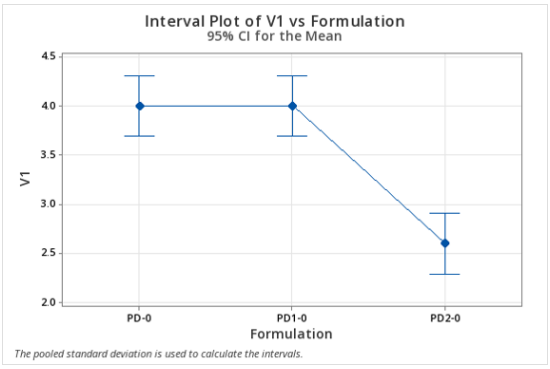

(b) Interval V_1 PD family.

Figure B.1: Data for V_1, PD family.

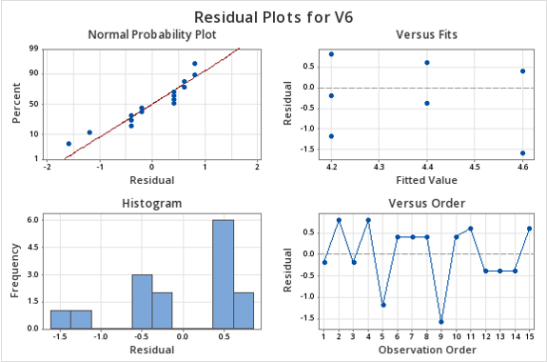

(a) Residual V_6 PD family.

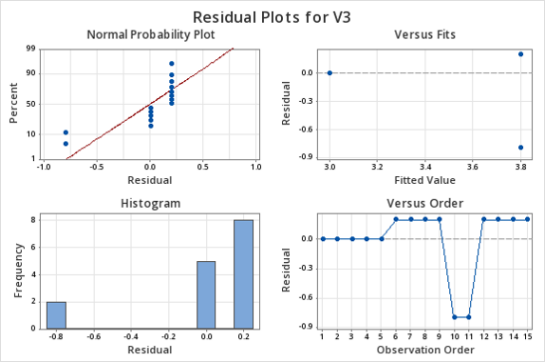

(b) Residual Analysis V_3 PD family.

Figure B.2: Data for PD family, V_3 and V_6.

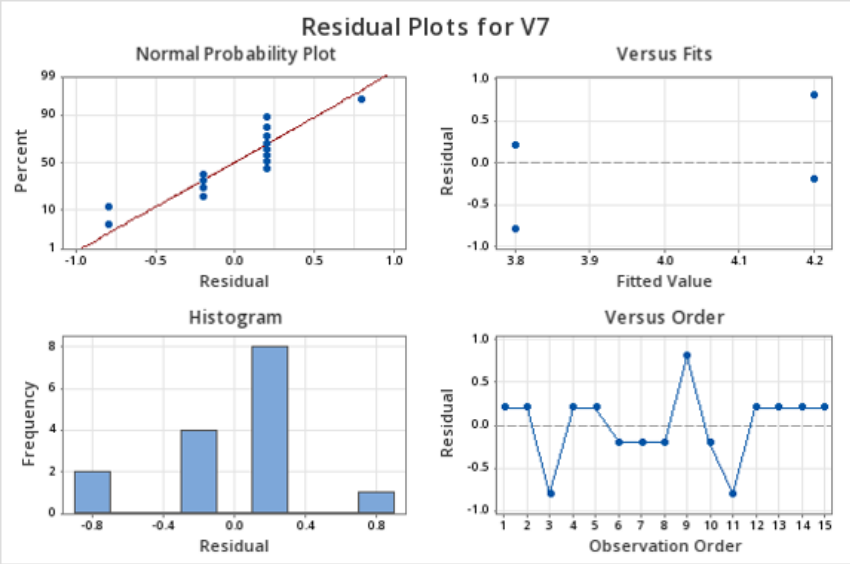

Figure B.3: Residual Analysis V_7, PD family.

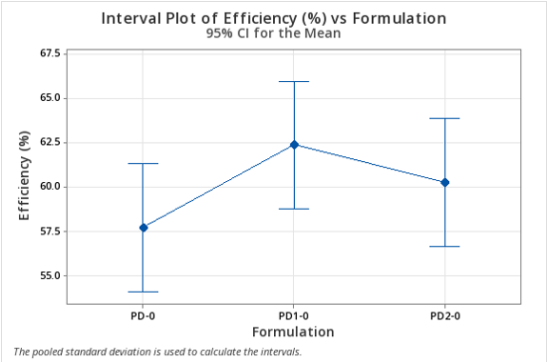

(a) Interval Efficiency PD family.

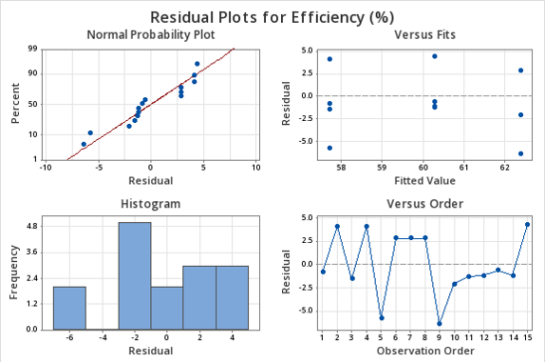

(b) Residual Analysis Efficiency PD family.

Figure B.4: Data for PD family, Efficiency.

B.2 ES Data

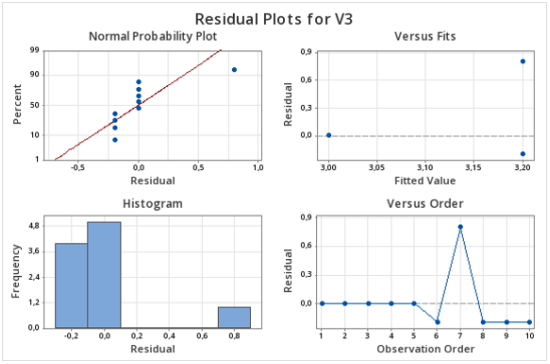

(a) Residual Analysis V_3, ES family.

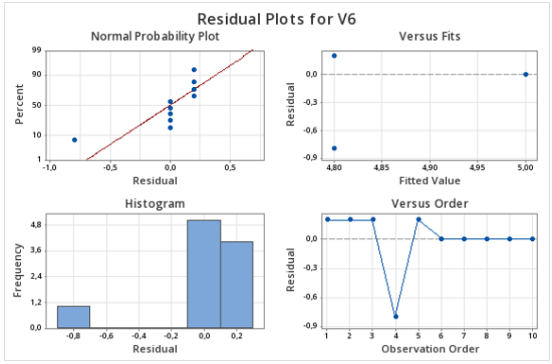

(b) Residual Analysis V_6, ES family.

Figure B.5: Data for ES family, V_3 and V_6.

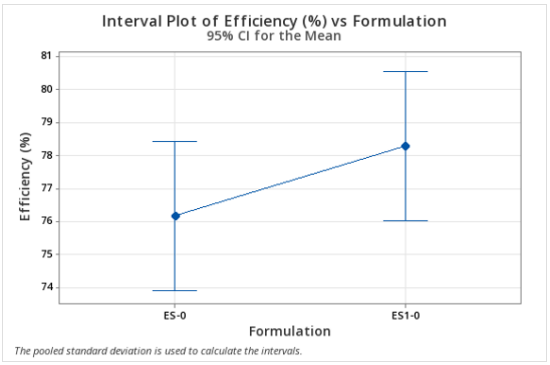

(a) Interval for Efficiency ES family.

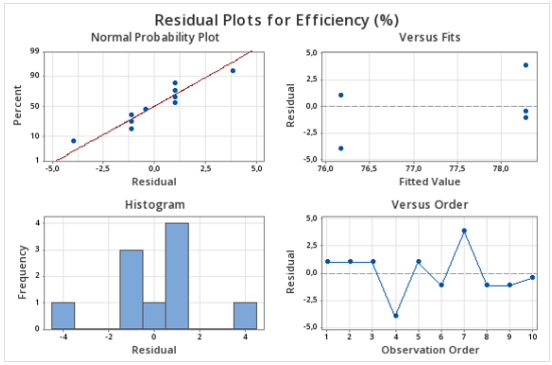

(b) Residual Analysis Efficiency ES family.

Figure B.6: Data for ES family, Efficiency.

B.3 NT Data

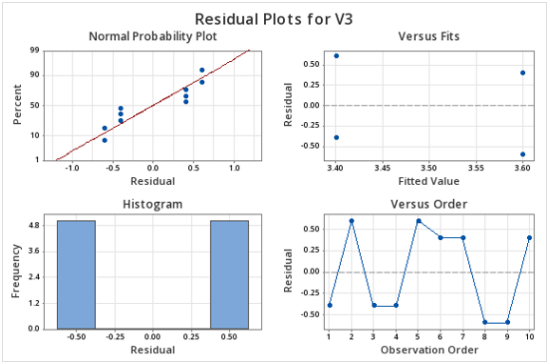

(a) Residual Analysis V_3, NT family.

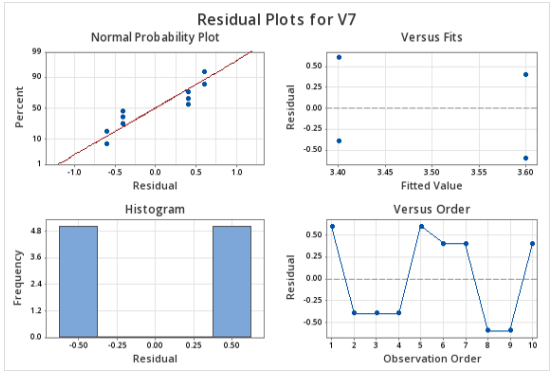

(b) Residual Analysis V_7, NT family.

Figure B.7: Data for NT family, V_3 and V_7.

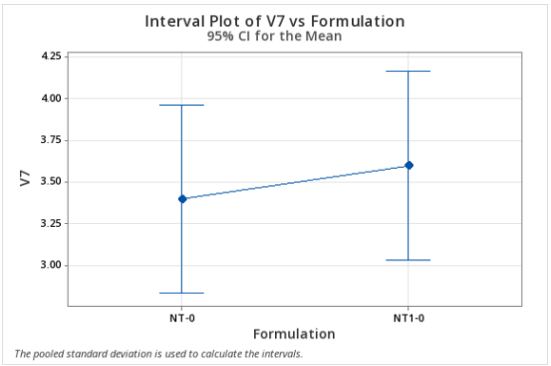

(a) Interval for Efficiency NT family.

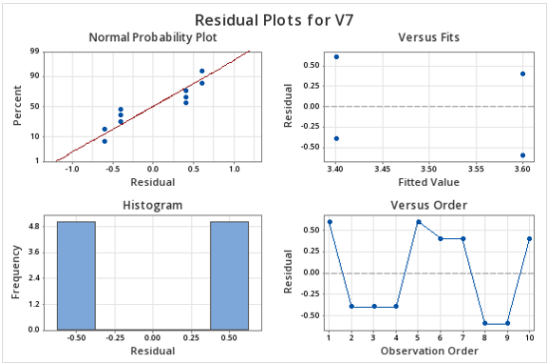

(b) Residual Analysis Efficiency NT family.

Figure B.8: Data for NT family, Efficiency.